1-1-2013

Subsurface Imaging and Petrophysical Analysis of the South Georgia Rift Basin, South Carolina

Olusoga Martins Akintunde
University of South Carolina

SUBSURFACE IMAGING AND PETROPHYSICAL ANALYSIS OF THE SOUTH GEORGIA RIFT BASIN, SOUTH CAROLINA

by

Olusoga Martins Akintunde

Bachelor of Technology
Federal University of Technology, 1992

Master of Technology
Federal University of Technology, 1997

Master of Science
Stanford University, 2005

Submitted in Partial Fulfillment of the Requirements

For the Degree of Doctor of Philosophy in

Geological Sciences

College of Arts and Sciences

University of South Carolina

2013

Accepted by:

Camelia Knapp, Major Professor

Pradeep Talwani, Committee Member

James Knapp, Committee Member

Manika Prasad, Committee Member

Lacy Ford, Vice Provost and Dean of Graduate Studies

DEDICATION

To my family members

ACKNOWLEDGEMENTS

Funding for this dissertation was provided through the $10M grants from the United States Department of Energy (DOE) for the geological characterization of the South Georgia Rift (SGR) basin for CO_2 storage (under Award Number DE-FE0001965), and I am extremely thankful to the DOE. I wish to thank the American Association of Petroleum Geologists (AAPG) Foundation for the award of the 2012 W. David Wiman Memorial Grant. The Department of Earth and Ocean Sciences (EOS) awarded me a teaching assistantship for the spring 2013, and I am very appreciative of the EOS funding assistance. The department assisted me with partial funds to attend the fall 2011 Student Expo organized by the Society of Exploration Geophysicists (SEG) and the AAPG.

Special thanks to my Doctoral Committee Members: Professors Camelia Knapp, James Knapp, Manika Prasad and Pradeep Talwani for their tremendous support with my dissertation. I have benefited and learned a lot from their wealth of experience and expertise. I carried out this work under the direction and meticulous supervision of Dr. Camelia C. Knapp (my primary/academic advisor), and I would like to specially thank her for her outstanding advisement and generous support. I am also very thankful to Dr. James H. Knapp for his unflinching support, helpful feedback and great insights notably into the tectonics aspect of this work as well suggestions for structural interpretation.

I learned new things from his knowledge of regional tectonics and structural geology. My sincere appreciation also goes to Dr. Manika Prasad notably for her expert advice and outstanding support with the rock physics part of this dissertation. Access to the laboratory facilities, at the rock abuse laboratory at the Colorado School of Mines, which I used for the rock physics studies, was made possible by her. I benefited a lot too from the vast experience and expertise of Dr. Pradeep Talwani in terms of his helpful reviews and feedback on the findings from our SeisData6 paper involving new constraints on the buried rift basins from the reanalysis of the SeisData6 seismic profile across the Coastal Plain of South East Georgia. Dr. Talwani also helped with links and access to useful materials/papers including the Norris Lightsey well logs that I used for the petrophysical study.

I would like to express my appreciation to Dr. John Shafer, Mike Waddell, Dr. Adrian Addison, Duke Brantley and Mark Evans from the Earth Sciences Resources Institute (ESRI), Columbia, South Carolina as well as David Heffner and Darrell Terry of Department of Earth and Ocean Sciences for their contributions to this work. Mr. Mike Waddell was very helpful with procurement of the digital versions of the well logs including the ones from the Norris Lightsey. These well data were originally provided by the Southern Company based in Georgia. Special thanks too to Drs. Scott Howard and Bill Clendenin of the South Carolina State Geological Survey for unrestricted access to the sandstone cores used in this study. They both provided helpful comments on the geology of the SGR basin. Basalt samples from Clubhouse Crossroads were provided by Dr. Paul Olsen of Lamont-Doherty Earth Observatory, Columbia University, New York. X-

ray computed tomographic images were acquired by the assistance of Dr. Mike Batzle and George Radziszewski of the Colorado School of Mines (basalt samples) and by Dr. Jessica Maisano and the UT Austin XCT team (Palisade/Diabase sills). XRD analysis was performed by the Mineral Lab Inc, in Golden Colorado. Thin section and photomicrograph on the Dorcehster-211 basalt sample were provided by Dr. James Rine of the Weatherford Laboratories in Houston, Texas. I thank Darrell Terry, a great friend and colleague for his helpful reviews and feedback. David Heffner assisted a lot especially during our visits to the South Carolina Geological Survey to examine and request core samples. My thanks also go to other members of the Geophysical Exploration Laboratory and the Tectonics and Geophysics Laboratory for their friendships. I gratefully acknowledge my roommate (from January 2011-May 2013), Dr. Patrick Roughen, and my long time friend from Stanford, Dayo Adeogba, for their support and friendships. I thank my friends from the RiverBend Community Church in Lexington, SC, as well from the All Nations Prayer Network (ANPN) for their prayers and encouragement. All my family members – Edmund, Jumoke, Titi, Seun – and my parents deserve my appreciation for their support, love and prayers all through my educational career. Finally, I am very thankful to the LORD for His grace, mercies, goodness, strength, blessings, protection and love that enabled me to complete my PhD and other previous degrees. Now to the King eternal, immortal, to God who alone is wise, be honor and glory forever and ever. Amen (1 Timothy 2:17).

ABSTRACT

The Triassic-Jurassic South Georgia Rift (SGR) basin, buried beneath Coastal Plain sediments of southern South Carolina, southeastern Georgia, western Florida, and southern Alabama, consists of an assemblage of continental rift deposits (popularly called red beds), and mafic igneous rocks (basalt flows and diabase sills). The red beds are capped by basalts and/or diabase sills, and constitute the target for supercritical CO_2 storage as part of a Department of Energy funded project to study feasibility for safe and long-term sequestration. This study addresses key stratigraphic, structural and petrophysical issues critical to determine subsurface suitability for CO_2 storage as well as improved understanding of the Triassic basin's evolution and underline characteristics. Also unlike shale-capped CO_2 reservoirs, very little is known about the ability of basalts and diabase sills to act as viable seals for CO_2 storage.

New interpretations from reprocessed SeisData6 Coastal Plain, supported by analysis of well data, substantiate the presence of a buried Triassic basin in South East Georgia that is about 2.2 km deep and 170 km wide. It appears to coincide with the subsurface convergence of the southwest and northeast extensions of the Riddleville and Dunbarton basins that are subsidiaries of the main SGR basin. Contrary to previous study, this basin does not have basalt. Our data show no clear evidence for the Augusta fault that was identified in other studies in the vicinity of the Piedmont-Coastal Plain

boundary in Georgia and South Carolina. Petrophysically, the SGR basin manifests distinct porosity-permeability regimes that are influenced by the depositional environments. New results also indicate the presence of thick, confined porous red beds with average porosity as high as 14%. However, the red beds' permeability is generally low and shows large numerical variations both locally and regionally. Low permeability is caused by poor sorting, small pore throats and tectonically induced compaction and diagenesis. Changes in porosity and permeability with depth are highly significant within the SGR basin, and suggest a compacted basin with a history of uplift and erosion. Analyses further show that the basalt flows and diabase sills in the southern South Carolina part of the SGR possess low porosity, high seismic velocity, and density that are favorable to caprock integrity.

PREFACE

The goal of my dissertation is to develop new seismic and petrophysical attributes (such as velocity, density, porosity, and permeability) of the Triassic-Jurassic formations of the South Georgia Rift (SGR) basin necessary for improved understanding of the basin as well its potential to safely and permanently store CO_2. The Triassic-Jurassic South Georgia Rift (SGR) basin, buried beneath Coastal Plain sediments of southern South Carolina, southeastern Georgia, western Florida, and southern Alabama, consists of an assemblage of continental rift deposits (popularly called red beds or sandstone), and mafic igneous rocks (basalt flows and diabase sills). The red beds are capped by basalts and/or diabase sills, and constitute the target for supercritical CO_2 storage as part of a Department of Energy (DOE) funded project to study the SGR's geological feasibility for long term sequestration. This geological characterization study is part of the growing response to the global need and urgency to mitigate rising concentrations of CO_2 in the atmosphere.

Prior to the industrial revolution (around 1750-1850), global average atmospheric CO_2 was varying slightly between 180 and 280 parts per million by volume (PPMV, Tans, 2012). But since the industrial revolution, atmospheric concentrations of CO_2 have increased significantly to present levels of between 390 to 395 PPMV (Tans, 2012).

This increase has caused a doubling of the global mean surface temperature from 0.4 to 0.8^{o}C with tendency to significantly impact global climate change in weather patterns (Schaef et al., 2009). The rise in atmospheric CO_2 levels has been attributed to continued increase in global energy use through expanded consumption of fossil fuels (EIA, 2007). The 20th century particularly experienced a tremendous increase in energy consumption. This was caused by expanding human populations worldwide and development of new technologies that rely heavily on combustion of hydrocarbon fuels. The Intergovernmental Panel on Climate Change projects that average global atmospheric CO_2 concentration will reach about 750 PPMV by 2100 (EIA, 2007). Consequently, the challenge of this 21st century is to stabilize atmospheric CO_2 concentrations at 550 PPMV, which are approximately twice preindustrial concentrations (Albritton and Meira Filho, 2001). In order to achieve this based on estimates provided by Albritton and Meira Filho (2001), global emissions must be continuously reduced so that by 2050 global emissions are 15 $GtCO_2$/yr (15 billion tons of CO_2 per year) and by 2100, emissions would be 50 GtCO2/yr less ($1GtCO_2=10^9$ metric tons of $CO_2=10^{12}$kg of CO_2). To meet the global expectations of reducing CO_2 emissions from sources (such as power generation, iron and steel production, coal mine, heavy manufacturing, and hydrocarbon generation), geologic sequestration is considered one of the preferred choices for near-term mitigation.

Geologic sequestration involves capture, separation, transport, and injection of CO_2 into geologic repositories such as deep and unminable coal seams, deep saline aquifers, and mature oil and gas fields. According to Lumley et al. (2010), 4 billion tons

(Gt) of CO_2 must be stored for geo-sequestration to make any impact on reducing global CO_2 emissions. Current projections based on active geo-sequestration projects around the world indicate the need for a dramatic increase in commercial CO_2 projects by a factor of 1000 or more to achieve the 4Gt/year (Lumley et al., 2010). It is as a result of this that the push to select and characterize potential sites for CO_2 storage appears to be gaining considerable attention. Of the three geologic sequestration options for Carbon Capture and Storage (CCS), storage in deep saline aquifers has been projected to hold the most combined promise in terms of storage capacity, proximity to emission sources, and state-of-the art technology (Bachu et al., 1994, Bachu, 1996; and, Hovorka et al., 2006). Deep saline aquifers have very minimal socio-economic benefit for domestic purpose as drinking water and for agricultural usage due to depth of occurrence and high concentrations of dissolved solids.

In order to be considered suitable for CO_2 storage, a geologic repository (for instance a saline aquifer as the case with the SGR) must have enough pore space (porosity) in which to store CO_2, high permeability with a trapping mechanism (an overlying caprock or seal) to ensure containment of the CO_2 in the pore space and prevent vertical migration into overlying freshwater aquifers. In particular, porosity and permeability are critical for evaluating reservoir storage capacity, injectivity, and seal integrity for subsurface CO_2 storage. Also, the continuity and integrity of the overlying caprock are important requirements (Akintunde et al., 2013b). The true regional extent of the basalt flows that may serve as CO_2 seals is unknown. The composition, structure, and thickness of the target reservoir rocks for storage must be known.

This dissertation is divided into five chapters to address the key research issues associated with the determination of CO_2 storage potential of the SGR basin and to provide new insights into the evolution and tectonics of the basin. Chapter one focuses on newly identified constraints for the buried Triassic basin from reprocessing and integrated interpretations of the 200 km regional SeisData6 reflection profile across the Coastal Plain of Southeast Georgia. New results from rock physics studies involving laboratory based techniques and petrophysical analysis of well data are presented in Chapter two. Furthermore, chapter two provides new information on the local and regional distribution of porosity and permeability and how these rock properties may have been impacted by depositional and/or post depositional processes. An investigation of the tectonic controls on porosity and permeability behavior of the SGR's Triassic-Jurassic formations is discussed in Chapter three. In Chapter four; the focus is on permeability predictions in the Triassic red beds of the SGR basin. A rock physics fluid substitution modeling study, to investigate whether or not the SGR's Triassic reservoir would be suitable for subsurface CO_2 monitoring (should injection be undertaken), is discussed as part of Chapter four. A summary of research goals, as well as the key and new research accomplishments are presented in Chapter five.

TABLE OF CONTENTS

LIST OF TABLES

LIST OF FIGURES

CHAPTER 1

NEW CONSTRAINTS ON BURIED BASINS AND REGIONAL IMPLICATIONS FOR SUBSURFACE CO_2 STORAGE FROM THE SEISDATA6 SEISMIC PROFILE ACROSS THE SOUTHEAST GEORGIA COASTAL PLAIN

1.1. OVERVIEW

Reprocessing of the SeisData6 Coastal Plain profile was motivated by the need to provide enhanced subsurface imaging critical to site characterization studies for CO_2 storage within the South Georgia Rift (SGR) basin. The objectives were to identify and interpret subsurface reflectors for evidence of the buried Triassic basin and its underlying characteristics. Our new interpretation, supported by analysis of well data, has helped substantiate the presence of a Triassic basin beneath the Coastal Plain sediments in South East Georgia. This basin is about 2.2 km deep and 170 km wide and appears to coincide with the subsurface convergence of the southwest and northeast extensions of the Riddleville and Dunbarton basins that are subsidiaries of the main SGR (Akintunde et al., 2013a). It is characterized by distinctively higher seismic velocities relative to the overlying Coastal Plain sediments and manifests a series of sub-horizontal reflectors below the topmost reflector.

We reinterpreted the topmost reflector to originate from a change in velocity

and density between the Cretaceous-Cenozoic Coastal Plain sediments and the underlying Triassic rocks. This does not always originate from the Pre-Cretaceous basalt contrary to previous interpretations. The interpreted absence of basalt from this study is consistent with Heffner et al. (2012) showing that basalt is not prevalent throughout the SGR basin. Seismic discontinuities in the southeast of the basin suggest Triassic normal faults. Our reprocessed and reinterpreted SeisData6 show no clear evidence for the Augusta fault that was identified in other studies in the vicinity of the Piedmont - Coastal Plain boundary in Georgia and South Carolina.

1.2. INTRODUCTION

The South Georgia Rift (SGR) basin is believed to be the largest and probably the most geologically complex Mesozoic graben of the Eastern North-American Passive Margin (ENAM). It covers an area of about 100,000 km^2 and it was formed during crustal extension associated with the breakup of Pangea and later opening of the North Atlantic Ocean. The separation of the African and North American plates, the formation of the Atlantic Ocean and the associated zones of weakness in eastern North America have been stated as the initial events in the breakup of Pangea (Chowns and Williams, 1983). The breakup of Pangea started in late Triassic (about 215 to 175 million years ago), producing a zone of rifting from North Africa to the Gulf of Mexico and along the east coast of North America. Block-faulted basins were produced by this rifting though considerable changes in the relative positions of the continents took place in late Jurassic time. In addition, the closeness of the southeastern part of North America to

the triple junction between the North Atlantic, South Atlantic, and the Gulf of Mexico makes this an area susceptible to complex rifting and transform faulting (Chowns and Williams, 1983; and, McBride et al., 1989).

The ENAM-SGR basin consists of rocks buried beneath the Coastal Plain in parts of Georgia, South Carolina, Alabama and Florida (Figure 1.1). According to Knapp et al. (2012), the ENAM is most significant due to the complexity and regional extent of this mature Mesozoic passive margin rift system encompassing: (1) a large volume and regional extent of related magmatism, (2) a preserved complete stratigraphic column that records the post-rift evolution in several basins, (3) preserved lithospheric-scale pre-rift structures including Paleozoic sutures, and (4) a wide-range of geological, geochemical, and geophysical studies both onshore and offshore. The short-lived but most voluminous magmatic event associated with the initiation of rifting, the Central Atlantic Magmatic Province (CAMP), is one of the most significant magmatic events in North America (Knapp et al., 2012).

The Coastal Plain developed after the Triassic-Jurassic splitting of North America from Africa and the opening of the Atlantic Ocean. The Coastal Plain is a wedge of sediments which thickens seaward and extends from the Fall line to offshore in the Atlantic Ocean. These Late Cretaceous to Early Cenozoic sediments reach thicknesses exceeding 5 km and originate from the subaerial erosion of the Appalachians (Cook et al., 1981, Snipes et al., 1993).

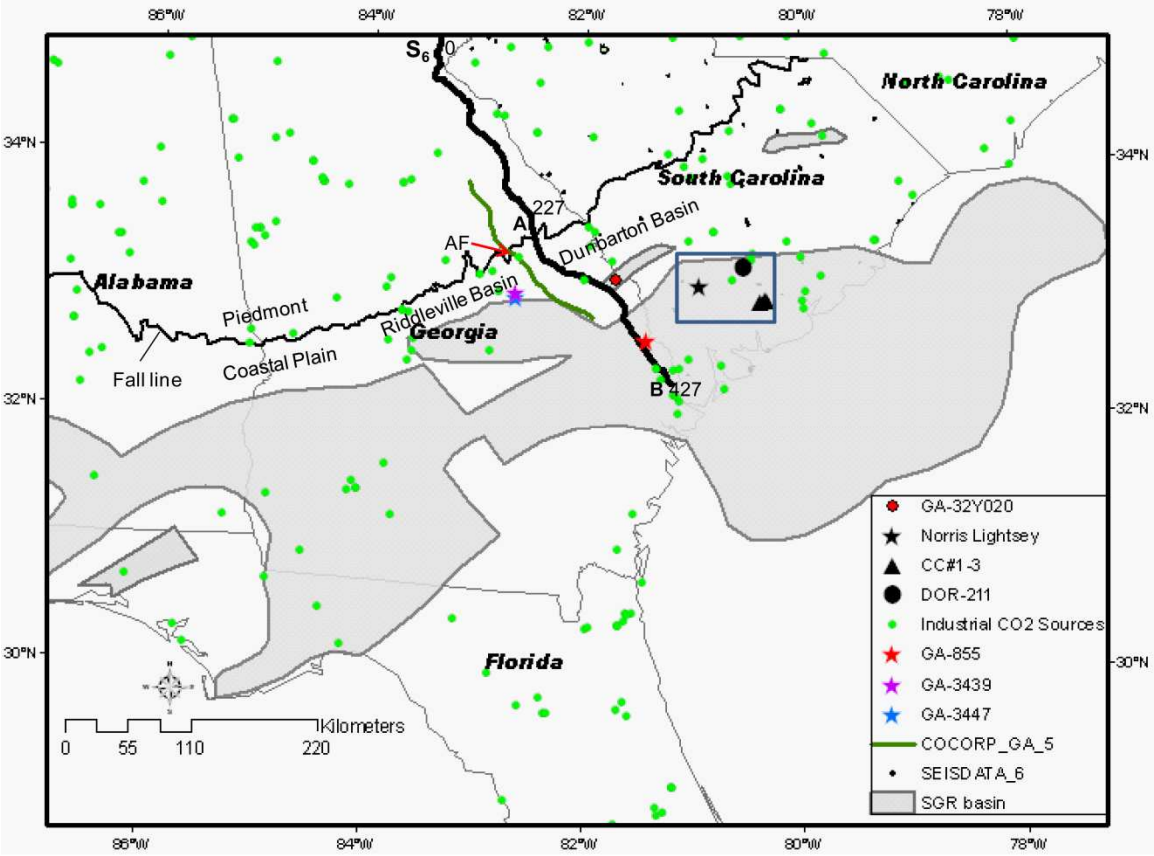

Figure 1.1: The South Georgia Rift (SGR) basin shown in gray below the Coastal plain covering parts of Georgia, South Carolina, Alabama, and Florida (modified from McBride et al., 1989). Seisdata (S_6) seismic profile lies between the Riddleville and Dunbarton basins and falls within areas postulated to be covered by basalt and/or diabase based on previous studies by Chowns and Williams (1983) and McBride et al. (1989). The Fall Line separates the coastal plain from the Piedmont province. The coastal plain segment of S_6 shown as AB is approximately 200 km (124 mi). The location of the Augusta fault (AF) was interpreted on the Consortium for Continental Reflection Profiling (COCOPR) GA-line 5 by Cook et al. (1981). It was thought to crop out to the northeast of the GA-line 5 and initially projected by Behrendt (1986) to intersect S_6 close to the boundary between the piedmont and coastal plain. Also displayed are locations of several wells in Georgia (GA-855, GA-32Y020, GA-3439, and GA-3447) and South Carolina (Norris Lightsey, Clubhouse Crossroads #1-3, and Dorchester-211) used in this study to calibrate the seismic data. Green dots represent industrial sources of CO_2.

SeisData6 (S_6) is one of the three multichannel regional seismic profiles in both Georgia and South Carolina with significant penetrations of the Coastal Plain (Figure

1.1). The three lines were acquired by Seisdata Services for the United States Geological Survey (USGS) in 1981 as part of a series of studies related to the Charleston, South Carolina, earthquake of 1886. The total length of the three profiles is 1,350 km, extending from the Piedmont province to the Coastal Plain across South Carolina and Georgia. Four vibrators were used for data collection and a summary of the data acquisition parameters is provided in Table 1.1. A previous seismic analysis of these profiles was carried out by Behrendt (1986) in order to investigate whether the Appalachian decollement, suggested as a probable cause of the 1886 Charleston earthquake, extends offshore or not. Our current interest in the S6 profile lies in its strategic location within buried Triassic-Jurassic rocks beneath the Coastal Plain that are the targets for the ongoing United States Department of Energy (DOE) funded project for geological characterization of the South Georgia Rift (SGR) basin for geological storage of CO_2 from stationary sources.

A key attraction in the SGR basin for CO_2 storage (and motivation for subsurface characterization) is due in part to the presence of Triassic-Jurassic formations occurring at depth intervals that are deeper than the 1 km needed for supercritical CO_2 storage. At a depth below surface of 0.8 to 1 km, CO_2 injected into the subsurface under normal geothermal and near hydrostatic pressure conditions will exist in a supercritical state (Albritton et al., 2001). In this state, CO_2 has a gas-like compressibility, viscosity, and surface tension with liquid-like densities and can flow more easily within the confined reservoir. Pore water in rocks near the center of Dunbarton basin is characterized by a dissolved solids content of about 11,000 mg/L (Marine and Siple, 1974) thereby enabling

their classification as deep saline formations. Chemical analyses of water from the Triassic red beds (Marine and Siple, 1974) reveal much higher chloride near the center of the basin (6,720 mg/L) when compared with water from the Coastal Plain sediments (1.5 mg/L) and crystalline metamorphic rock (1,260 to 1,400 mg/L). These buried formations are also within proximity to known surface sources of CO_2 (Figure 1.1).

Behrendt (1986) suggested the S_6 Coastal Plain profile crossed a buried Triassic basin in southeastern Georgia. However, bad data quality, arising from incorrect receiver geometry, hinders reliable interpretation of reflectors critical to improved understanding of key features of regional stratigraphic and structural significance. We reprocessed the approximately 200 km long S_6 Coastal Plain profile (AB in Figure 1.1) in order to unravel key characteristics of the buried basin as well as evaluate regional significance of the delineated geologic features of interest. The seismic reprocessing was aided by the availability of recent and improved processing techniques such as line geometry, residual statics correction, true amplitude recovery, velocity analysis and normal moveout correction, common-midpoint stacking, migration, depth conversion and other seismic imaging enhancement tools for improved subsurface imaging compared to the previous analysis of the SeisData 6 seismic line (Behrendt, 1986). Application of recent processing techniques has the ability to improve reflection continuity as well as enhance images of subsurface reflectors and/or features that were previously not seen. It is important that the subsurface seismic imaging yields a post-stack migrated depth section that is most suited for seismic-well correlation. This is a key component of our study.

Table 1.1: Summary of Vibroseis-Source Seismic Data Acquisition

S/N	Acquisition Design	Parameters
1	Sweep length	18 s
2	Sample rate	4 ms
3	Spread length	6.7 km
4	Group interval	67 m
5	Channels	96
6	Geophones per group	24
7	Maximum fold	24
8	Record length	6 s

1.3 OBJECTIVES OF STUDY

A number of unanswered questions on the stratigraphic and structural characteristics of the buried Triassic basin emanate from the previous interpretations of the S6 seismic record by Behrendt (1986). This study is designed to address these important unresolved issues that have regional implications and that are also important to the task of subsurface regional evaluation for CO_2 sequestration. These issues are:

1. The true characteristics in terms of stratigraphical, structural composition, extent and thickness of an inferred Triassic buried basin.

2. Whether or not there is a basaltic layer on top of the Triassic sediments, and what implications the presence or absence of basalt in this study area would have on the regional significance of this mafic igneous deposit within the main SGR basin as well as on its potential to serve as regional seal for CO_2 storage.
3. Whether or not the south east dipping Augusta fault (Figure 1.1), which approximately trends along the Piedmont-Coastal Plain boundary in Georgia and South Carolina, extends underneath the Coastal Plain sediments.
4. Whether or not this buried basin has any relationship with the Riddleville basin and Dunbarton basin in Georgia and South Carolina

1.4. METHODS OF STUDY

In order to fully address the above issues, a three-step approach that is different from the method employed for the initial analysis of the S_6 profile was implemented. Previous interpretations of the line employed line drawings that were based on visually correlating a large number of adjacent seismic traces using their characteristic waveforms (Behrendt, 1986). The new approach involves: (1) reprocessing of the S_6 Coastal Plain profile using newer seismic imaging techniques to produce a post-migrated depth-converted section, (2) interpretation of the depth section based on a geologically constrained seismic interpretation, and (3) analysis and correlation of nearby Georgia well data with the reprocessed seismic section to substantiate interpretation.

The seismic imaging steps consist of: (1) initial data analysis to understand noise and signal characteristics, and (2) appropriately designed and applied workflows involving key processing steps necessary for signal enhancement relative to the

background noise. The initial data analysis from of the entire 1451 shot gathers, based on frequency and amplitude discrimination between noise and signal, reveal a dominant presence of anomalously high amplitude, and low frequency spikes in the data (Figures 1.2 and 1.3). These spikes are attenuated by applying a low cut, high pass filter (Figure 1.3). There are also low frequency groundroll and seismic reverberations (Figures 1.2 to 1.5). The observed noise ranges from coherent to random and it varies both spatially and temporally. Consequently, it is important to apply the correct filter which takes into consideration the space and time variations (Figures 1.2 to 1.4) and such that no harm is done to the data. The S_6 data has a bandwidth of 5-90 Hz and the dominant frequencies range between 10 and 60Hz.

The seismic processing and imaging steps (Table 1.2) were designed based on the data needs vis-à-vis an understanding of the characteristics of the signal and noise from the initial data analysis. The goal is to produce a reliable image of the subsurface geology. These processing steps (Table 1.2) are: vibroseis correlation, geometry assignment, trace editing, elevation statics, true amplitude recovery, deconvolution, residual statics correction, velocity analysis and Normal Move Out (NMO) correction, common mid-point stacking, post-stack enhancement, post-stack time migration and depth conversion to yield a good quality image suitable for stratigraphic interpretation and subsequent correlation with well data. Proper assignment of the 2D land geometry is a critical aspect of these processing steps, and is a part of the reason for reprocessing. This must be done correctly to ensure the best possible imaging of desirable reflectors for reliable interpretations. The reliability of other critical tasks such as velocity analysis

and stacking depends on the accuracy of the 2D source-receiver geometry. The ProMAX 2D land geometry tool was used to assign the correct source and receiver information (such as source and receiver stations as well as their x and y coordinates) obtained from observer records during field acquisition.

Vibroseis correlation enables the zero phase correlation of the field data with the vibroseis's sweep signal to produce a correlated data that looks like a conventional seismic record from an impulsive source. Trace editing helps to identify and attenuate high amplitude, low frequency spiky traces and noise bursts as well as muting unwanted refracted arrivals. Elevation statics corrects traces to the final or a common datum. Loss of amplitudes due to attenuation and wavefront spreading is compensated for with the true amplitude recovery. The pre-stack band pass filter helps to condition the data set within the desirable frequencies and at the same time attenuate any undesirable frequencies not accounted for during trace editing.

Deconvolution was applied to improve data resolution as well as to remove the effects of the noise caused by the convolution of the source signal and the earth's reflectivity. Residual statics corrects for irregularities in source and receiver elevations not account for during geometry and elevation statics. Reliable velocities for normal moveout correction, stacking and post-stack migration are obtained from velocity analysis. NMO corrects for the hyperbolic moveout caused by differences in reflection arrival time between zero and non-zero offsets. For long offsets, non-hyperbolic

moveout may occur and this can be corrected using long offset and anisotropy corrections (Al-Chalabi, 1973; Castle, 1994).

Following NMO correction, the data is stacked using velocities obtained from velocity analysis. Stacking is the summation of signals or traces from the same common midpoint. It helps to remove random noise thus boosting the overall signal to noise ratio. Prior to stacking, the data must be sorted from the shot domain to the Common Midpoint (CMP) domain and this is done before NMO correction. A post-stack enhancement involving the application of Frequency-Distance (F-X) deconvolution was carried out to aid the removal of residual random noise. Post-stack migration helps to reposition events on the seismic data to the supposedly true locations both spatially and temporally. Migration implementation was based on the finite-difference technique (Claerbout and Doherty, 1972). The time-migrated section was converted to depth using the interval velocities from velocity analysis.

All preprocessing, processing and postprocessing steps including parameter testing and quality control were executed using the ProMAX 2-D seismic processing and analysis software. Additional information concerning the underlying physics and applications of these processing techniques can be found in Sheriff and Geldart, 1983, and Yilmaz (2001). The reprocessed S_6 coastal plain seismic-depth section is shown in Figure 1.6. Interpretation is focused on the upper 2000 m because (1) that section contains the information needed for delineation of the target subsurface reflectors and

(2) the seismic data acquisition design does not provide significant penetration below the upper 2 s (Behrendt, 1986).

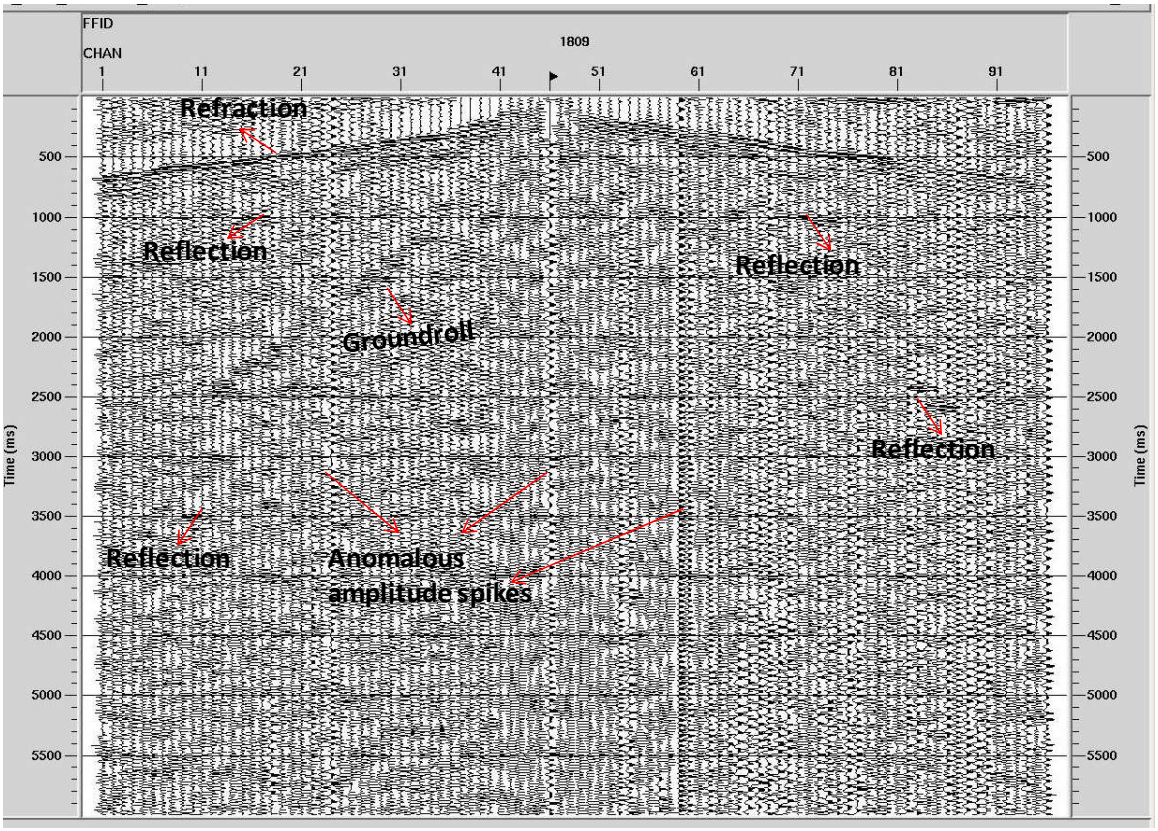

Figure 1.2: Shot gather with field file identification number 1809 before low cut, high pass filter. The main seismic events such as primary reflections, and the high amplitude, low frequency spiky traces and groundroll stand out.

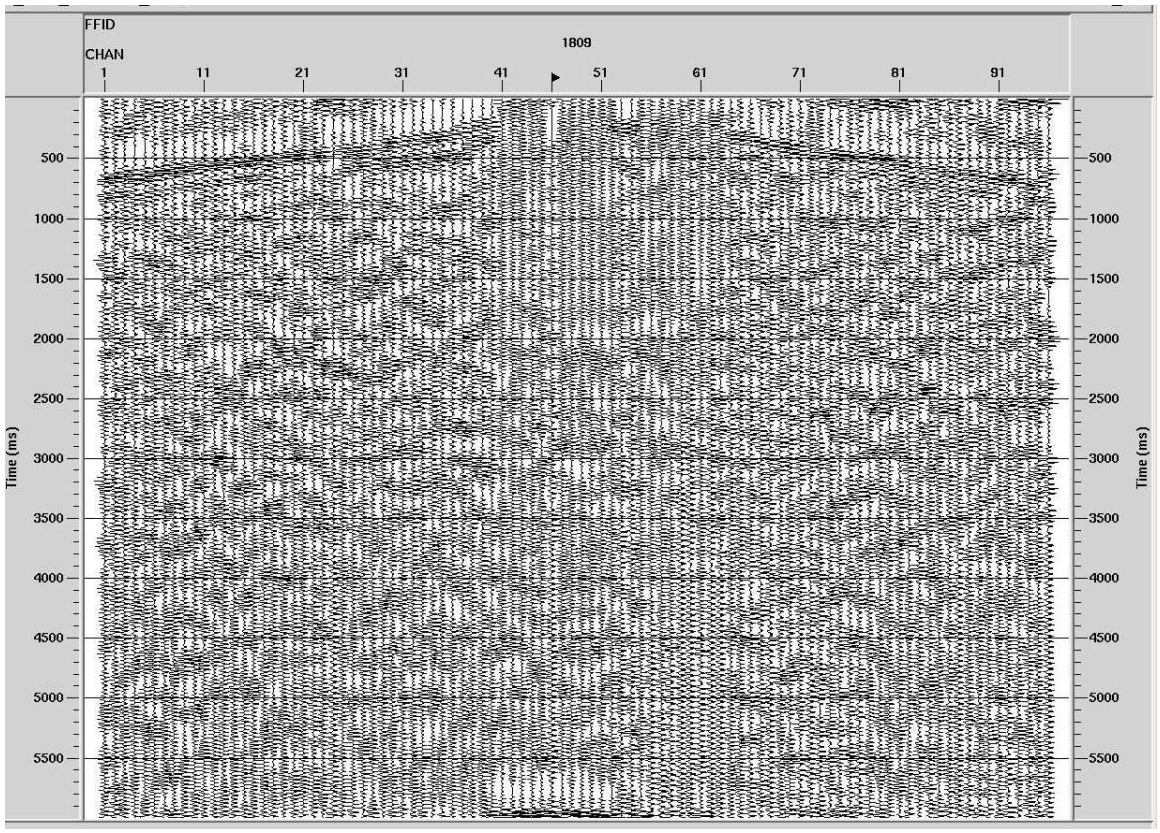

Figure 1.3: Shot gather 1809 after low cut, high pass filter. The low cut filter helps to attenuate the high amplitude and low frequency noise.

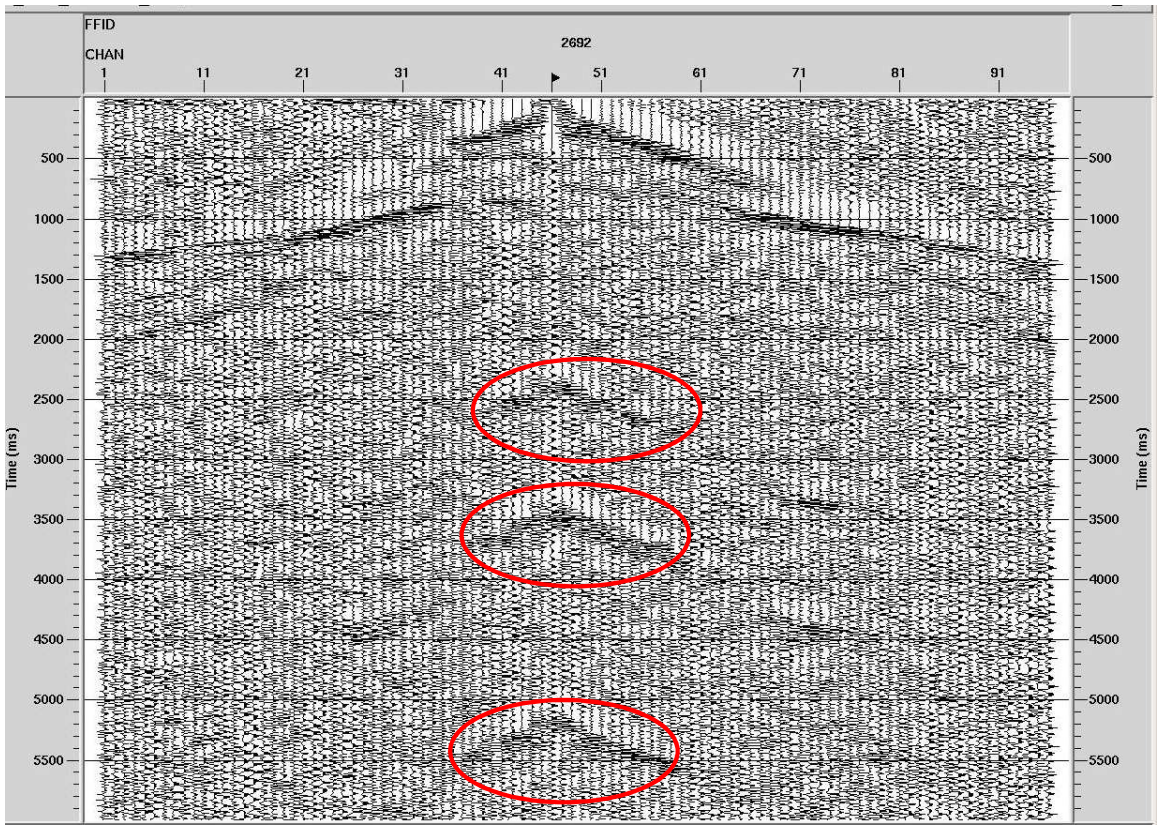

Figure 1.4: Shot gather 2692 showing seismic reverberations (in red circles)

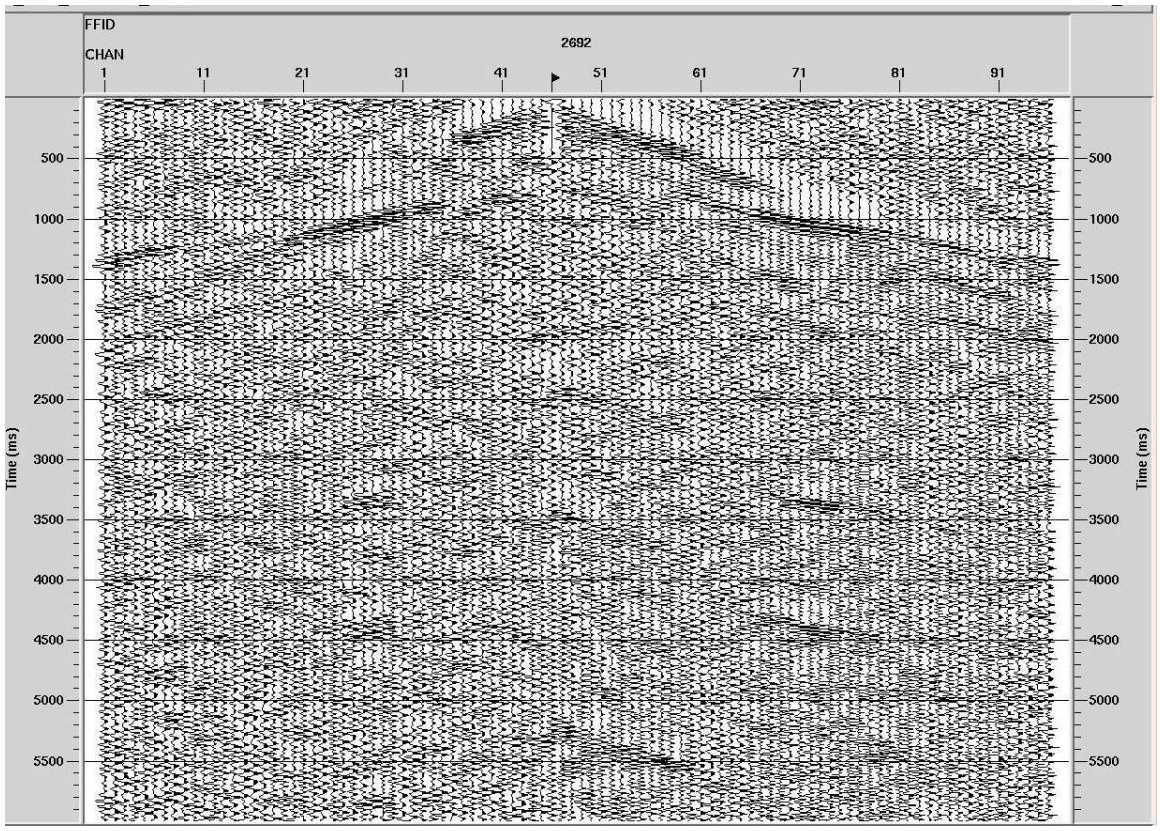

Figure 1.5: Shot gather 2692 after removing the seismic reverberations.

Table 1.2: Key Seismic Processing and Imaging Steps

S/N	Seismic Processing Sequence	Key Parameters/Applications
1	Vibroseis correlation	Very first input trace; sweep and output lengths: 18s, 6s
2	Geometry assignment	Straight line based on appropriate source-receiver values
3	Trace editing	Removal of noisy/bad traces
4	Elevation statics	5000 m/s velocity
5	True amplitude recovery	Spherical divergence and attenuation corrections
6	Band pass filter	8-10-80-90 Hz
7	Deconvolution	Spiking deconvolution with operator length, 4ms
8	Residual statics	External model cross correlation and sum autostatics
9	Velocity analysis	Semblance, gather, and velocity function stack panels
10	Normal moveout correction	Stacking velocity derived from velocity analysis
11	Stacking	Common depth point stack using stacking velocity
12	Post stack enhancement	F-X deconvolution and two-dimensional spatial filtering
13	Post stack migration	Fine difference time migration
14	Time/depth conversion	Interval velocity derived from normal moveout-corrected velocity

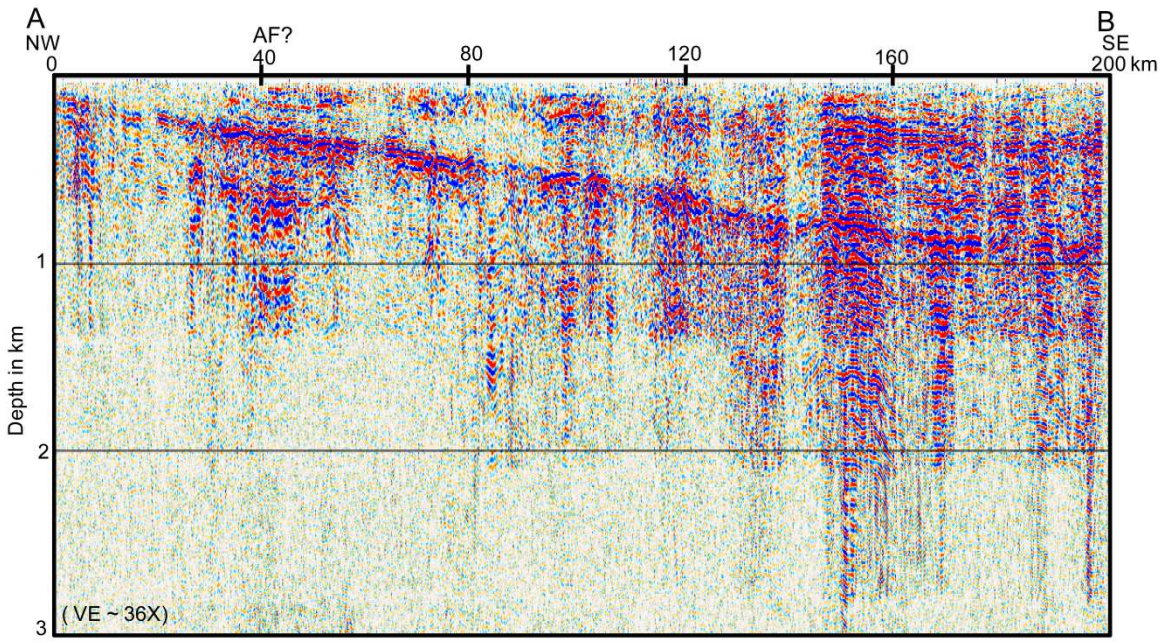

Figure 1.6: Reprocessed SEISData6 coastal plain seismic section showing the high-amplitude northwest-southeast-dipping reflector AB previously interpreted as the J horizon (Behrendt, 1986; McBride et al., 1989). AF indicates the projected intersection of the Augusta fault with the S_6 coastal plain seismic profile based on Behrendt (1986). VE stands for vertical exaggeration. The seismic time section was converted to depth using interval velocities derived from the stacking velocities.

1.5. RESULTS AND DISCUSSION

Key observations and analyses of the interpreted depth section (Figure 1.7) in correlation with nearby Georgia well data are discussed in the following section.

Reinterpretation of the Topmost Reflector

The prominent northwest-southeast (NW-SE) reflector “AB”, which is dipping southeast (Figure 1.6) shows seismic characteristics that resemble what was previously interpreted as the “J” horizon (Behrendt, 1986). Previous interpretation of the occurrence or presence of the “J” horizon is based on the premise that it occurs as a

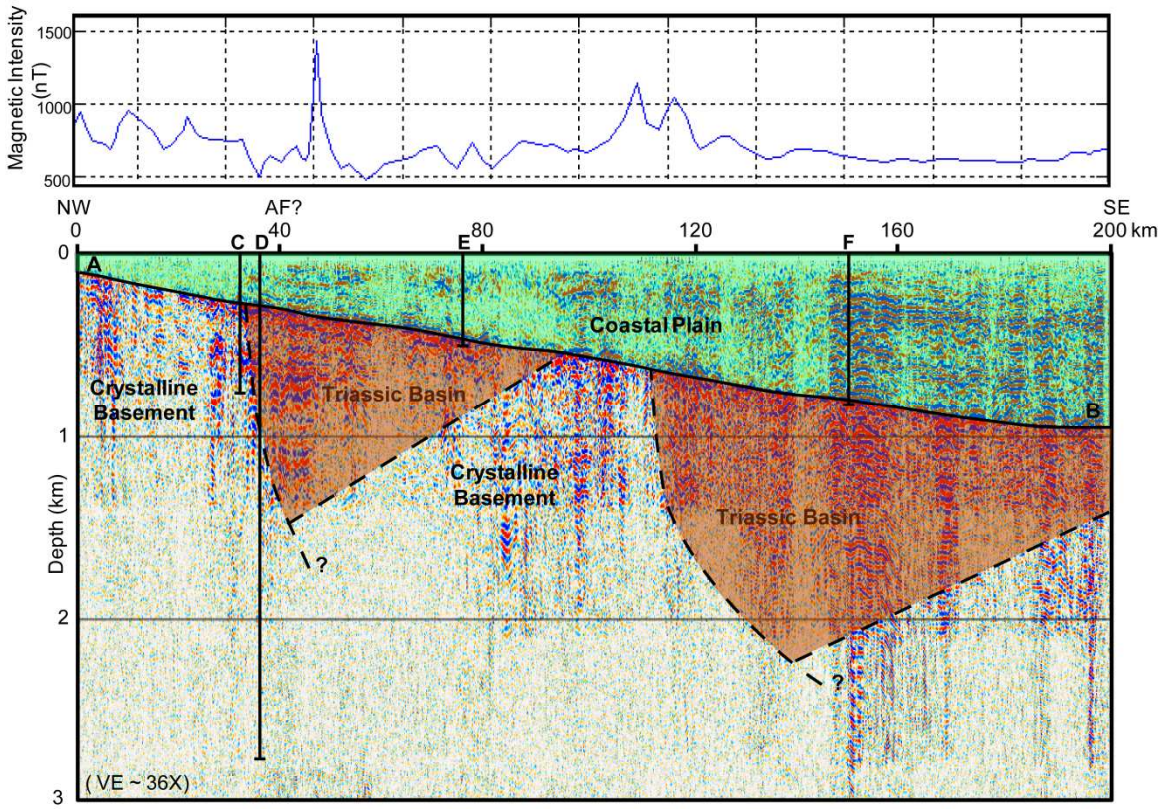

Figure 1.7: Interpreted SEISData6 coastal plain seismic section showing the delineated Triassic basins (orange) below the Cretaceous coastal plain sediments (green). Four nearby Georgia wells with penetrations of non-volcanic rocks directly below the coastal plain are shown as C (GA 3439; total depth, 800 m), D (GA 3447; total depth, 2867 m), E (GA 32Yo20; total depth, 422 m), and F (GA 855, total depth, 816 m). Correlation of the seismic data with these wells helped substantiate that the AB reflector is an unconformity at the base of the coastal plain sediments. Basin fault boundaries are shown as curved lines terminating within the crystalline basement. The magnetic profile (on top) was reconstructed from Behrendt (1986) based on a compilation from the U.S. Geological Survey open-file maps of the area (Daniels and Zeitz, 1978). AF = Augusta fault; VE = vertical exaggeration.

reflector where Coastal Plain sediments rest directly on top of a high-velocity basaltic/igneous layer, and so the term Jurassic ("J") reflector (McBride et al., 1989). The "J" reflector received considerable attention in the 1980s as a distinct, regional geologic marker widespread throughout the SGR basin, and that it is either below or at the base

of the Coastal Plain unconformity (Dillon et al., 1983). The term "J" reflector originated from Schilt et al. (1983) based on seismic correlations with the Clubhouse Crossroads basalt flows (Figure 1.1) from three drill cores in the southern region of South Carolina (Behrendt et al., 1983; Gohn et al., 1983; Gottfried et al., 1983; Hamilton et al., 1983; and Schilt et al., 1983). The age of the "J" basalt as determined by Lanphere (1983) on the Clubhouse Crossroads Basalt is early Middle Jurassic (184 Ma). Its emplacement resulted from the effects of pronounced igneous activity that has been associated with the formation of the SGR basin and the onset of sea floor spreading associated with continental margins formation (Holbrook and Kelemen, 1993). It is known to be chemically similar to the Central Atlantic Magmatic Province (CAMP) basalt flows and to be associated with offshore basalt described seismically as "seaward-dipping reflectors (SDRs)" (Holbrook and Kelemen, 1993; Goldberg et al., 2010). These SDRs were emplaced during the early opening of the Atlantic Ocean (Goldberg et al., 2010).

We interpret the high-amplitude horizon (AB) to correspond to the base of the Cretaceous Coastal Plain sediments and transition to the underlying Triassic rocks. This interpretation is corroborated by the characteristics NMO-corrected interval velocities, derived from velocity analysis for both within and at the base of the Coastal Plain strata, ranging from 2,100 m/s to 2,500 m/s. These values are well within the range of Coastal Plain velocities reported in Bonini and Woollard (1960). The interval velocities for the underlying Triassic strata are higher than that of the Coastal Plain but do not exceed 4500 m/s reflecting known seismic velocities for the Triassic sedimentary rocks (McBride et al., 1989).

Our new interpretation of the “J” horizon is substantiated by the analysis of four nearby wells in Georgia (Figures 1.6 and 1.7) which show that this high-amplitude, sub-horizontal reflector is not associated with the pre-Cretaceous basalt reflector but rather corresponds to the base of the Coastal Plain. Popenoe and Zietz (1997) and Snipes et al. (1993) describe the base of the Coastal Plain as a sub-Cretaceous, post-rift unconformity that onlaps the Triassic sedimentary and crystalline metamorphic rocks. We believe that this strong, NW-SE dipping reflector (“AB” in Figure 1.7) results from the acoustic impedance contrast between the overlying poorly consolidated and low-velocity Coastal Plain sediments and the underlying, well consolidated and high velocity Triassic sedimentary and metamorphic rocks below.

The absence of a Pre-Cretaceous basaltic layer directly below the Coastal Plain within the study area is strongly supported by a thorough analysis of three nearby Georgia wells. GA 855 (closest to the SW end of the profile) reaches a total depth of 816 m (2,677 ft) and penetrates Triassic sediments directly below the Coastal Plain at 705 m (Figures 1.7 and 1.8). GA 32Y020 covers a total depth of about 422 m and encounters Triassic sedimentary rocks at around 419.3 m. GA 3447 provides significant penetration of the Triassic sedimentary rocks below the Cretaceous sediments from 336 m to 2,536 m, and metamorphic rocks from 2,537 m to 2,867 m. Furthermore, the GA 3439 well, drilled to a total depth of 800 m, shows that the Coastal Plain sediments are mainly underlain by metamorphic rocks from 335 m to 800 m.

The Buried Triassic Basin

Using the seismic-well correlations, we interpret the series of sub-horizontal reflections below the "AB" reflector to be indicative of the Triassic-basin fill, with thickness varying from 1,000 m to around 2,200m. This buried basin is an extension of the main SGR basin that is thought to be a complex Mesozoic graben (Popenoe and Zietz, 1977; and Daniels et al., 1983) formed during crustal extension associated with the breakup of the supercontinent Pangea and later opening of the Central Atlantic Ocean. McBride et al. (1987) described it as the southernmost and largest of the series of narrow, elongate onshore early Mesozoic basins of the eastern North America. Chowns and Williams (1983) described the SGR to be an extremely large, early Mesozoic basin with an area of approximately 100, 000 km2 and basin-fill thickness of 3,500 m. Studies by McBride et al. (1989) and Petersen et al. (1984) described the SGR as a composite of sub-basins and individual synrift, half-grabens separated by intervening structural highs. It was suggested by Chowns and Williams (1983) and Swanson (1986) that the formation of the Mesozoic SGR basin was probably influenced by the presence or reactivation of zones of basement weakness in the Southern Appalachians. The tectonically induced rifting events also led to pronounced igneous activity within the SGR basin (Dietz and Holden, 1970). This igneous activity was characterized by the presence of basalt flows, emplacement of diabase sills and dikes and large-mafic and ultra-mafic intrusions (Daniels et al., 1983). These igneous rocks have been described by Phillips (1983) as normally magnetized materials, suggesting that they formed during the Late Triassic-Early Jurassic time interval of predominantly normal polarity. Most

radiometric ages for eastern North American Mesozoic basalts and diabase fall within the range of 170 – 200 million years (Phillips, 1983 and Hames et al., 2000) thus supporting an Early Jurassic age.

Absence of basalt on top of the sedimentary strata shows that the southeastern Georgia part of the SGR basin falls outside of the preserved occurrences of the basalt flow within the SGR basin (Heffner et al., 2012). This contradicts previous work that the S6 Coastal Plain profile falls within a region thought to contain pre-Cretaceous basalt flows (Behrendt, 1986, and McBride et al., 1989). Two well-known examples of preserved occurrence of the Jurassic basalt within the SGR basin are found in the Clubhouse Crossroads (CC1, CC2, and CC3) and Dorchester 211 wells (DOR-211) in southern South Carolina (Figure 1.1). The CC1, CC2, and CC3 wells reached total depths of 792 m, 907 m, and 1,152 m and penetrated 42 m, 131 m, and 256 m respectively of basalt (Gohn et al., 1983b). DOR-211 was drilled to a total depth of 632 m and penetrated 32 m thick of basalt (Reid et al., 1986).

Our interpretation is consistent with the known subsurface geology of the buried Triassic basin under the Savannah River National Laboratory, South Carolina. This sub-basin is about 40 km from S_6 (Marine and Siple, 1974, and Domoracki, 1995). Studies by Marine and Siple (1974) show that there is no basalt on top of this Triassic basin and that the basin-fill consists predominantly of mudstone, poorly sorted sandstone, and poorly sorted fanglomerate present near the basin margin. The absence of basalt could be due to the effects of uplift and considerable erosion during Late Jurassic-Early

Cretaceous. Erosion might have also led to the removal of some parts of the Triassic sediments (Marine and Siple, 1974) and exposure of the metamorphosed crystalline basement as seen in the northwestern part of the profile.

Structurally, the delineated buried Triassic basin may be fault-bounded and characterized by asymmetric half-graben features based on the inferred or probable fault boundaries between the Triassic basin sedimentary rocks and crystalline basement rocks (Figure 1.7). The reflection discontinuities towards the end of the southeastern parts of the profile suggest presence of faults resembling graben-like features. Presence of grabens and half-grabens are not uncommon in many of the fault-bounded sub-basins within the SGR basin (Talwani, 1977, Ackerman, 1983, Hamilton et al., 1983, Schilt et al., 1983, Petersen et al., 1984 and Ratcliffe et al., 1986). Ratcliffe et al. (1986) and Swanson (1986) show that these basin-bounding normal faults were formed during the Paleozoic orogeny and reactivated during the Mesozoic extension. Behrendt (1986) reported the possibility of reactivation of these Triassic normal faults as reverse faults in Late Cretaceous and Cenozoic. Though the focus of our interpretation is on the buried basin, the observed seismic discontinuities also extend to the Coastal Plain suggesting the likelihood of presence of faults that may have been reactivated during Cretaceous and early Cenozoic. The lack of reflections in the lower part of the imaged profile (Figures 1.6 and 1.7) is probably indicative of the presence of crystalline basement complex rock of pre-Mesozoic age.

Relationship with Riddleville and Dunbarton Basins

The Riddleville basin of east central Georgia and the Dunbarton basin in the Central Savannah River area of South Carolina ((Domoracki, 1995) are two identified buried Triassic basins (Siple, 1967, Daniels et al., 1983; Marine 1974, Marine and Siple 1974, and Petersen et al., 1984) that are subsidiaries of the main SGR basin. Both are within proximity to the SeisData6 Coastal Plain profile. Daniels and Zietz (1978) discovered the Riddleville basin on the basis of its low magnetic signature, and this was later confirmed by wells in the area of the magnetic low susceptibility (according to Daniels et al., 1983). In addition, Piedmont crystalline rocks have been recovered from wells on the north side of the basin (Daniels and Zietz, 1978). Red beds recovered beneath the Cretaceous in deep coreholes that are characterized by a magnetic low led to the discovery of the Dunbarton basin (Siple, 1967). Like the Riddleville basin, the Dunbarton basin is reported to be enclosed by a subcrop of crystalline rocks (Marine, 1974). Petersen et al. (1984) pointed out that the formation of both basins appears to be controlled by pre-existing structures. The Riddleville basin is described as a half-graben formed along a south east dipping listric border fault, while the Dunbarton basin has been described as an asymmetric graben with possible normal faults on both its northwest and southeast sides. Petersen et al. (1984) suggested a similar structural relationship.

The observed sub-horizontal Triassic reflectors below the prominent reflector “AB” are possible indicators of the subsurface extensions of the east-west trending

Riddleville and Dunbarton Triassic basins. Behrendt (1986) had implied the possible crossing of the Riddleville basin by S_6 Coastal Plain profile towards the south-east end of the line. Daniels et al. (1983) linked the Riddleville basin with the Dunbarton Triassic basin in southern South Carolina and noted that both are two interconnected basins separated from the main rift by a broad horst of crystalline basement. Aided by the seismic-well correlations, we observed magnetic lows within parts of the basin penetrated by Triassic sedimentary red beds (Figure 1.7). The very high magnetic intensity observed towards the northeastern part of the basin may be caused by the presence of a buried, highly magnetic body/intrusion within the near-surface rocks or the edge of the basin. The corresponding gravity is generally low with a value of -10 mgals (Behrendt, 1986). It increases to about 5 mgals and then decreases to -10 mgals towards the edge of the basin (Behrendt, 1986). The observed gravity low and the corresponding high magnetic intensity suggest the source of the anomaly could also be due to presence of an isolated, mafic intrusion and/or a dike within the crystalline metamorphic rocks. Both Dunbarton and Riddleville basins are reported to be enclosed by crystalline metamorphic rocks (Chowns and Williams, 1983). The estimated basin-fill thickness of between 1 and 2.2 km is in agreement with the known thicknesses of basin-fill for both the Dunbarton and Riddleville basins (Chowns and Williams, 1983). Seismically, there appears to be a slight difference in the nature of the sub-horizontal Triassic reflections from GA 3447 towards the south east end of the basin. It is possible that this could be due to S_6 line penetration of both the Riddleville and Dunbarton basins. The basins are related, but differ in the degree of composition of basin-fill. The

presence of subsurface heterogeneities even within similar lithologies can cause changes in the seismic response. Based on the seismic image and magnetic characteristics, lithologic similarity and the strategic location of S_6 Coastal Plain profile (in between Riddleville and Dunbarton basins as shown in Figure 1.1), the delineated Triassic basin appear to be the subsurface convergence of the southwest and northeast extensions of the Riddleville and Dunbarton basins. Consequently, we refer to the buried basin imaged by the S_6 Coastal Plain seismic profile the Ridlleville-Dunbarton Triassic basin.

No indication of Augusta Fault

The Augusta fault has been described as a major, low-angle, extensional normal fault that originated during the Alleghanian extension and appears to dip toward the southeast (Maher, 1987). The Augusta fault was identified approximately at the Piedmont-Coastal Plain boundary in Georgia and South Carolina and is exposed near the city of Augusta, Georgia. Hatcher et al. (1977) had previously interpreted the Augusta fault to be a major crustal structure, separating older greenschist facies rocks of the southern Augusta terrane (previously referred to as Belair belt) in the hanging wall from younger amphibolites facies rocks of the northern Savannah River terrane (previously referred to as Kiokee belt) in the footwall (Maher, 1987, Maher et al., 1994).

Analysis of seismic reflection data by Cook et al. (1981) and Petersen et al. (1984) indicated that the Augusta fault extends to at least mid-crustal levels and that it is probably associated with the development of the Mesozoic-age rift basins beneath the

Coastal Plain. Interpretation of this fault by Cook et al. (1981) was based on identification of a series of numerous seismic reflections that suggest a southeasterly dip of 10 degrees on what was interpreted to be the Augusta fault. However, as pointed out by Iverson and Smithson (1983), this trend of southeast-dipping reflections is nearly 20 km wide, whereas the Augusta mylonite zone appears to be less than 1 km wide. A near absence of reflections within 25 km of the Augusta fault was also reported in Iverson and Smithson (1983). Bramlett et al. (1982) submitted that the Augusta fault must flatten at depth (about 2 km) in order to correspond to events identified by Cook et al. (1981) as Augusta fault reflections. Given these diverging views in the interpretations of the Augusta fault, it is unclear and very unlikely if the observed near absence of reflections around point A in close proximity to GA wells 3439 and 3447 (Figures 1.6 and 1.7) can be associated with the subsurface projection of the Augusta fault. Behrendt (1986) had implied a possible intersection of the Augusta fault by the S_6 Coastal Plain seismic profile towards the northwest end of the line (marked AF as shown in Figure 1.6). We attribute this observed near absence of reflections and/or change in the reflection character to two possibilities: (1) the presence of non-reflective metamorphic rocks of the Piedmont Province beneath the Coastal Plain as indicated by the correlation of seismic and well data, (2) the effects of subsurface transition of the Piedmont Province to the Coastal Plain, involving a change in lithology from the metamorphic rocks of the Piedmont Province to the buried Triassic sedimentary rocks. There is no evidence that the Augusta fault extends to beneath the Coastal Plain in the study area.

1.6. REGIONAL IMPLICATIONS

The identified topmost S_6 reflector has been associated with top of basalt flows or diabase sills where previously seen and used to interpret the regional presence of the "J" reflector from several Georgia, COCORP (Consortium for Continental Reflection Profiling) and USGS seismic lines (Dillon et al., 1979; Behrendt et al., 1983; Hamilton et al., 1983; Lamphere, 1983, and Schilt et al., 1983). Contrary to this existing paradigm of the last 25 years, here, we reinterpret this topmost reflector to be the base of the Coastal Plain sediments. Therefore, the long standing hypothesis that this horizon, popularly called the "J" horizon, is mainly associated with a basaltic layer throughout the SGR basin is challenged. This assertion is consistent with a recent analysis of sub-Coastal plain wells and seismic lines (outside of S_6) by Heffner et al. (2012) that show that the "J" horizon is not ubiquitous within the SGR basin. These findings raise a fundamental question regarding the significance of this horizon as a regional geologic marker. The "J" horizon was recognized as a highly conspicuous, high-amplitude and two-cycle reflection that separates the thinner, upper section of the SGR basin from the thicker underlying, Triassic strata and/or Piedmont crystalline rocks (McBride et al., 1987). These characteristics were previously used to interpret the regional presence of the "J" reflector from several Georgia, COCORP and USGS lines (Lamphere, 1983, Schilt et al., 1983, Hamilton et al., 1983; Dillon et al., 1979 and Behrendt et al., 1983).

Furthermore, the true geographical extent of the Pre-Cretaceous basalt has remained unknown in spite of previous efforts by Chowns and Williams (1983),

Gottfried et al. (1983) and McBride et al. (1989) to delineate its areal extent. Its postulated regional extent within the SGR basin was based on seismic correlations with limited and scattered drill-hole data. Consequently, an understanding of its geographical extent is important if it were to serve as an effective, regional seal for CO_2 storage. Based on the results of this study and the additional well controls presented in Heffner et al. (2012), the basalt distribution on a regional, basin scale appears to be mostly concentrated within the square shown in Figure 1.1. This covers the Clubhouse Crossroad (CC) and Dorchester (DOR) 211 wells. Consequently, we estimate its onshore areal extent to be about 2,700 km^2 to 2,800 km^2.

The absence of basalt from the study area does not preclude subsurface CO_2 storage. Evidence abounds in southern South Carolina for the presence of basalt flows (Clubhouse Crossroads and Dorchester 211 wells) and diabase sills on top of the Triassic red beds (Figures 1.8 and 1.9). The interior of basalt flows, if present within the formations, can serve as additional capping unit to CO_2-red beds reservoir capped by diabase sills. Diabase sills and basalt (especially the interior of flows) do exhibit low porosity and permeability that favor caprock integrity (Akintunde et al., 2011). In addition, the sills can form important confining units if these occur in multiple units both below and on top of the sedimentary unit. An excellent example of this is seen in the Norris Lightsey #1 well. The Norris Lightsey #1 well is located about 80 km from the S_6 profile and 55 km from the Clubhouse Crossroad wells (Figure 1.1). It was a wildcat petroleum exploration well drilled in Northwest Colleton County, South Carolina. It was drilled to a depth of about 4,000 m and encountered over 3,100 m of Triassic sediments.

Regionally, this study has shown that the base of the Coastal Plain in the SGR basin overlies different types of rocks such as Triassic sedimentary rock, volcanic and non-volcanic rocks (Figure 1.9). Adequate characterization of these rocks through additional drilling and seismic studies will be vital to any regional and site-specific exploration studies. Given the association of buried Triassic sub-basins within the SGR basin with half-grabens (Ratcliffe et al., 1986 and Swanson, 1986), the likelihood of faults within the basin could pose a big risk to sequestration, especially if these were active and leaking. A detailed characterization of the leaking or sealing capacity of these probable faults will be necessary as well.

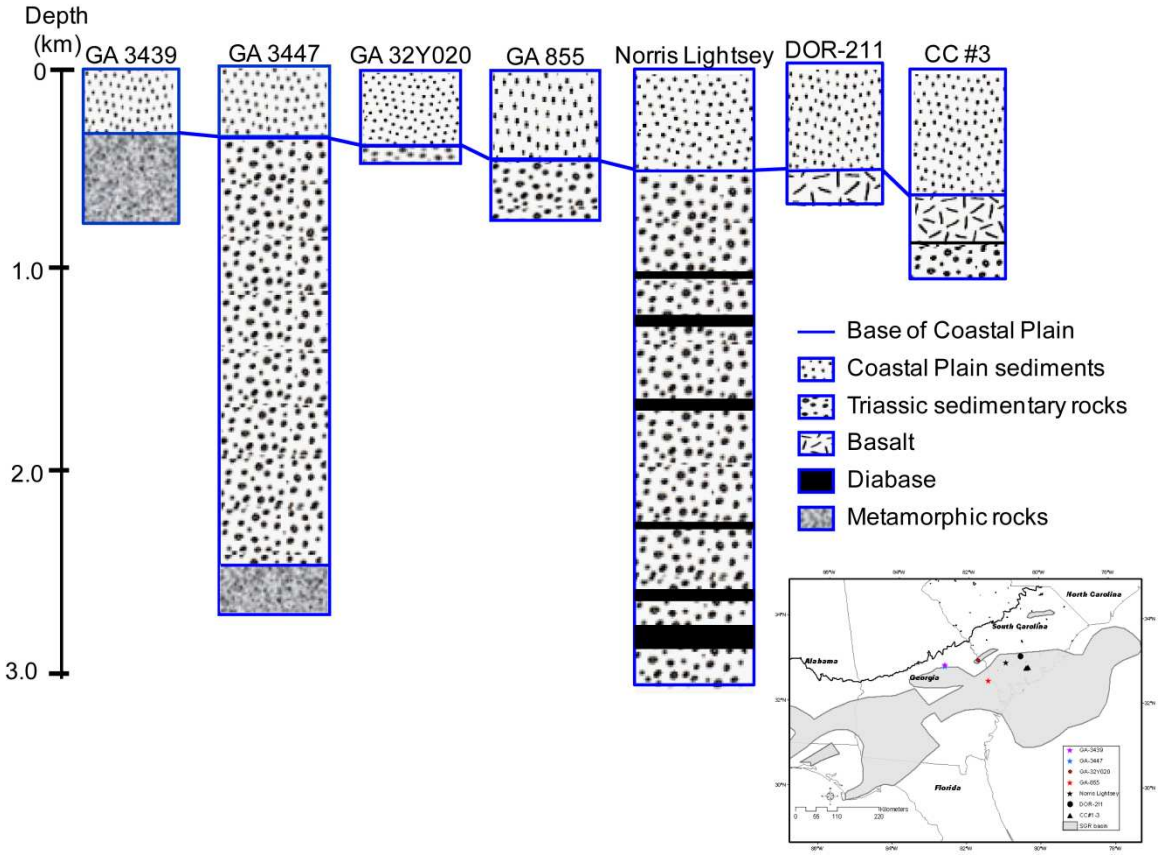

Figure 1.8: Stratigraphy of the buried Triassic-Jurassic South Georgia Rift basin based on information from Georgia (GA) and South Carolina (SC) wells (Akintunde et al., 2013a).

DOR-211 is Dorchester 211 well and CC3#3 is the Clubhouse Crossroads well #3. Notice the absence of basalt and diabase in the GA wells. The location map is shown in the inset.

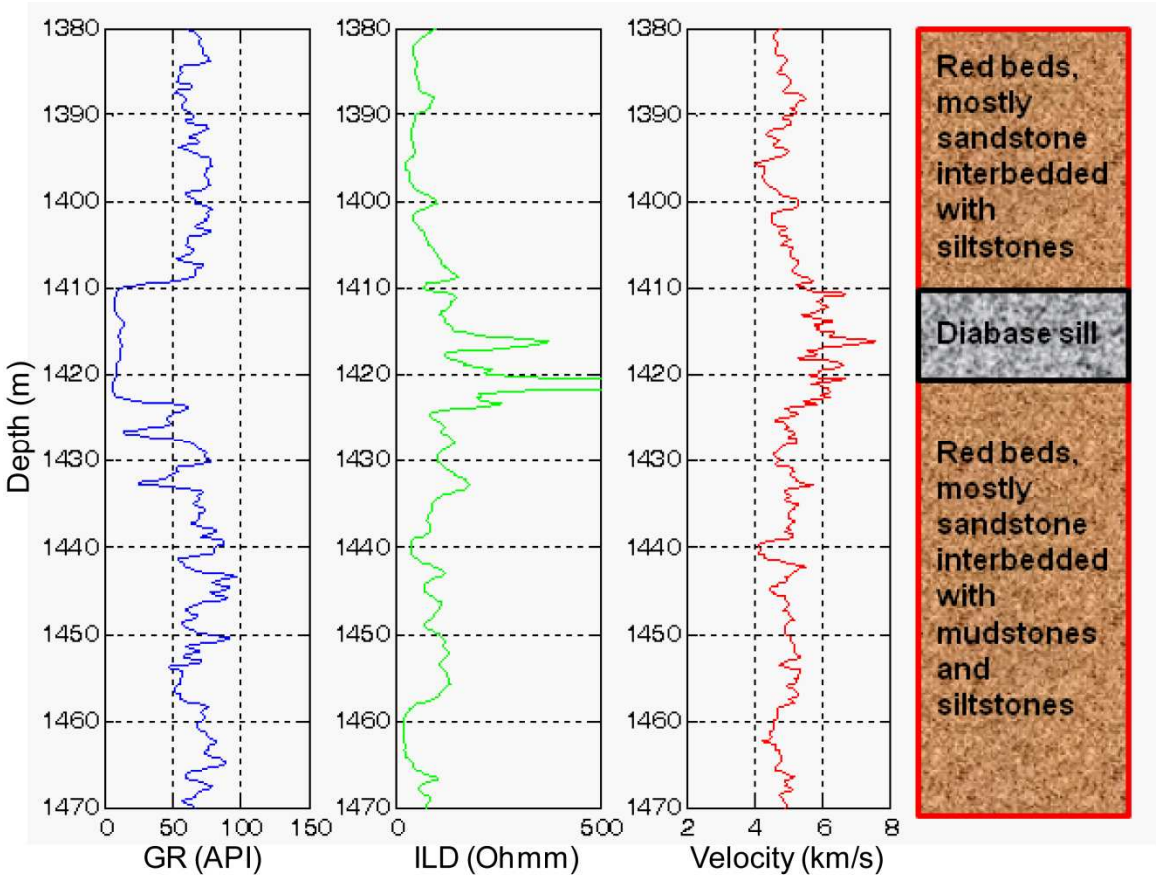

Figure 1.9: A depth section from the Norris Lightsey well in South Carolina. The diabase sill is easily delineated from the underlying Triassic unit by its low gamma ray (GR), high resistivity (deep induction resistivity log, ILD, in ohm-meter), and high velocity (sonic log in kilometers per second).

1.7. Conclusions

The purpose of this research involving Reprocessing and reinterpretation of the USGS SEISData6 reflection seismic profile across the Coastal Plain of Southeastern Georgia was to delineate basin-scale geologic features of interest to the ongoing site

characterization studies for CO_2 storage within the SGR basin. The SGR basin is a composite of sub-basins covering Jurassic-Triassic rocks that are buried below the Cretaceous and Cenozoic Coastal Plain sediments in parts of South Carolina, Georgia, Alabama and Florida. A key, significant discovery from the analysis of the newly imaged S6 seismic line is the substantiation of the presence of a buried Triassic basin inferred to be the subsurface convergence of the previously named Riddleville and Dunbarton basins in Georgia and South Carolina, herein named the Riddleville-Dunbarton basin. A prominent topmost reflector, which we reinterpreted to be the base of the Coastal Plain sediments, separates this basin from the overlying Coastal Plain sediments.

Our seismic analysis further shows that this basin is characterized by distinctively higher seismic velocities relative to the overlying Coastal Plain and manifests a series of sub-horizontal reflectors below the topmost reflector. This reflector, popularly referred to as the "J" basalt reflector, was previously interpreted to correspond to the top of a basalt layer. Based on our interpretation, no basalt was encountered on S6 contrary to previous analyses. Compositionally, the basin fill is mostly sedimentary rocks though juxtaposed in the north east by Piedmont metamorphic rocks. Our new seismic imaging results corroborated by interpretation from nearby Georgia well data suggest that no-pre-Cretaceous rocks are present above the delineated Triassic basin. The lack of Jurassic-age basalt from the study area implies uplift or subsidence, erosion, and possible effects of fault reactivation. It also strengthens the recent findings of a recent study of wells and seismic data (outside of S_6 regional profile) by Heffner et al. (2012) that emphasize the restrictive distribution of basalt within the main SGR basin.

Regionally, our new results show that the base of the Coastal Plain in the study area, and by extension, the SGR basin, overlies different types of rocks that include Triassic sedimentary strata and other non-volcanic rocks. Consequently, we believe that, for the purpose of CO_2 sequestration studies within the SGR basin, attention should be paid to areas that are within the restrictive distribution of basalt and/or diabase sills that (where present with the required geographical extent) could serve as potential caprocks to the underlying, confined Triassic sedimentary rocks. In addition, the potential for the occurrence of faults, which can be either sealing or leaking, would need to be properly evaluated, both locally and regionally within the SGR basin, given the inferred presence of half-grabens in parts of the basin.

CHAPTER 2

PETROPHYSICAL CHARACTERIZATION OF THE SOUTH GEORGIA RIFT BASIN FOR SUPERCRITICAL CO_2 STORAGE

2.1. OVERVIEW

A key consideration for CO_2 sequestration site selection is the ability to demonstrate the presence of a porous reservoir with adequate storage capacity. In addition, subsurface suitability for CO_2 storage will depend on reservoir injectivity and seal integrity that are both closely related to rock properties such as porosity and permeability. Also unlike shale-capped CO_2 reservoirs, very little is known about the ability of basalts and/or diabase sills to act as viable seals for CO_2 storage. Therefore, with this study, we designed and carried out a series of physics-based laboratory experiments on selected samples considered strategic to the goal of unraveling the key rock attributes necessary to study feasibility for CO_2 storage. Experiments involved porosity, permeability and acoustic velocity measurements on samples from four sites within the basin: Sumter, Berkeley, Dorchester-211 and Clubhouse Crossroads. These were supplemented with existing laboratory data from Dunbarton and Norris Lightsey wells and data with penetrations of these target rocks. Interpretations and analyses of experimental data were aided with lithologic and thin sections descriptions of cores, X-ray diffraction (XRD) data and X-ray Computed Tomographic (CT) images.

The new results show that the SGR basin has confined porous rocks that may be capable of storing significant quantities of CO_2. Reservoir thicknesses as high as 420 m and an average porosity as high 14% were obtained. Results also show that the SGR basin manifests distinct porosity-permeability regimes that are influenced by the depositional environments. These are: (1) high-porosity, low/medium permeability zone; (2) medium/low porosity, low permeability zone; (3) low porosity, low permeability zone, and, extremely low porosity and low permeability zone. The high-porosity, low/medium permeability zone is associated with lacustrine deposits and consists of fine-grained Triassic sandstones with interbedded layers of siltstone and mudstone. The medium/low porosity, low permeability zone is dominated by fluvial fine-to very fine-grained sandstone, while the extremely low porosity and permeability zone are characterized by fluvial and alluvial-fan deposits.

Furthermore, the presence of low permeability red beds is a prominent occurrence within the SGR basin. This characteristic, which is substantiated by physical examination of cores and analysis of thin section, is caused by poor sorting and small pore throats. Also, our analysis supported by high resolution X-ray Computed Tomographic images shows that the basalt flows and diabase sills possess physical properties (high seismic velocities and densities and low porosity), petrophysical characteristics and micro structural properties consistent with sealing requirements and favorable to caprock integrity. However, rock mechanics/geomechanical tests as well as seismic characterization of these target seals will be necessary to further determine caprock integrity and continuity.

2.2. Introduction and Motivation

The occurrence of deep saline sandstone formations (popularly called red beds) that are capped by mafic igneous rocks such as basalt flows and/or diabase sills motivates the interest to conduct a petrophysical study to help unravel key attributes of rocks that are important not only for the purpose of CO_2 storage within the Triassic-Jurassic SGR basin but also to provide new understanding into the evolution of the Triassic-basin fill. The focus of this petrophysical study is on locations within southern South Carolina (Figure 2.1) where geologic evidence abounds for potential Triassic-Jurassic formations (Gohn et al., 1983b; Gohn, 1983; Smyth, 2007; Goldberg et al., 2010) that are worth evaluating for storage capacity, reservoir quality and injectivity as well as seal viability for the purpose of subsurface CO_2 storage (Table 2.1). According to the Carbon Sequestration Atlas of the United States and Canada, there is a high concentration of carbon sources located over the SGR Basin. The proximity of carbon sources to promising CO_2 geologic storage formations adds to the relevance of this investigation. If the Triassic/Jurassic saline formations within the SGR Basin prove to be a suitable carbon storage option, then the co-location with substantial carbon sources makes carbon sequestration very attractive.

Of critical importance to these characteristics (Table 2.1) are the need to understand the local and regional distribution of porosity and permeability, and how these reservoir properties may be impacted by depositional environments. Results of analysis of experimental data and petrophysical interpretation of well logs carried out to

evaluate these properties and their potential implications for supercritical CO_2 storage are presented.

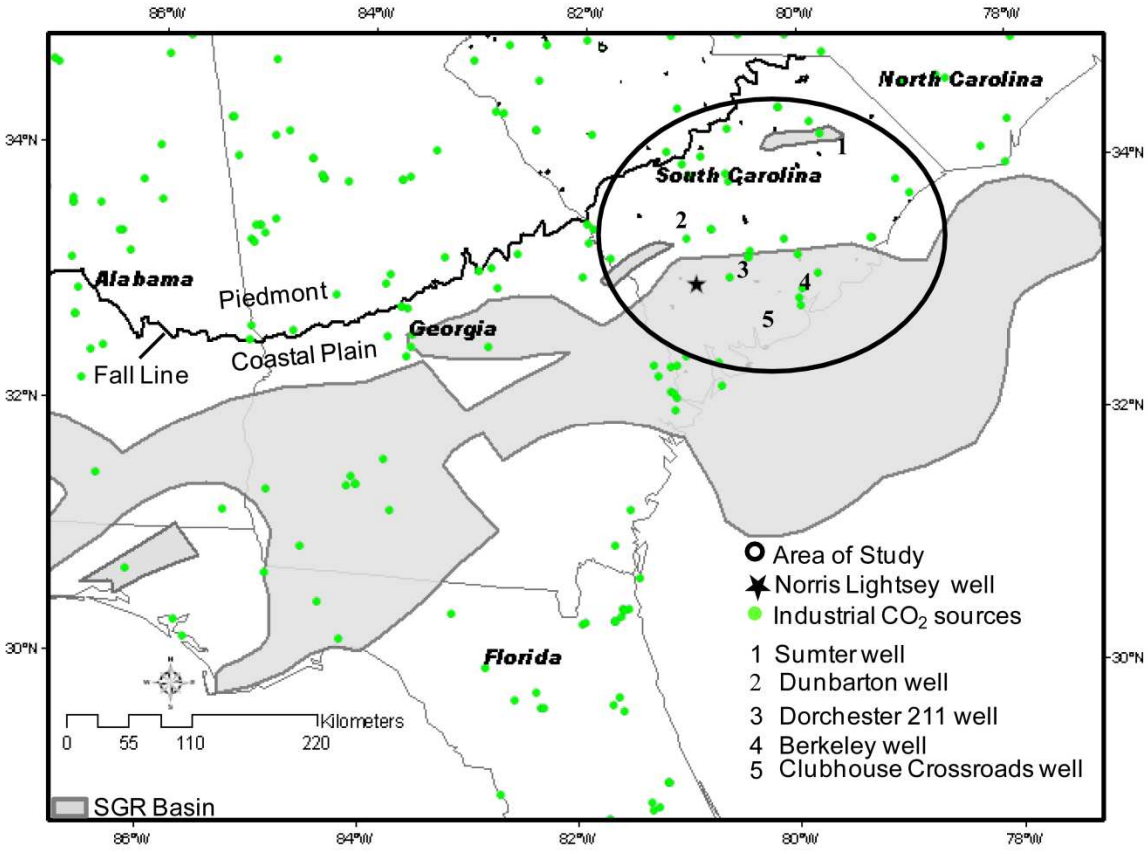

Figure 2.1: Map (modified from McBride et al., 1989) showing locations of the samples for petrophysical study. The study locations are within the South Georgia Rift basin.

Table 2.1: Critical rock properties for subsurface CO_2 storage

CO_2 Storage Requirements	Critical Rock Properties/Characteristics
A reservoir with adequate storage capacity	Porosity, permeability, reservoir thickness
Reservoir injectivity/unrestricted fluid flow	Porosity, permeability, reservoir thickness
Trapping mechanism to ensure containment of CO_2	An overlying caprock or seal
Seal integrity and viability	Porosity, permeability and thickness
Knowledge of the physics of CO_2-rock interactions for the purpose of subsurface monitoring	Porosity, density

2.3. WHY SUPERCRITICAL CO_2 STORAGE?

At depth below 800 m, CO_2 injected into the subsurface under normal geothermal conditions with near hydrostatic pressures will exist in supercritical state (Burruss et al., 2009). In this state, CO_2 has gas-like compressibility, viscosity, and surface tension with liquid-like densities. The consequence of this is that CO_2 can flow more easily within the confined reservoir and more storage per unit volume can be achieved. Also, supercritical CO_2 is immiscible and soluble in water (Koide et al., 1993). The CO_2, due to its buoyancy, will typically move up-dip in geologic formations, and tend to accumulate in traps enclosed by a seal. On a short-term, the stored CO_2 can be trapped by structural or stratigraphic seals as observed in hydrocarbon accumulations. Also, the dissolved and immiscible CO_2 can travel within the formation over long residence times in form of hydrodynamic trapping (Bachu et al., 1994). The long-term trapping usually takes the form of solubility and/or mineral trapping (Koide et al., 1993).

2.4. OBJECTIVES

The key, fundamental research question of this study is to determine whether or not the SGR basin is suitable for supercritical CO_2 storage. In order to be considered suitable for CO_2 storage, a geologic repository (for instance a saline aquifer as the case with the SGR) must have enough pore space (porosity) in which to store CO_2, high permeability and trapping mechanism (an overlying caprock or seal) to ensure containment of the CO_2 in the pore space and prevent any vertical migration into overlying freshwater aquifers. In particular, porosity and permeability are critical for evaluating reservoir injectivity and seal integrity for subsurface CO_2 storage. Both

properties are needed to determine the effective CO_2 storage capacity. In addition, the ability to model and understand the physical interactions of the CO_2 reservoir systems under in situ conditions is dependent on the reservoir porosity (Table 2.1). Also, the continuity and integrity of the overlying caprock are important requirements. For this study we are concerned with local and regional understanding of rock properties (porosity and permeability) that are vitally important to the determinations of reservoir quality, storage capacity and injectivity. We are also interested in knowing how these rock properties may have been impacted by depositional and/or post depositional processes. We also want to know if the physical properties, internal composition and micro structure of the target seals are favorable to caprock integrity.

2.5. METHODS

The study approach involves implementation of the following methods and analyses: (1) lithologic analysis of cores and deep wells, (2) petrophysical interpretation of existing well data, (3) laboratory measurements to determine porosity, permeability, density and P-wave velocity, (4) X-ray diffraction analysis and X-ray computed tomographic scans on samples from study locations, and (5) interpretation of thin sections. Analysis of cores based on visual examination of rock samples was carried out to obtain first hand information and insights into type and nature of lithology, mineralogical and textural composition, fabric as well as identification of any structures such as vugs, joints, bedding and fractures within the rock.

This was followed by petrophysical analysis of existing well data to provide evidence for the occurrence of confined porous reservoirs, indicate presence of overlying seals, gain understanding into the spatial, regional distribution of the target reservoirs and seals, as well as yield input (such as porosity and thickness of reservoir units) necessary for storage capacity determination. Although the SGR-CO_2 project currently has information on 252 wells that were previously drilled for ground water and oil exploration (Heffner et al., 2012), the majority of these wells did not recover the target reservoir seals. Besides, most of the wells occur at shallow depths and lack the necessary petrophysical data for porosity determinations. Consequently, this petrophysical analysis has focused on the Norris Lightsey well in southern South Carolina part of the basin (Figure 2.1). This well, based on the analysis of the other wells in the project database, represents the most significant penetrations of the target red bed reservoirs and seals for CO_2 storage.

Additionally, standard measurements of porosity and permeability were carried out on borehole samples from Sumter, Berkeley, Clubhouse Crossroads and Dorchester-211. Measurements were done using the Automated Core Measurement System (CMS-300) which is a product of Core Laboratories Incorporation (Keelan, 1986). It combines porosimeter and permeameter in one instrument to determine porosity and permeability. It also takes into account the Klinkenberg correction (Klinkenberg, 1941). Furthermore, the CMS-300 system has the capability to carry out measurements on up to twelve 1.5 inch diameter samples at up to confining stresses of between 800 and 10,000 psi. However, it only accommodates samples within a permeability range of 0.1

microdarcy to 5 darcies and a pore volume range from 0.02 cc to 25 cc. Our tested samples were made into cylindrical plugs of 1.5 inches diameter and about 2 inches long for the measurements. Porosity is determined from the porosimeter by gas expansion method based on Boyle's law. The sample is pressurized with helium and the pressure is allowed to stabilize. The helium is then expanded into a chamber of accurately known volume and the pressure is allowed to stabilize again. The pore volume is then calculated from the initial and final pressures using Boyle's law. The permeameter consists of a sample holder and pressure gauges on each side and a calibrated orifice from which the fluid flow rate can be determined. It is routinely measured by passing an inert gas like helium or nitrogen through the rock sample. The pressure drop across the sample and the flow rate are measured. From these measurements as well as the length and cross sectional area of the sample, permeability is determined using Darcy's law (Darcy, 1856). For this analysis, measurements of porosity were done at room conditions and permeability at low confining stresses (300 to 900 psi that does not exceed the overburden pressure at the depth from which the sample was taken). Apart from the gas expansion method based on Boyle's law, porosity can be measured from knowledge of the bulk and solid volume and by displacement techniques (Schon, 2011). Indirect techniques such as logging using sonic and density and by correlation between porosity and other rock properties such as density, velocity and stress changes may allow for determinations of porosity. Both porosity and permeability can also be determined from Nuclear Magnetic Resonance (NMR) measurements (Schon, 2011).

The predetermined parameters for porosity are usually the total volume, pore volume, grain volume and weight or mass of the rock sample.

Density for each of the 1.5 inches diameter samples was calculated from knowledge of the diameter, length and mass. Following plugging of samples, the lengths and diameter were re-measured with the Vernier Caliper to ensure accuracy for density determinations (to within plus or minus 0.005). Sample mass was determined from a standard laboratory mass measuring device. In order to ensure accuracy, four measurements of each of these physical quantities were made and the average taken. Density was subsequently calculated from knowledge of the volume and mass of each cylindrical sample.

The new experimental data were supplemented with existing porosity and permeability data from the Dunbarton (Marine and Siple, 1974, Marine, 1974) and Norris Lightsey wells. The Norris Lightsey data were acquired by Core Laboratories Incorporation, Dallas, Texas in 1984, as part of exploration activities for hydrocarbon.

In order to support interpretations of porosity and permeability data on the target sandstone/red beds, petrographic studies of these target samples based on analyses of thin sections were carried out. Thin sections involve rock preparation for analysis with a polarizing petrographic microscope. These are made from a small slab of a rock sample glued to a glass slide, and subsequently ground smooth until the sample is 0.03 mm (30 microns).

Ultrasonic P-wave velocity measurements (under bench top/static/ambient conditions) were carried out on the basalt and diabase samples. These measurements were performed to aid interpretation of porosity and permeability as well as to help make a distinction between basalt flows and diabase sills. Measurements were carried out using the pulse transmission experimental technique (Prasad, 1997, 2002). It consists of a digital oscilloscope and a pulse generator which generates the P-wave signals (Figure 2.2). In the pulse arrival technique, waves (typically at 1 MHZ) are generated using the piezo-ceramic crystals that convert an electrical impulse into mechanical energy. As displayed in Figure 2.3, two piezo-ceramic transducers are coupled to two sides of the sample and a measurement of the time it takes for a wave to travel from one end to the other is taken. The system delay time or trigger (which must be taken into account when calculating velocity from the measured travel times) is determined by taking the head-to-head time. The pulse transmission method of measuring velocity at room conditions can be extended to incorporate the effects of anisotropy, fluid saturations, and stress changes under low and high frequencies on (Biot 1956a, b; King, 1966, Nur and Simmons, 1969, and, Prasad, 2002). This work represents and presents the first core-scaled ultrasonic laboratory study on the SGR's mafic igneous rocks such as basalt flows and diabase sills.

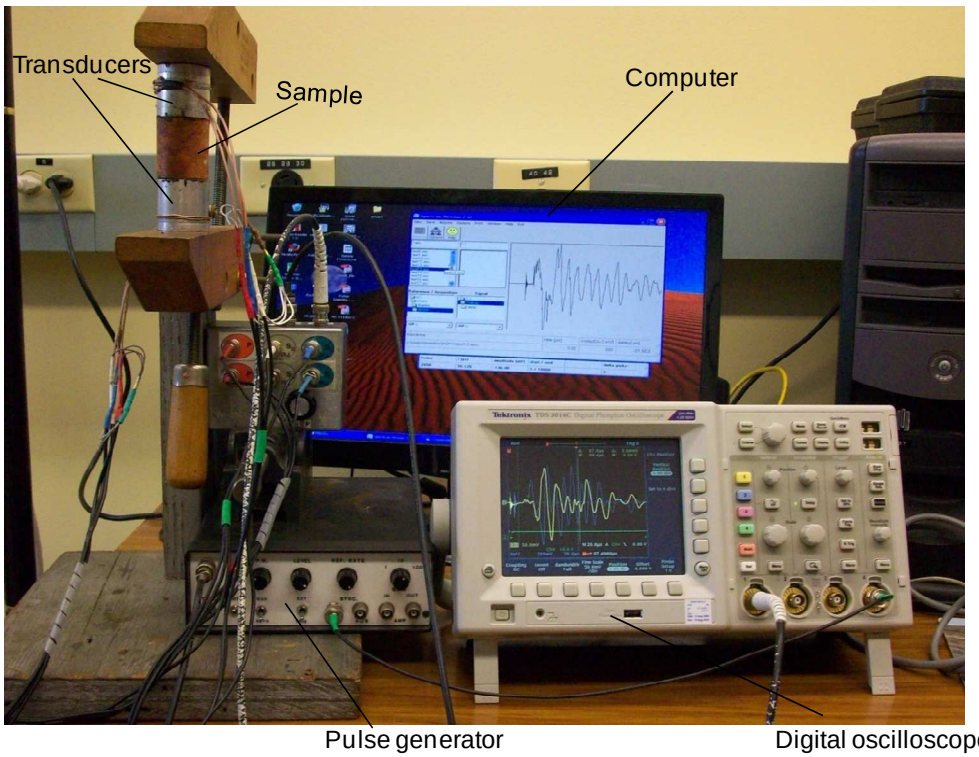

Figure 2.2: Laboratory setup for ultrasonic velocity measurements. Facilities provided by the Rock Physics Laboratory at the Petroleum Engineering Department at the Colorado School of Mines, Golden, CO).

In addition, X-Ray Diffraction (XRD) analysis on sandstone/red beds samples was carried out to enable identification and quantification of bulk and clay minerals and other components that may appear too small to be identified in thin-section. This was also done in order to have insights into the degree of elemental compositional and textural maturity of the sandstone samples. A small portion of the sample was ground to about 400 mesh in a steel swing mill, packed into a well-type holder and then scanned with the diffractometer over the range 3 to 61 degrees. The ground samples were also prepared as oriented mounts by mixing ground sample with distilled water, drawing the mixture onto a cellulose acetate filter and then rolling the deposited

material onto a glass disk. The oriented mounts were scanned over the range 2 to 30 degrees; treated with glycol and then re-scanned over the range 2 to 22 degrees. Presence of clay minerals can be identified by analyzing the oriented mounts. The relative peak areas/heights on the XRD scans and the X-ray diffractometer determined elemental compositions are used to estimate the mineral concentrations. Also depending on the sample composition, the detection limits range from less than 1% to approximately 5%. The XRD results, shown in Table 2.2, are presented as approximate mineral weight percent concentrations.

Micro X-ray Computed Tomograhy (MXCT) was performed on basalt flows and diabase in order to produce images that can be used to interpret internal composition and micro structural properties. MXCT is a non-destructive technique that enables visualization of the inner features in the interior of opaque solid objects. The image is generated by directing X-rays through a certain thickness (slice) of the object being scanned from multiple orientations and measuring their resultant decrease in intensity. A specialized algorithm is typically used to reconstruct the distribution of X-ray attenuation in the slice plane (Ketcham and Carlson, 2001). The X-ray attenuation is fundamentally a function of X-ray energy as well as the density and atomic number of the material being imaged. High-resolution, micro X-ray CT differs from conventional medical CT-scanning in its ability to resolve details as small as few microns in size, even when imaged objects are made of high density and low-contrast materials. Due to the non-availability of diabase sill samples from our study area, samples from the Palisade

Sills in the Newark series (in New York and New Jersey) that are considered analogues of the SGR basin diabase sills were obtained and analyzed.

2.6. RESULTS

The key, substantial findings from the various analyses and methods that we have used, and how these relate to subsurface evaluation of the Triassic-Jurassic SGR basin for supercritical CO_2 storage are presented as follows. Estimates of how much CO_2 may be stored within the confined porous rocks are also clearly discussed in this section.

The Basalt Flow Deposits

The Clubhouse Crossroads (CC-1, CC-2 and CC-3), and the Dorchester -211 (DOR-211) wells in southern South Carolina (Figure 10) are two examples of known occurrence of Jurassic age basalt flows (Lanphere 1983, Hames et al. 2000) within the SGR Basin that could serve as viable CO_2-reservoir seals. The CC-1, CC-2, and CC-3 wells covered total depths of 792 m, 907 m, and 1152 m and penetrated 42 m, 131 m and 256 m thicknesses respectively of basalt (Gohn et al., 1983b). DOR-211 covered a total depth of 632 m and penetrated a 32 m thick of basalt deposit (Reid et al., 1986). These basalt flows have been studied for geologically, tectonic and regional significance (Chowns and Williams, 1983; Akintunde et al., 2011; and, Heffner et al., 2012). However, a knowledge of the physical properties of these rocks that is necessary to assess seal's viability is lacking. Shown in Figures 2.2 and 2.3 are X-ray CT scans of cores from these wells. The highly vesicular flow top (Figure 2.3) is characterized by spheroidal pores and appears to have undergone significant alteration. The alteration may result from

weathering, erosion, magmatic and other tectonic processes based on petrographic and geochemical evidence (Gottfried et al., 1983). The interior of flow typically retains the dark color and the fine-to-median grained characteristics (Figures 2.3 and 2.4). The vesicles within the flow top are represented by the black spheroidal pores in the CT image. The presence of olivine and pyroxene are represented in white. The significant difference in the gray shades between the flow top and the flow interior is due to variations in the mineralogical composition as well as the proportion of pore space. The interior of the flow consists of minerals such as plagioclase, pyroxene and olivine (Gottfried et al., 1983). Also, these do not have pores and are dominated by minerals resulting in the whitish, gray color. Additional insights into the texture and internal composition of the basalt flow interior are provided in the thin section/photomicrograph shown in Figure 2.5 for the DOR-211 sample. The fine-grained, porphyritic and crystalline nature of the sample can be seen coupled with the presence of yellowish olivine, black augite, and gray stratiated plagioclase phenocrysts in a ground mass of whitish feldspar. Slight textural and mineralogical alteration, common in basalt, can be seen in the yellowish clasts (olivine-normative/altered basalt) as well. This is possibly caused by magmatic processes or local/regional scale metamorphism associated with extensional tectonic movements of the SGR Basin.

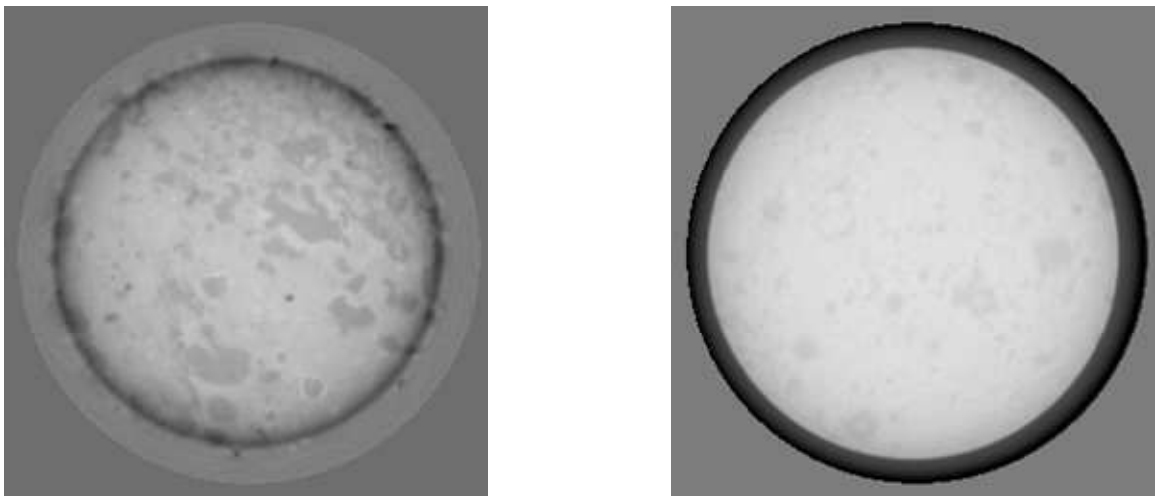

Figure 2.3: X-ray computed tomographic (CT) images of basalt flows encountered at the Clubhouse Crossroad Well -2 (CC-2). The highly vesicular top of flow at 726 m and an interior layer at 802 m are illustrated on the left and right. The CC-2 flow interior at 802 m appear fresh, un-weathered and show physical characteristics similar to the DOR-211 sample (Figure 2.4).

The basalt flow layers above the top of flow are generally denser, fresher and characterized by higher seismic velocities than the flow top. The densities measured were 2.72 g/cm3 and 2.89 g/cm3 for the CC-2 and DOR-211flow interiors and 2.28 g/cm3 for the CC-2 flow top (Figures 2.4 and 2.5). Ultrasonic measurements yielded P-wave velocities (Vp) of 3.70 km/s for the CC-2 flow top as well as 6.20 km/s and 6.75 km/s for the CC-2 and DOR-211 flow interiors at 802 m and 605 m. With the exception of the flow top that produces porosity of 14.34 % and permeability of 0.045 mD, near-zero porosity and permeability values were obtained for the interior layers.

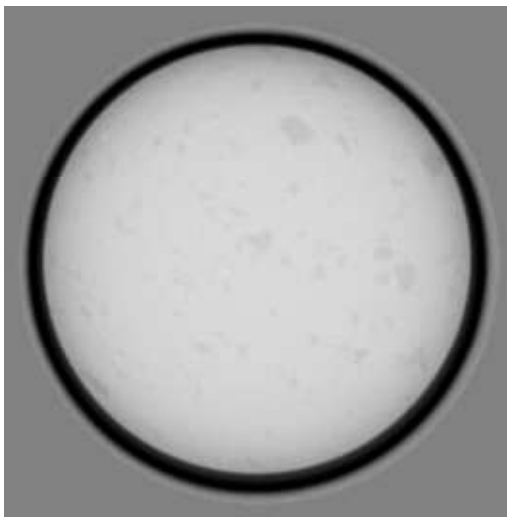

Figure 2.4: X-ray computed tomographic image of an interior basalt layer encountered at Dorchester-211 (DOR-211) well at 605 m.

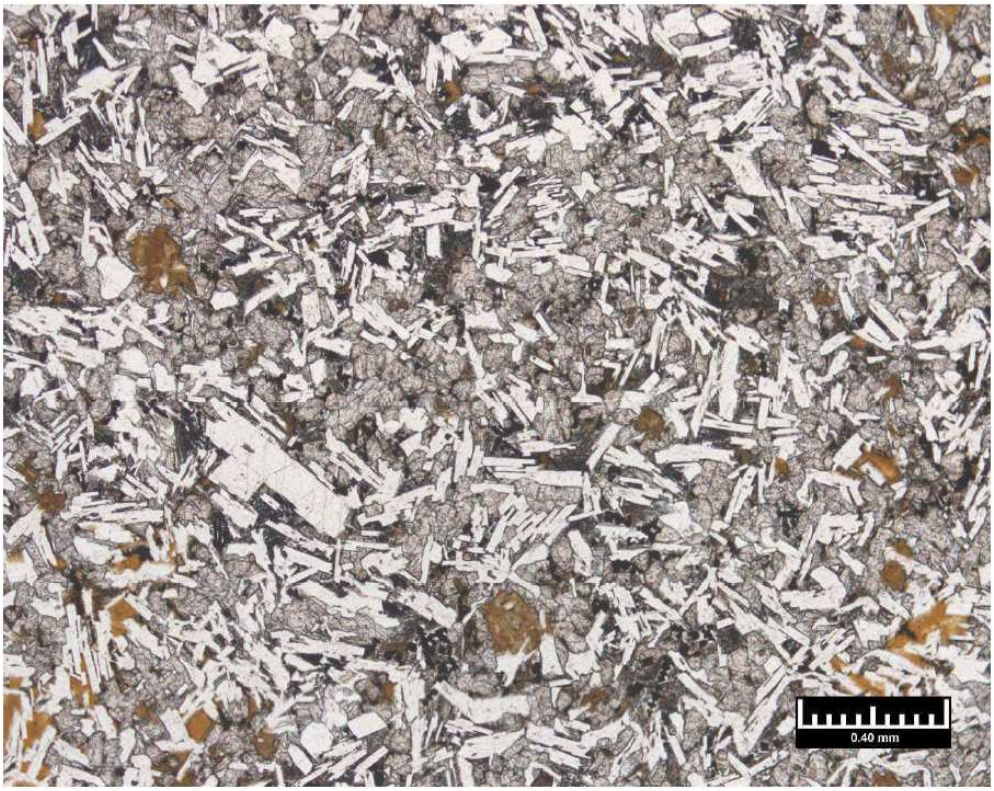

Figure 2.5: A thin section of Dorchester-211 basalt flow at 600 m in plain white light

The Diabase/Palisade Sills

An extensive suite of diabase sills that could serve as caprocks exists within the SGR basin (Figure 2.6). The diabase sills are distinct in geophysical borehole logs from the target red beds by higher resistivity, lower gamma ray and higher seismic velocity (Figure 2.6). As illustrated in the Norris Lightsey well, the target diabase sills occur well below the 0.8 km to 1 km depth required for supercritical CO_2 storage and range in thicknesses from 1.5 to 124 m (Figure 15). This well was a wildcat drilled to a depth of about 4,000 m in northwest Colleton County, SC. It encountered over 3,100 m of Triassic red beds confined above and below by diabase sills.

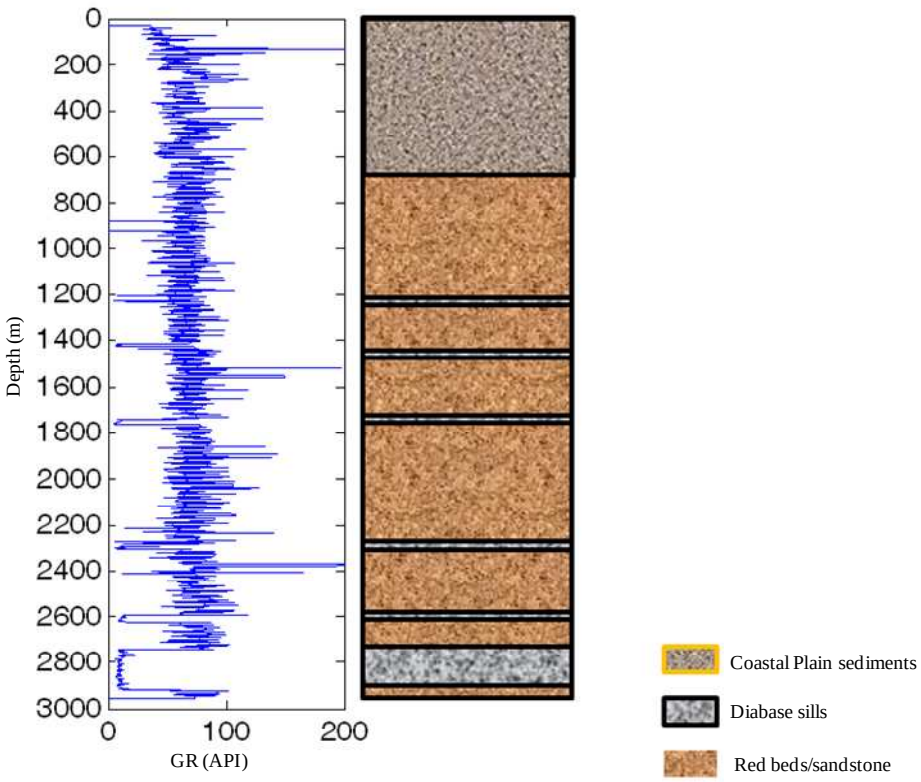

Figure 2.6: Gamma ray and simplified lithology logs from the Norris Lightsey well showing multiple intervals of Triassic red beds that are confined above and below by diabase sills.

In order to provide a detailed view into the internal composition and micro structure of these sills X-ray CT imaging was carried out on near-surface outcrop samples of Palisade/diabase sills (Figure 2.7). Non-availability of diabase cores from the Norris Lightsey well necessitates the use of the near-surface outcrops. The principal minerals are plagioclase, pyroxene and olivine though interstitial growths of accessories such as biotite, quartz and potassium feldspar can be seen. The X-ray CT images/scans (Figure 2.7) do not reveal any internal features that could compromise caprock integrity. These sills are fresh, hard rocks and with no indication of any void, opening or pathway that could cause fluid movement.

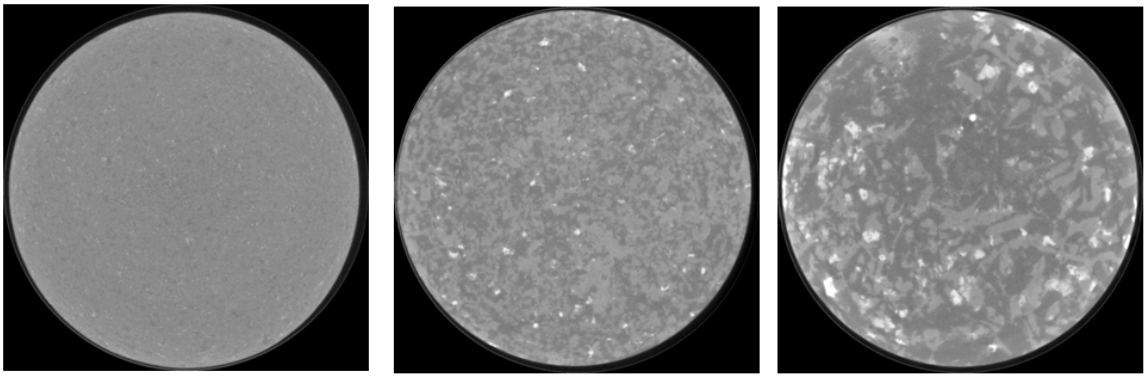

Figure 2.7: X-ray Computed Tomography (CT) scans on samples of diabase/palisade sills. From the left to right are samples within 2 m, 20 m and 200 m respectively of the base of sill. Changes in gray levels are indicative of variations in the density of minerals.

Most of the diabase encountered in the SGR basin is phaneritic because of the diabasic (intergranular) to ophitic texture depending on grain size. The observed change in gray levels in the CT images (Figure 2.7) is reflective of the differences in the mineralogical composition and texture of the tested samples. The whitish marks

represent olivine and pyroxene, and mineralogical alterations caused by possible crystallization processes are common within the diabase. Olivine is particularly susceptible to alteration and in thin sections has been shown to correspond to pseudomorphs of serpentine, idingsite, and magnetite (Chowns and Williams, 1983). Relatively uniform P-wave velocities (5.20 - 5.50 km/s), and densities (2.98 g/cc to 3.00 g/cc,) respectively, were observed for the diabase/palisade sills. Because these are much shallower samples occurring within 250 m from land surface, the velocity values are lower than the sonic-derived values from the log (Figure 1.9) that shows values exceeding 6 km/s as well as the values obtained for the basalt flow interior. The characteristic high velocities are reflective of velocity values seen in impermeable and non-porous rocks with proven seal integrity either for hydrocarbon or CO_2 sequestration. Also, the lack of pores and/or interconnectivities within the base of the diabase sills (Figure 2.7) will enhance the ability to retard upward migration of CO_2 into the overlying layers.

Basalt Flows versus Diabase Sills

For the purpose of subsurface characterization and in order to assess their effectiveness as CO_2 reservoir seals, it is important to make a distinction between basalt flows and diabase sills. Based on the core-scale laboratory measurements, the interior of the SGR basalt flow could serve as a seal because it is dense, impermeable and non-porous. In addition, the overlying, highly vesicular and porous top of flow has the ability to contain and mineralize the CO_2 that may tend to migrate upward or escape from the

interior layer (Schaef et al., 2009; Goldberg et al., 2010). The ability of the highly vesicular basalt flow tops to rapidly absorb and chemically react with CO_2-saturated pore water forming stable carbonate minerals makes basalt formation a potential geologic storage option for CO_2 (McGrail et al. 2006; Schaef et al., 2009; Goldberg et al., 2010). However, the non-homogeneous nature of the basalt flow (McGrail et al., 2006 and Planke et al., 1999) coupled with its restrictive occurrence within the SGR Basin (Heffner et al., 2012 and, Akintunde et al., 2013b) could be an issue for the regional scale subsurface potential for CO_2 storage. In this situation, more drilling would be needed to support seismic evidence for delineation of true geographical extent of the basalt flows. Also, the rate of basalt mineralization can be different for different geologic environments. Hence, an understanding of the SGR-basalt CO_2-brine interactions as a function of temperature, pressure and rock composition would be necessary. In contrast, the diabase sills appear to exhibit very little variations in measured velocities and densities. Also within the SGR Basin and unlike the basalt flows, evidence from deep borehole abounds for the occurrence of these sills at depths that favor supercritical CO_2 storage.

The Red Beds Reservoir

The late Triassic-Early Jurassic red bed units are overlain by and /or interbedded with basalt flows as seen in the Clubhouse Crossroad well-3 (Gottfried et al., 1983). Intrusion of these red beds by diabase sills is evident from the Norris Lightsey well (Figure 2.6). Apart from the Norris Lightsey well, the CC-3 well remains the only other

well with deep penetrations of the red beds. Located in southwestern Dorchester County near Charleston South Carolina (Figure 10), CC-3 was drilled alongside CC-1 and CC-2 by the U.S. Geological Survey between 1975 and 1977. It penetrates 121 m of red beds between 1031 m and 1152 m. This formation is overlain by 256 m of basalt flows, and 775 m of Cretaceous and Cenozoic sediments of the Coastal Plain. There are no geophysical borehole logs for the CC-3 red bed section. Interpretation of cores, well and XRD data (Table 2.2) together with analysis of existing geologic records from Gohn et al. (1983); Marine and Siple (1974) and Marine (1974) enable identification of two dominant facies of red beds representative for the SGR Triassic-basin fill. These are fine-to-medium-grained and coarse-grained sandstones or conglomeratic sandstones (Figure 2.8). The fine-to-medium grained facies are poorly sorted and well consolidated. These are primarily reddish sandstones commonly interbedded with mudstones and siltstones. Thin layers of conglomerate and shale are also present.

Table 2.2: Sandstone Composition from X-ray Diffraction Analysis on selected samples from Sumter, Berkeley and Clubhouse Crossroads-3 wells (CC-3-1 and CC-3-2)

Mineral Name	Sumter	Berkeley	CC-3-1	CC-3-2
Quartz	35%	19%	18%	19%
K-feldspar	21%	8%	6%	22%
Plagioclase feldspar	-	12%	<5%	13%
Mica/Illite	5%	24%	29%	5%
Smectite	22%	15%	15%	14%
Chlorite	-	-	10%	5%
Kaolinite	10%	10%	-	-
Calcite	-	-	12%	19%
Hematite	-	< 5%	5%	<5%

The dominant minerals based on the XRD analysis of selected samples from Berkley, Sumter and Clubhouse Crossroads-3 (CC-3-1) include quartz, feldspar, smectite and illite/mica (Table 2.2). The coarse-grained facies are well-indurated based on the core examination. These are mostly characterized by poorly sorted coarse-grained to conglomeratic sandstones and interbedded mudstones. The mudstones are similar to the ones encountered within the fine-to-medium grained facies. An excellent example of these facies is found directly below the fine-grained sample in the CC-3 well (Figure 2.8). The significant color change in the coarse-grained sample is due to presence of granitic and other detrital clasts such as granodiorite, mylonite, microbreccia and basalt. The dominant minerals in the coarse-grained sample are quartz and feldspar based on

XRD analysis and thin sections (Figure 2.9). The XRD data (Table 2.2) indicates lack of textural and compositional maturity for both the fine-grained and coarse-grained samples due to their high proportions of unstable grains and/or lithic fragments. This substantiates the petrological evidence for the lack of maturity of these red beds reported in Gohn et al., 1983.

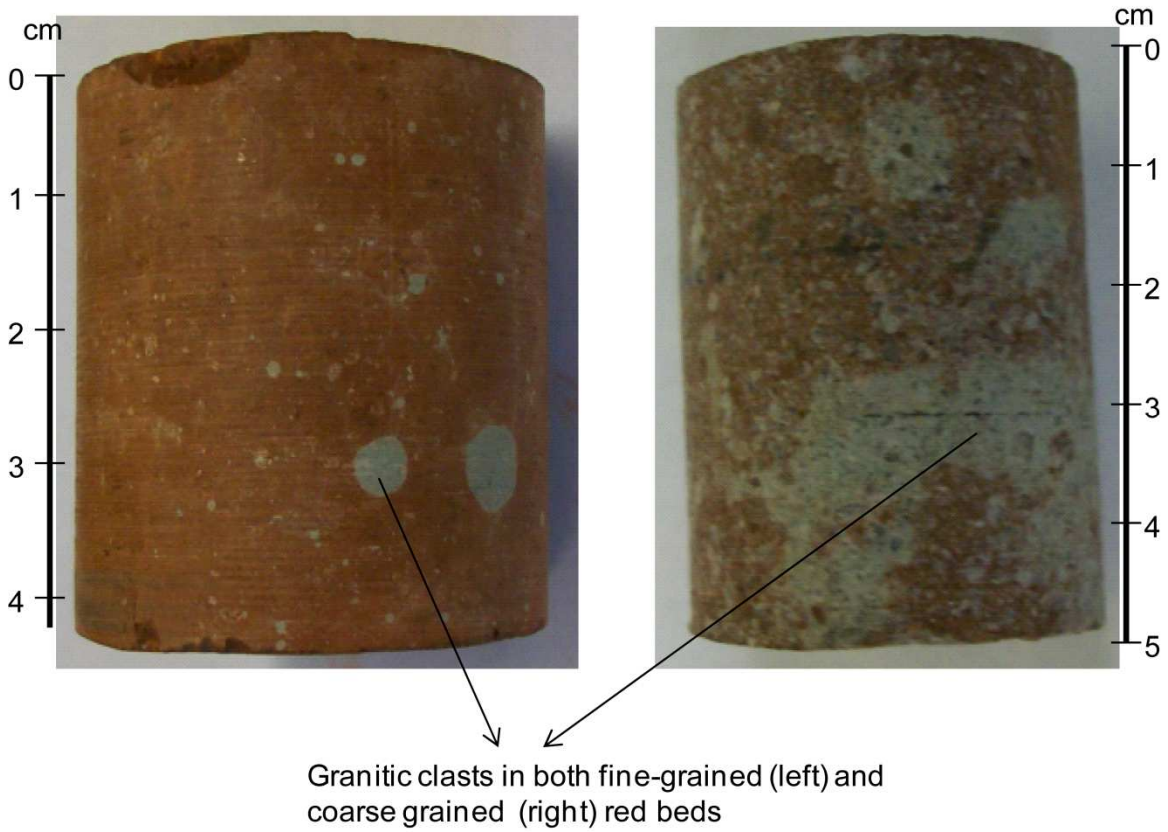

Figure 2.8: Triassic red bed cores (1.5 inches diameter) recovered from the CC-3 well. Left is fine-grained sandstone sample at depth of 1047 m while the core on the right is coarse-grained/conglomeratic sample at depth of 1146 m. The grayish color green seen on the fine-grained sample are small pockets of siltstone and granite clasts and the ones on the coarse-grained are predominantly granitic clasts.

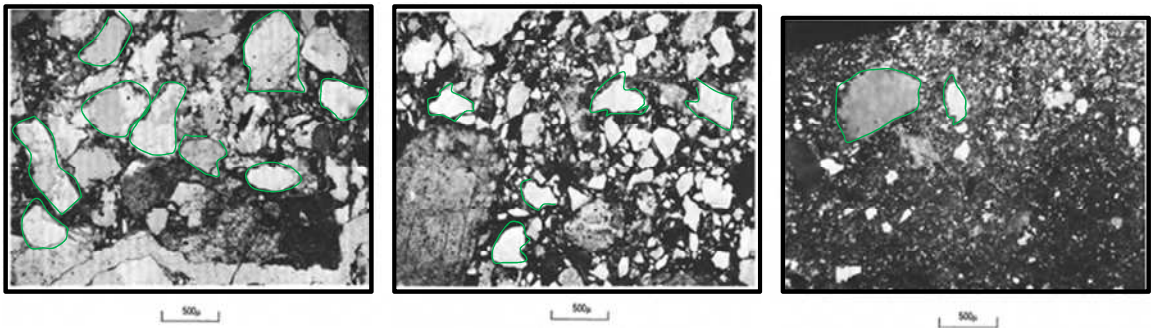

Figure 2.9: Photomicrographs (modified from Gohn et al., 1983) of thin sections of coarse grained sandstones within close proximity of the coarse grained sample at 1046 m that we used in this study (Figure 8 above). From left to right are sandstone at 1146.9 m (in plane light), 1146.6 m (in plain light) and 1146.7 m (in crossed nicols). Poor sorting and poor moderate rounding of grains (green colored marks) can be seen in all three sections.

The poorly sorted character of both fine and coarse-grained sediments could have a significant impact on the permeability of these formations. Poorly sorted and fine-grained sandstone usually has smaller pore throats with a consequent reduction in permeability. Photomicrographs of thin sections (Figure 2.9) provide evidence for poor sorting and moderate to poor rounding of grains within the coarse-grained sediment.

Porosity and Permeability of sandstones/Red Beds

Experimentally derived porosity and permeability values on samples from Berkeley, Sumter, Dunbarton, Norris Lightsey and Clubhouse Crossroads -3 wells (Figure 2.1) identify four distinct porosity-permeability regimes within the SGR Basin (Table 2.3 and Figure 2.10). These are: (a) a high porosity, medium/low permeability zone associated with the Norris Lightsey well's lacustrine deposits, (b) a medium/low porosity, low permeability zone observed in the Berkeley and Sumter fluvial sandstones, (c) a low porosity, low permeability zone associated with Dunbarton and Berkeley fluvial

deposits, and (d) an extremely low porosity and permeability associated with fluvial-alluvial deposits found in the Clubhouse Crossroads (CC-3) red beds.

The lacustrine origin for the high porosity medium/low permeability zone derives from the recovery of pollen and spore assemblages from drill cuttings of gray-green shales between 1373 and 2184 m depth in the Norris Lightsey well (Traverse 1987). These deposits according to Traverse (1987) resemble lacustrine sequences in other exposed basins (Olsen et al., 1991). Evidence for lacustrine deposition from this study comes from the analysis of the Norris Lightsey well logs (Figure 1.9). The presence of lacustrine deposits within the SGR Basin is also supported by Ziegler (1983) who identified a prominent belt of seismic reflections near the middle of the Triassic sequence in the South Georgia basin as lacustrine. Of importance to subsurface evaluation for CO_2 storage are the observed significant variations in the porosity-permeability distribution especially within the high porosity, medium/low permeability associated with the Norris Lightsey's lacustrine fine-grained sandstones. Though there are no thin sections for the Norris Lightsey well, the presence of fine-grained siltstones (Figure 1.9) provides indication of poor sorting. The fine-grained siltstones are generally characterized by very limited and/or fewer less interconnected pores with a consequent reduction in permeability.

The variation in the amounts of silt and clay particles as well as the differences in grain sizes could be a plausible explanation for the Norris Lightsey permeability-porosity trends. A high porosity-low permeability trend can also be observed within this zone.

Given the volumetric relationship between porosity and permeability, it appears logical to expect high porosities to correspond to high permeability within the same formation. However, this is not always the case in this study area. It is possible for a rock sample to have high porosity and low permeability. Unlike porosity that depends primarily on the volume properties of the pores, permeability is a function of both the volumetric and geometric properties of the rock pores (Prasad, 2003). Any variation in pore geometry will affect permeability. As pointed out in Mavko et al. (2003), two sandstone samples can exhibit the same porosity and microstructure, but different average grain sizes leading to the larger grain size with a higher permeability. In addition, the relatively high percentage of silt and clay for the Norris Lightsey samples (Core Lab. Report, 1984) suggests a possible cause of the low permeability. This (according to the Core Lab. Report) may be partially due to a shattering of the matrix material by the impact of the sidewall sampling device.

Table 2.3: Porosity and permeability measurements

S/N	Sample ID	Porosity (%)	Permeability (mD)	Source (Year)
1	Sumter	10.6	0.16	This study – WL (2011)
2	Berkeley_1	13.3	0.15	This study – WL (2011)
3	Berkeley_1*	13.0	0.10	This study – CSM(2011)
4	Berkeley_2	8.6	0.01	This study – WL (2011)
5	Berkeley_2*	8.9	0.01	This study – CSM (2011)
6	Dunbarton	6.3	0.016	Marine and Siple, 1974; Marine, 1974
7	Norris Lightsey_1	22.6	1.5	CL (1984)
8	Norris Lightsey_2	23.8	2.2	CL (1984)
9	Norris Lightsey_3	24.2	6.7	CL (1984)
10	Norris Lightsey_4	27.7	3.7	CL (1984)
11	Norris Lightsey_5	28.1	8.9	CL (1984)
12	NorrisLitghtsey_6	32.5	6.9	CL (1984)
13	Clubhouse Crossroads-3_1	2.6	0.001	This study – WL(2012)
14	Clubhouse Crossroads-3_2	2.1	0.0023	This study – WL (2012)

*Measurements of the Berkeley samples were repeated at the Weatherford and CSM laboratories. Core-derived porosity measurements for the Norris Lightsey fall within the range of log-derived porosity values (Table 3). Data sources: WL – Weatherford Laboratories, Golden, Colorado, USA; CSM – Rock Abuse Laboratory, Colorado School of Mines; CL – Core Laboratory Petroleum Engineering, Dallas, Texas)

The interpreted fluvial/continental and fluvial/alluvial origins for the medium/low porosity, low permeability zone as well as the low/extremely low porosity and low/extremely low permeability zones is based on lithological similarities with exposed analog basins characterized by deposition in these environments. These exposed Triassic-Jurassic basins are prominent within the Newark Super group and other parts of south eastern United States (Gohn et al., 1983b; Olsen et al., 1991). The

absence of textural and mineralogical maturity in the sandstones within these zones based on XRD analysis (Table 2.2) favors deposition by fluvial processes.

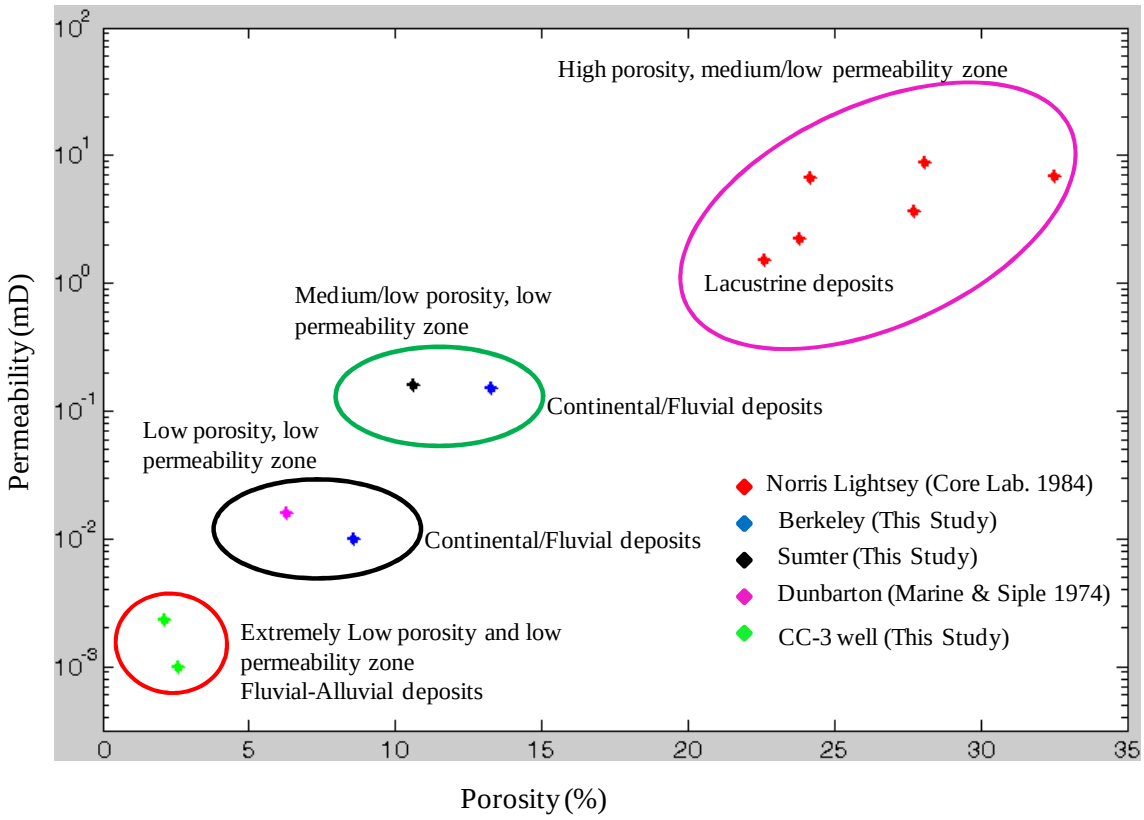

Figure 2.10: Permeability-porosity distribution model based on experimental data (Akintunde et al., 2013b).

Another evidence for fluvial deposition from this study derives from a reanalysis of cores of Triassic red beds from Dunbarton (Figure 2.1) shown in Marine and Siple (1974). The lithology and depositional history of the poorly sorted Dunbarton red beds is consistent with the geology of fluvial deposits as shown in Miall (1996). The basis for the interpreted fluvial/fluvial-alluvial depositional environment for the low/very low porosity and permeability for the Triassic red beds recovered from the Clubhouse

Crossroad (Figure 1.9) and was based on geologic evidence from Gohn et al. (1983) and Lindholm et al. (1979). While the low/very low porosity-permeability of the fluvial-alluvial deposits may appear unique to the SGR Basin, low/very low porosity-permeability is not uncommon in poorly sorted fluvial sandstones (Nelson 2004). The low porosity and permeability markers within these zones are due to the poor sorting and small pore throats exhibited by these sandstones (Figures 2.8 and 2.9).

Estimation of CO_2 Storage Capacity

The amount of CO_2 that can be stored within the confined porous reservoir (Figure 2.6 and Table 2.4) must be taken into consideration to decide whether or not subsurface storage would be a worthwhile effort. Porosity values were derived from red bed intervals in the Norris Lightsey well (Figure 2.1). These were calculated over the intervals with reservoir and seal presence (Table 2.4). A variety of well logs was used to aid accurate interpretations for porosity, and an example is shown in Figure 2.11. Porosity (ϕ) was calculated from the sonic log using the Wyllie time average formula:

$\phi = (\Delta t - \Delta tma)/ (\Delta tf - \Delta tma)$,

where Δt is acoustic transit time, Δtma is acoustic transit time of the rock matrix and Δtf is acoustic transit time of interstitial fluids (Wyllie et al., 1956). The inputs into this formula are all in μsec/ft. Acoustic transit time was obtained from the sonic log and 52.6 μsec/ft and 89 μsec/ft were used as the acoustic transit time of the rock matrix and acoustic transit time of interstitial fluid (brine) respectively (Mavko et al., 2003). Because of the significant variations in the log-derived porosity measurements, an

average value was used in the storage capacity calculations. It is important to note that the core-derived porosity measurements (Table 2.3) fall within the range of the log-derived values (Table 2.4). The differences are due to the difference in scale of measurements.

For storage capacity estimation, a theoretical approach based on the DOE-NETL equation (DOE 2008) was used. It estimates CO_2 storage capacity (GCO_2) based on the following expression:

$$GCO_2 = A \times h \times \phi \times \rho \times E,$$

where A is the geographical area covered by target reservoir and seal, h is reservoir thickness, ϕ is reservoir porosity, ρ is density of CO_2 and E is storage efficiency factor.

A reasonable, projected minimum value of 5, 000, 000 (m^2) was used for the geographical area, which covers the region penetrated by red beds and diabase within the study locations. Reservoir thickness determined from well logs and a density of 700 kg/m^3 was used for supercritical CO_2 (Burruss et al., 2009). The storage efficiency is the ratio of used space for CO_2 storage to the available space multiplied by 100 and an estimate of 10% was used based on petrophysical interpretations from well logs and core measurements. The results show that 3.73 to 13.23 Gt CO_2 may be stored within the study area (Table 2.4).

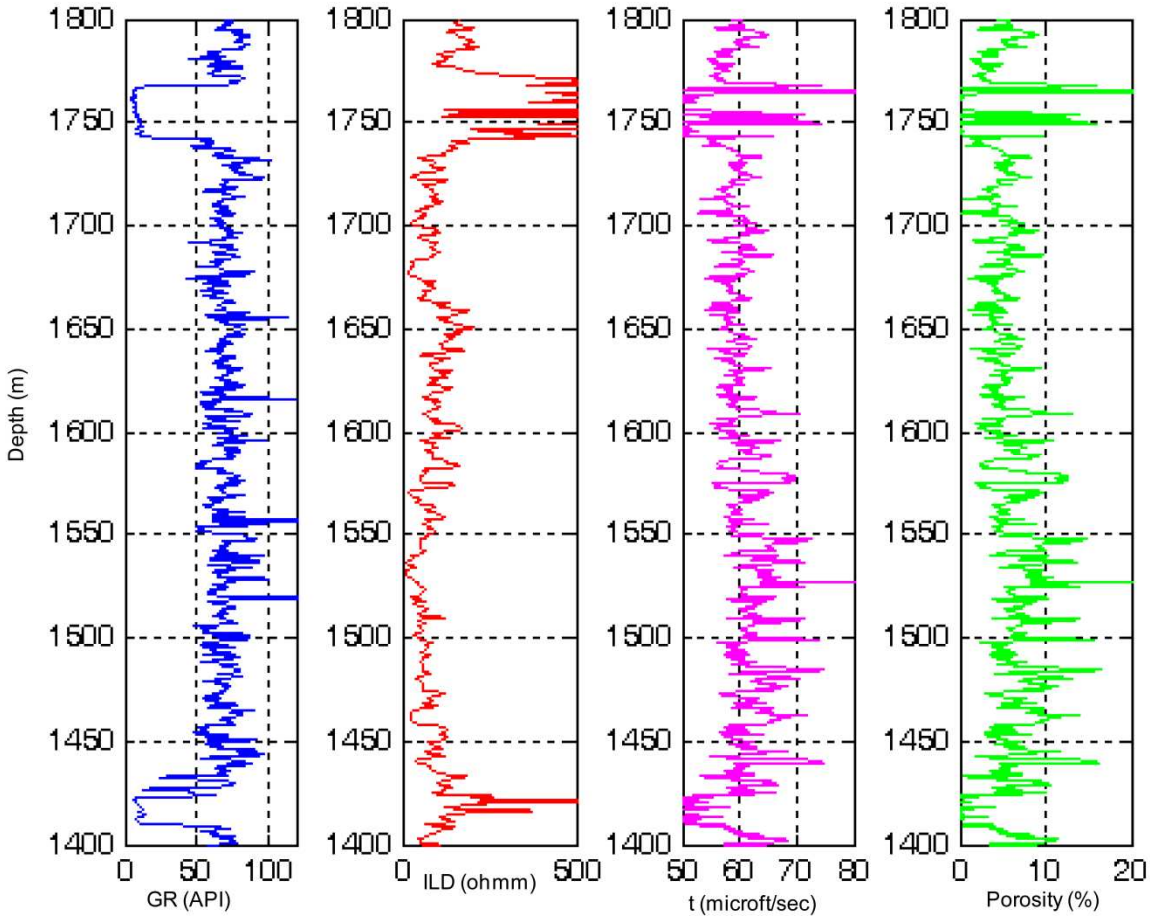

Figure 2.11: Gamma ray (GR), deep induction resistivity (ILD), acoustic transit time (t) and porosity.

Table 2.4: Storage capacity estimation over target intervals

Depth interval (m)	Thickness (m)	Area (m^2)	Density of CO_2 (kg/m^3)	Porosity range (%)	Average porosity (%)	Storage efficiency (10%)	CO_2 storage capacity (Gt)
1240 - 1390	150	5000000	700	5 - 22	7.1	10	3.73
1433 - 1733	300	5000000	700	5 - 20	7.7	10	8.10
1780 - 2200	420	5000000	700	1 - 10	3.7	10	5.44
2310 - 2580	270	5000000	700	1 - 22	14	10	13.23

2.7. DISCUSSION OF RESULTS

The SGR Basin has never been previously explored for carbon sequestration in terms of key rock properties significant for CO_2 storage. This research is concerned with evaluating the critically important reservoir/seal properties necessary to study the feasibility for subsurface storage of CO_2. New experimental and petrophysical results indicate that porous, deep and thick saline Triassic red bed formations with potential for supercritical CO_2 storage do exist within the basin. Injectivity tests and reservoir simulation models will be necessary to know how much can be safely and permanently stored under dynamic reservoir conditions (temperature, pressure and time as well as the kinematics of the rock-CO_2/brine interactions). This would be important in order to design strategies for long-term storage should CO_2 injection be undertaken.

Basalts and/or diabase sills (Figures 2.3-2.7) in the area of interest have the physical properties and microstructural conditions required for cap rock integrity. Unlike the top of flow characterized by high porosity, near-zero porosity and permeability values were obtained for the interior of basalt flows. These are consistent with sealing requirements and suggest the basalt may provide viable seals to prevent upward migration of CO_2 into the overlying Coastal Plain sediments. The presence of significantly high pores within the flow top is responsible for the relatively high porosity.

Additionally, the non-porous and impermeable nature of the interior layers is consistent with their characteristics high velocity values. These are extremely tight, dense rocks with no obvious sign of weathering and any significant micro-structural features that could compromise cap rock integrity. The weathered, poorly consolidated nature and low density of the top of flow are responsible for the low Vp.

However, the diabase sills present a more viable option for further characterization within the SGR Basin in view of the restrictive regional extent of the basalt flow (Akintunde et al., 2013a). The high velocities of the diabase sills are similar to velocity values seen in impermeable and non-porous rocks with proven seal integrity either for hydrocarbon or CO_2 sequestration. The X-ray CT scans (Figure 2.7) do not reveal any internal features that could compromise the caprock integrity. These sills are fresh, hard rocks and with no indication of any void, opening or pathways that could cause fluid movement. The lack of pores and/or interconnectivities within the base of the diabase sills would enhance the ability to retard upward migration of CO_2 into the

overlying layers. In addition, multiple layers of diabase in association with the confined red beds or sandstone units provide an added advantage for increased physical trapping and/or multiple storage units. Additional studies involving seismic imaging, micro-seismic characterization, borehole imaging, and geomechanical tests are necessary to further evaluate the seal integrity and continuity.

On the basis of porosity-permeability analysis (Figure 2.10), two end members or regions of porosity-permeability distribution have been recognized within the SGR Basin. The fluvial/fluvial-alluvial dominated sandstones where the porosity and permeability are lower relative to the lacustrine dominated porosity-permeability region. In between these end members, there are significant variations in the porosity-permeability distribution. This has implications for the degree of reservoir quality and injectivity. These variations also suggest the presence of moderately to highly compartmentalized reservoir system within the SGR Basin. In the fluvial region, the poor sorting effectively limits the pores and pore throats within the rock and with a consequent reduction in permeability. Also, low permeability behavior is a common feature in the lacustrine region. The consequence of the low permeability is a restriction in subsurface fluid movement, which would impact reservoir injectivity. While the lacustrine deposits will be more viable for the SGR Basin CO_2 storage, a restrictive fluid movement will be unfavorable to commercial scale development should CO_2 injection be undertaken.

Besides the influence of depositional setting, effects of post depositional processes such as compaction and diagenesis are possible causes of the low porosity and permeability. However, the fact that these are deeply buried rocks, which in some areas are overlain by thick sequences of consolidated extrusive basalt flows and/or intrusive diabase sills, suggests preservation of the pores and pore throats. While this may hold, the occurrence within the Triassic red beds of pore-filling igneous clasts as observed in the CC-3 red bed section (Figure 2.8) is an indication of possible textural and mineralogical alterations that can reduce porosity and permeability. Considerable erosion during late Triassic to early Jurassic as well as tectonically induced events (such as faulting, emplacement of mafic igneous deposits, uplift and subsidence) that preceded sedimentation near the Triassic-Jurassic boundary may have triggered alterations and diagenesis within these sediments.

In view of the vastly expansive areal extent of the basin (about 100, 000 km^2), it is strategically and economically important, as part of site characterization studies to know which part of the basin to focus future research efforts on and resources available for long-term storage feasibility studies. The Norris Lightsey area (Figure 2.1) offers the most promising reservoir conditions for subsurface CO_2 storage. In addition to the geo-sequestration significance of the results of this study, this work demonstrates the applicability of petrophysics or rock physics to regional site characterization in environmental related studies involving evaluating feasibility for CO_2 storage. Rock physics is commonly applied for monitoring and verification studies.

By implementing physics-based laboratory experiments on rock samples, key rock attributes that are strategic and extremely important to the goal of site selection and characterization can be determined. The integration of core scale petrophysical data from multiple wells provides the framework or basis to upscale core derived reservoir properties to regional scale. Seismically constrained 3D geo-reservoir modeling incorporating lithofacies and petrophysically derived rock properties can be implemented using recent geo-statistical rock physics techniques (Spikes et al., 2007; Grana and Rossa, 2010) to upscale to the regional scale. More data from coring, geomechanics and 3D seismic imaging would be needed to further characterize the geometry, regional extent and continuity of the petrophysically identified reservoirs and seals (Akintunde et al., 2013b).

2.7. CONCLUSIONS

Confined, porous Triassic red bed reservoir units with potential for supercritical CO_2 storage exist within the SGR Basin. Between 3.73 and 13.23 Gt of CO_2 may be stored for a single storage system (and up to 30.07 Gt for a stack storage system). A unique characteristic of the basin revealed by this study is the presence of distinct porosity-permeability regimes that are influenced by the depositional environments. These are: (1) a high-porosity, low/medium permeability zone; (2) a medium/low porosity, low permeability zone; (3) a low porosity, low permeability zone, and, (4) an extremely low porosity and low permeability zone (Akintunde et al., 2013b).

The high-porosity, low/medium permeability zone is associated with lacustrine deposits and consists of fine-grained Triassic sandstones with interbedded layers of siltstone and mudstone. The medium/low porosity, low permeability zone is dominated by fluvial fine-to very fine-grained sandstone, while the extremely low porosity and permeability zone are characterized by fluvial and alluvial-fan deposits. Presence of low permeability red beds is a common characteristic within the basin. The low permeability is caused by poor sorting and small pore throats.

Tectonically induced post depositional processes are also possible controls on the observed porosity-permeability trends. The basalt flows and diabase sills possess physical properties (such as high seismic velocities and densities), petrophysical characteristics and micro structural properties consistent with sealing requirements. The diabase sills are distinct from the basalt flows by exhibiting very little variations in velocity and density.

This work has shown that rock physics or petrophysics can be applied to subsurface characterization involving environmental related issues like carbon capture and storage. It is important as part of a regional site investigation to select an optimum location for drilling to understand changes or variations in reservoir properties at desirable resolution (cm/core/log scale) not provided at the seismic scale.

CHAPTER THREE

AN INVESTIGATION OF THE TECTONIC IMPLICATIONS OF THE POROSITY AND PERMEABILITY DISTRIBUTION WITHIN THE SOUTH GEORGIA RIFT BASIN

3.1. OVERVIEW

Porosity/permeability versus depth profile was constructed from the available laboratory measurements in Table 2.3 in order to investigate the tectonic significance of the pattern of porosity and permeability variations exhibited locally and regionally within the SGR basin. Both porosity and permeability change much with depth regionally than locally vis-à-vis considering each study locations (Sumter, Berkeley, Dunbarton, Clubhouse Crossroads-3 and Norris Lightsey). The observed changes in porosity with depth suggest a highly compacted, deformed basin.

Permeability is generally low at both shallow and deeper depths and shows significantly large numerical variations. It is likely that sediment deposition, which precedes igneous activity that led to extrusion of voluminous basalt flows and intrusion of diabase sills during late Triassic-Early Jurassic, may have been significantly impacted, but disproportionately, by tectonically induced compaction, lithification and diagenesis leading to large numerical variations in permeability changes with depth for the study locations. Also, both porosity and permeability exhibit negative correlation with depth for the study locations with the exception of the Norris Lightsey data.

In addition, both Dunbarton and Clubhouse Crossroads Triassic red beds samples show remarkably lower porosity and permeability when compare to the Norris Lightsey values. This behavior raises a fundamental question as to whether or not the basin-fill in these three locations is characterized by the same tectonic environment even though the rocks appear to be of the same age, lithologic composition and occur at near similar subsurface depths. Evidence from a suite of well logs penetrating the Norris Lightsey red beds shows a dramatic shift in acoustic travel time as well as in sonic-derived P-wave velocity below and above normally pressured intervals at depth. This abnormal shift may be triggered by possible faulting or fracturing within the red beds resulting in altered porosities and permeabilities at depth. Regionally, the linear and non-linear dependencies of porosities with depth indicate a basin with a history of uplift and erosion.

3.2. INTRODUCTION

In this study, we explore a possible link between rock physics and tectonic evolution of the SGR basin in the light of unraveling of geological observations of key tectonic importance from core-derived porosity and permeability data. This is an area of research that is different from the usual petrophysical interpretations of porosity and permeability data for reservoir and production applications notably in oil and gas exploration. Rock physics involves the study of rock properties such as porosity and permeability and how these are related to geophysical observations (Mavko et al., 2003). Porosity is the amount of pore space in a rock while permeability is the ability of

a rock to transmit fluid. Both are very important in assessing reservoir storage capacity as well as the degree of reservoir quality and compartmentalization for the purpose of oil and gas recovery, subsurface storage of CO_2 and any other dynamic reservoir systems that involve fluid movement. In addition, knowledge of porosity and permeability can be applied to basin modeling to better understand key information of importance to compaction and cementation history of a basin (Prasad, 2002). As pore space properties of rocks, porosity and permeability are primarily dependent on the size, shape, distribution, and packing or sorting of the rock's grains (Schon, 2011). Physical, chemical and geo-chemical processes including diagenesis and changes in the mineralogy are other factors that can influence porosity and permeability in rocks.

The focus of this study is on the role of tectonically induced post depositional processes on the present-day porosity and permeability within the Triassic-Jurassic SGR basin. The focus is on the tectonic interpretation of porosity/permeability depth profiles derived for the SGR red beds or sandstones. This is an area of research not previously examined for the SGR basin. We obtained new porosity and permeability information from Sumter, Berkeley, and the Clubhouse Crossroads well#3 using standard laboratory measurements carried out on 1.5 inch diameter core plugs. These measurements were carried out using the Core Measurement System (CMS) 300 which combines helium-based porosimeter (based on gas expansion by Boyles' law) and gas-based permeameter in one instrument to determine porosity and permeability. The permeability measurement from CMS-300 takes into account the Klinkenberg correction

(Klinkenberg, 1941). The porosity was measured at room conditions and permeability determined under low confining stresses.

Existing porosity and permeability data from the Dunbarton basin (Marine and Siple, 1974, Marine, 1974) and Norris Lightsey wells were used to supplement the new experimental data (Table 3.1). Core Laboratories Incorporation, Dallas, Texas in 1984, acquired the Norris Lightsey data (based on side wall coring) as part of efforts to explore for hydrocarbon resources. These datasets were initially interpreted in relation to the depositional environments and reservoir quality assessment as parts of geological characterization study aimed at evaluating subsurface suitability for CO2 storage within the SGR basin (Akintunde et al., 2011, and Akintunde et al., 2013).

Table 3.1: Depth-dependent Core derived porosity and permeability data for the study locations

Locations	**Depth (ft)**	**Porosity (%)**	**Permeability (mD)**
Sumter	690	10.6	0.16
Berkeley	1799	13.3	0.15
Berkeley	1826	8.6	0.01
Durbarton	2694	6.0	0.016
CC-3*	3435	2.1	0.0023
CC-3*	3760	2.6	0.001
Norris Lightsey	3241	22.6	1.5
Norris Lightsey	3243	23.8	2.2
Norris Lightsey	3412	24.2	6.7
Norris Lightsey	3475	28.1	3.7
Norris Lightsey	4938	27.7	8.9
Norris Lightsey	4994	32.5	6.9

*CC-3: Clubhouse Crossroad-3

3.3 OBJECTIVES

This study is concerned with interpreting the porosity/permeability variations with depth locally and regionally in order to (1) investigate the physical controls responsible for the present-day porosity and permeability as well as (2) gain new insights into the implications of the observed porosity and permeability changes for the tectonic evolution of the basin.

3.4. METHODS

The methodology involves the construction and analysis of porosity and/or permeability versus depth relationships for the study locations with available core-laboratory data (Table 3.1). This was aided by analysis of available thin section as well as the information on the lithologic composition of the Triassic-Jurassic formations.

3.5. POROSITY-DEPTH RELATIONSHIP

This study shows that there are significant changes in porosity versus depth both locally and regionally throughout the basin (Figure 3.1). Locally, the porosity changes by up to 44% and regionally by over 100% %. A reduction in porosity with depth is easily noticeable at most locations with the exception of the Norris Lighsey well. We do expect porosity to be lower in deeper, older rocks and show a decreasing linear trend with depth due to increasing effects of compaction and cementation. However, exception to this behavior is not uncommon and the Norris Lightsey porosity-depth relationship does manifest this departure. The Dunbarton and Clubhouse Crossroad samples occur within

proximity of the depths penetrated by the Norris Lightsey samples, but the porosities are distinctively and remarkably lower compare to the Norris Lightsey porosities.

Furthermore, the porosity decrease with depth is consistent with the normal compaction trend observed in most clastic formations. Based on the empirical formulation of Athy (1930), as shown in equation 3.1, sediment compaction is a function of the mean effective stress.

$$\phi(z) = \phi_0 \exp(-b.z) \qquad (3.1)$$

Where ϕ_0 is the porosity at reference depth (z=0), ϕ is porosity at the actual depth Z and b is a factor controlling the compressibility of the sediment. Schon (2011) based on Revi et al., 2002 introduced the effects of deformation/overburden stress and/or effective pressure and density into the compaction model to come up with equation 3.2

$$\phi(z) = \phi_c + (\phi_0 - \phi_c).\exp(-c.p.g.z) \qquad (3.2)$$

Where (p) is the porosity at effective pressure p, ϕ_c is the residual porosity (at p tends to infinity) and ϕ_o is the initial porosity at p = 0, g is the acceleration due to gravity and c is related to the compressibility of the rock.

3.6. PERMEABILITY-DEPTH RELATIONSHIP

The reduction in permeability with increasing depth below the surface follows the same trend in most of the study locations apart from the Norris Lightsey well (Figure 3.2). The changes in permeability vary between 56% and 93% for these locations where a linear decrease with porosity (Figure 3.1) is observed. Permeability changes by up to 83% in the Norris Lightsey well that is characterized by a non-linear relationship in the

porosity-depth model (Figures 3.1 and 3.2). The permeability values are generally low due to the fine-grained nature of the sediments, poor sorting, presence of small pore throats and poor rounding of grains (Marine, 1974, and Gohn, 1983). However, the permeability for other study locations including the shallow samples from Sumter and Berkley are much lower than that of the Norris Lightsey. In most parts of the study locations, the permeability-depth trend is consistent with the porosity-depth model (Figures 3.1 and 3.2) implying a relationship between porosities and permeabilities for the SGR Triassic red beds formations. This is supported by the observed strong positive correlation (with a correlation coefficient of 0.9861) between the Norris Lightsey's porosity and permeability as shown in Figure 3.3 (plotted for data points that fall within the correlation).

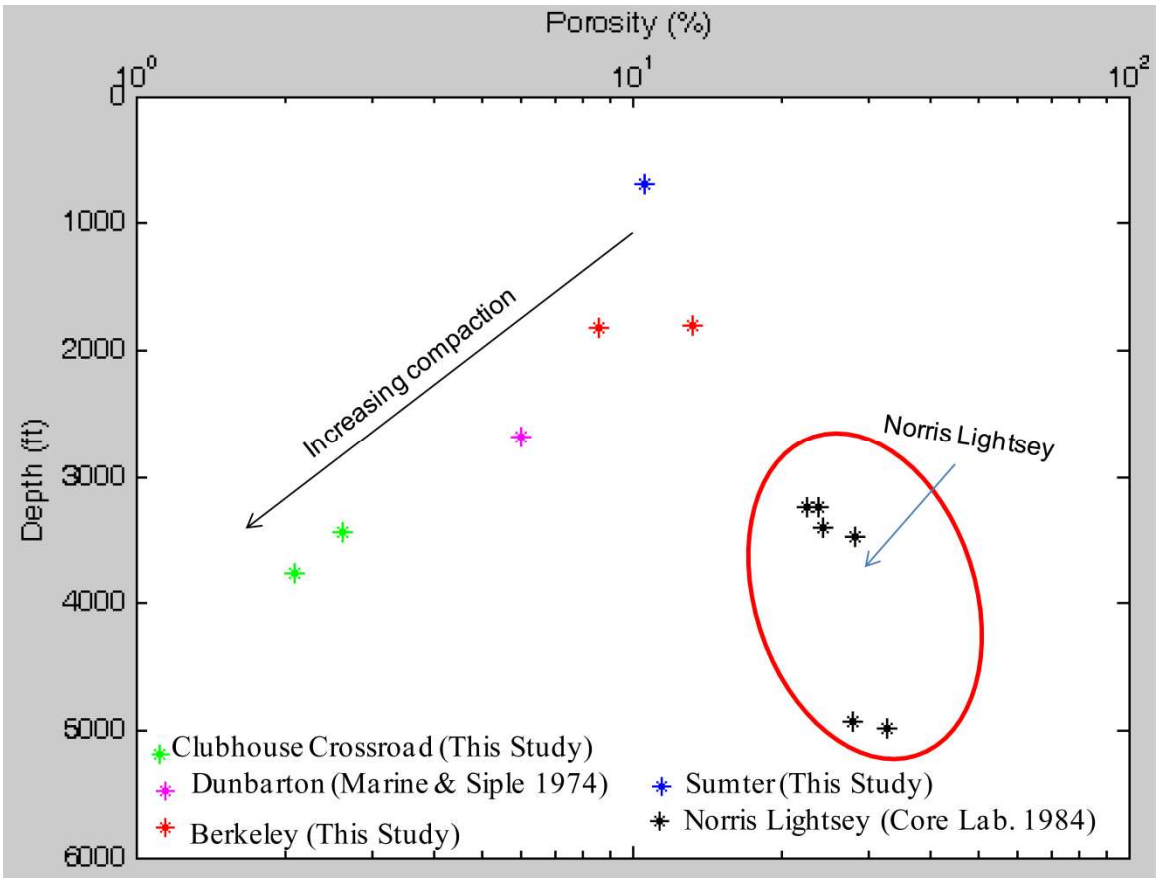

Figure 3.1: Porosity versus depth for the sampled locations

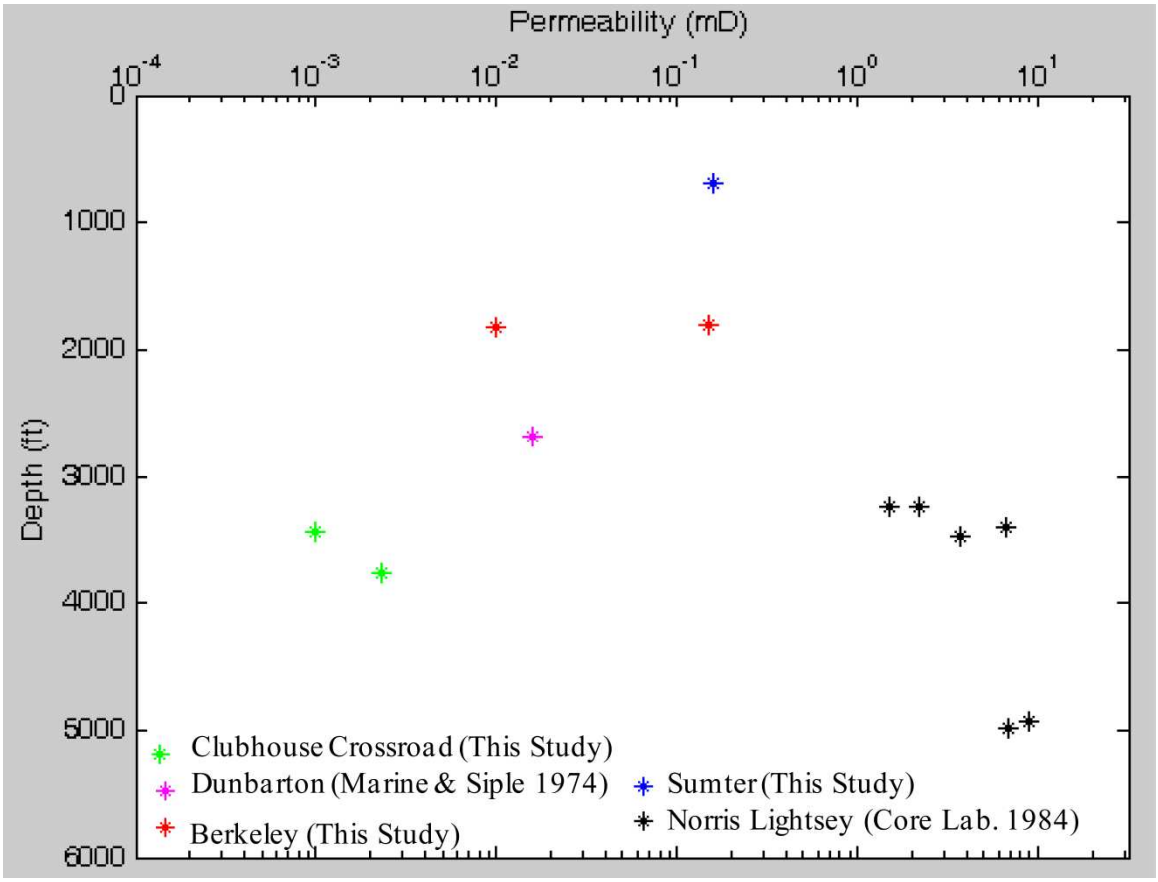

Figure 3.2: Permeability versus depth for the sampled locations

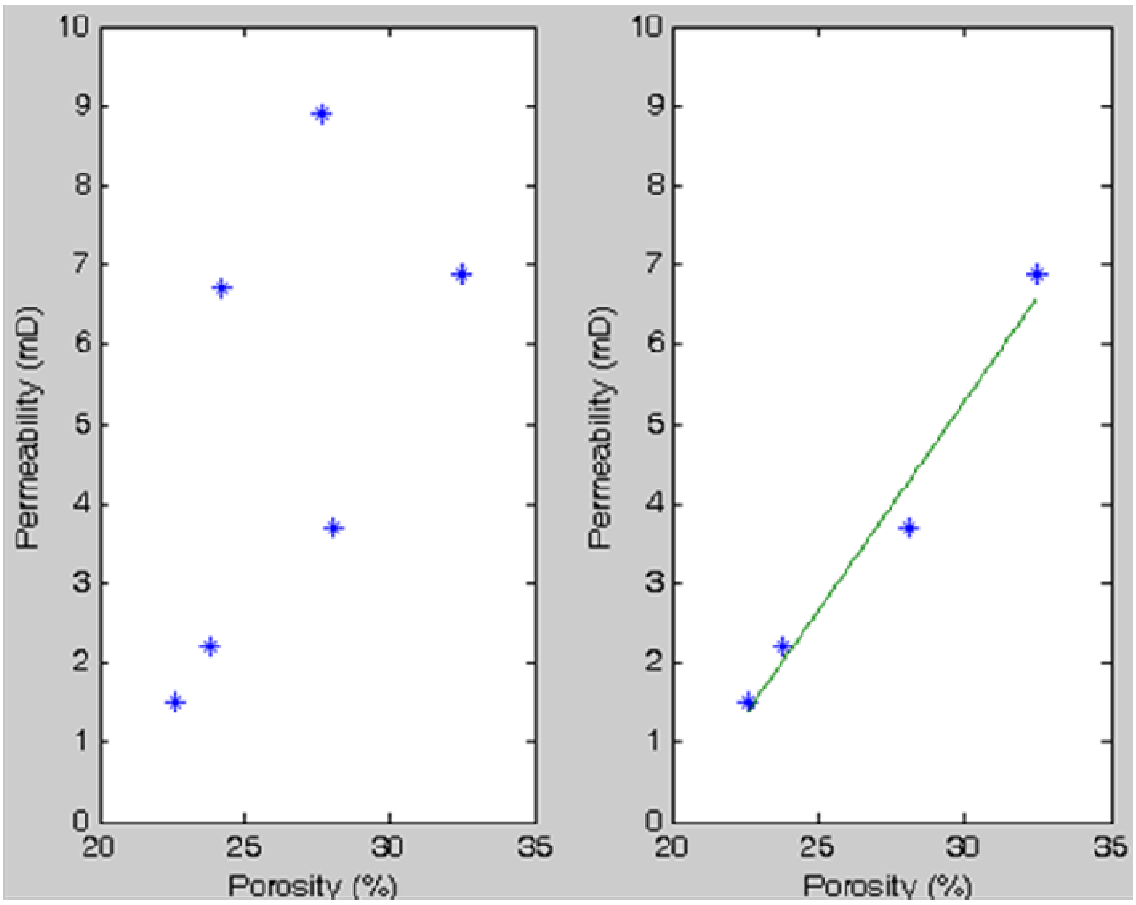

Figure 3.3: Porosity-Permeability plot for the Norris Lightsey. The plot on the left shows actual data points, while the line plot one on the right shows porosity and permeability data points with strong positive correlation 0.9861.

3.7. DISCUSSION AND REGIONAL IMPLICATIONS

Four key observations stand out in the porosity/permeability depth models (Figure 3.1 and 3.2): (1) a general lack of significant correlation of porosity/permeability with depth throughout the basin, (2) a linear decrease of porosity with depth for all other study locations with the exception of the Norris Lightsey, (3) the unusually higher porosities and permeabilities for the deeply buried Norris Lightsey red beds relative to

other parts of the basin such as Berkeley and Sumter wells that are shallower and the Clubhouse Crossroad-3 and Dunbarton wells that occur at near-similar depths, and (4) the non-conformity of the Norris Lightsey porosity-depth distribution with the normal compaction trend.

The first observation, whereby we see both a linear and non-linear increase in porosity/permeability with depth is often encountered in a basin that has undergone differential uplift and erosion (Bloch, 1991). Erosion and uplift in the basin possibly made the Triassic sediments to be nowadays at a shallower level than after being buried and compacted, thereby leading to altered porosity and permeability following original deposition, compaction and cementation. These rocks are all part of the Atlantic-type passive continental rift deposits, however there is no evidence to suggest that the sedimentary fill in these locations at present is what it was during the early cycle of sedimentation that accompanied rifting and continental separation.

It is likely that erosion during Jurassic removed large volumes of rocks including several parts of the top of the Triassic sediments as well as uncovering part of the crystalline basement rock. Furthermore, tectonic events including extrusion of basaltic flows and intrusion of diabase sills, which prostdate basin-filling during early to late Jurassic, likely have played a significant role in post depositional processes that can trigger induced porosity and permeability within the basin. The fact that the observed regional changes in the porosity-depth trend (Figure 3.2) lack a uniform pattern suggest that these post-rift events may have occurred disproportionately within or in some parts

of the basin. This in turn may lead to variations in the degree of tectonically induced physical processes that may influence porosity/permeability-depth distributions.

The observed linear decrease of porosity with increasing depth (with a negative correlation of about 0.9) provides a good indication of strongly compacted SGR red beds formations (Figures 3.2 and 3.4). The compaction model implies a porosity of about 15% at the near surface and then decreases significantly for the Triassic sediments such as the ones from the Clubhouse Crossroad-3 and Dunbarton wells. The possible occurrence of the Clubhouse Crossroad-3 red beds to within few tens of meters to the underlying crystalline basement rock as implied in seismic refraction study by Ackermann (1983) also suggests strongly compacted sediments. In addition, the SGR basin has a history of magmatism and deformation that is so far has not been proven to be contemporaneous throughout the basin. The preserved extents of these magmatic and deformed rocks are variable and may be highly restrictive to some parts of the basin like the Clubhouse Cross Roads (Heffner et al., 2012, and Akintunde et al., 2013a,). The presence of these preserved magmatic bodies like the 256 m thick of basalt flows on top of the Triassic sediments in the Clubhouse Crossroad-3 (Akintunde et al., 2013b) and the inferred underlying crystalline basement rock (Ackermann, 1983) will increase sediment compaction. This in turn will lead to loss of porosity as observed in the unusually low porosity for the Clubhouse Crossroad-3 red beds (Table 3.1 and Figure 3.2).

The third and fourth observations, involving the non-linear behavior of the Norris Lightsey porosity-depth distribution as well as its unusually higher porosities and

permeabilities relative to the Clubhouse Crossroad-3 and Dunbarton red beds occurring at near similar depths, present an issue of scientific importance to the tectonic evolution of the basin. As reported in Marine (1974) , analysis of Triassic samples from 5 wells within Dunbarton show extremely low permeability ranging from 4.5 * 10-6 mD to 1.6 * 10-2 mD over the depth range of 1272 ft to 4260 ft. Moreover, an average porosity of 6.3% was recorded for all Triassic samples tested. Poor sorting supported by thin sections descriptions is obviously one of the reasons for the low permeability observed in the Dunbarton and the Clubhouse Crossroad Triassic samples (Marine, 1974; Gohn, 1983, and Akintunde et al., 2013b). Due to the lack of cores for the Norris Lightsey well, we could not perform a petrographic study to help ascertain whether or not the red beds sequence has been subjected to any significant alteration compositionally and texturally to have impacts on the present day porosity and permeability. What we do know from the core laboratory data (Core Lab. Report, 1984) is the presence of significantly high amounts of silt and clay in the Norris Lightsey samples, and which may be partly responsible for the low permeability. This high value (based on the data acquisition information from Core Laboratories, Inc.) may be partially due to a shattering of the matrix material by the impact of the sidewall sampling device. The strong correlation between the measured porosities and permeabilities (Figure 3.3) adds confidence to the reliability of the Norris Lightsey data.

Analysis of available well logs from the Norris Lightsey well that penetrate similar depth intervals covered by the laboratory-derived porosity and permeability data (Figure 3.5) does justify or support the observed trend from the core-derived porosities.

Except for the difference in the scale of measurements, the sonic-derived porosity values show values show high porosities as high as 20% around 4300 ft and values greater than 20% can be seen around 3200 to 3600 ft. We see a similar trend in the porosity-depth relationship from the laboratory-measured data (Table 3.1 and Figure 3.2). P-wave velocities derived from the Norris Lightsey acoustic travel time (sonic) log are between 4-5 km/s and these are lower than the 5.5-6.7 km/s reported for the Dunbarton Triassic sediments at 3000-4000 ft (Marine, 1974). This analysis shows that the Dunbarton red beds are more compact and rigid than the Norris Lightsey sediments, and hence the much lower porosity and permeability.

Furthermore, the Norris Lightsey area may be separated from other parts of the basin or occurs in association with a system of horst and grabens. This in turn can potentially alter the rock's physical properties in contrast with other parts of the basin examined in this study (Figures 3.1 and 3.2). This would undoubtedly strengthen previous studies showing that the SGR basin may not be a single extensional basin but a system of sub- basins, half-grabens and grabens (Heffner et al. , 2012, McBride et al., 1989, Petersen et al., 1984, and Talwani, 1977).

The presence of a pre-existing structure like a fault or a fracture zone capable of perturbing the pore pressure at depth can induce secondary porosity. Evidence for an abnormal pore pressure condition likely trigger by fluid trapped in faulted red beds can be seen in the observed sharp increase in acoustic travel time (sonic) log from about 78 to 157 µsec/ft (50% change) at around 3450 ft (Figure 3.6). The sonic-derived P-wave

velocity equally reduces by 50% from 4 to 2 km/s at this interval. This type of change in acoustic behavior at depth is often associated with a discontinuity or a break in the rock. The gamma ray readings around this zone varies between about 40 to 100 API that are typical of red beds consisting of interbedded mudstone/siltstone and sandstone and so the observed change in the acoustic travel time log does not indicate transition to a different rock type. There is no gas in this formation since the signature from the deep induction resistivity tool is low (below 100 ohm m) at this interval. An overlay of the Neutron-porosity and bulk density (Figure 3.6) does not produce any crossover which may suggest presence of a gas-filled formation. The presence of faulted/fractured red beds is what may/can trigger such a change in velocity/acoustic travel time. The implication is that the Norris Lightsey well may have been located on a fault-bounded half graben which could impact porosities and permeabilities at depth. At depths above and below 3450 ft (Figure 3.6), the red beds appear to be normally pressured and so the observed shift in the acoustic travel time at 3450 ft is likely a result of an abnormal pressure condition caused by faulting or fracturing in the red beds. Faulting or fracturing following original deposition creates voids or openings in the rock's pore space thereby increasing both porosities and permeabilities for potential fluid storage and movement.

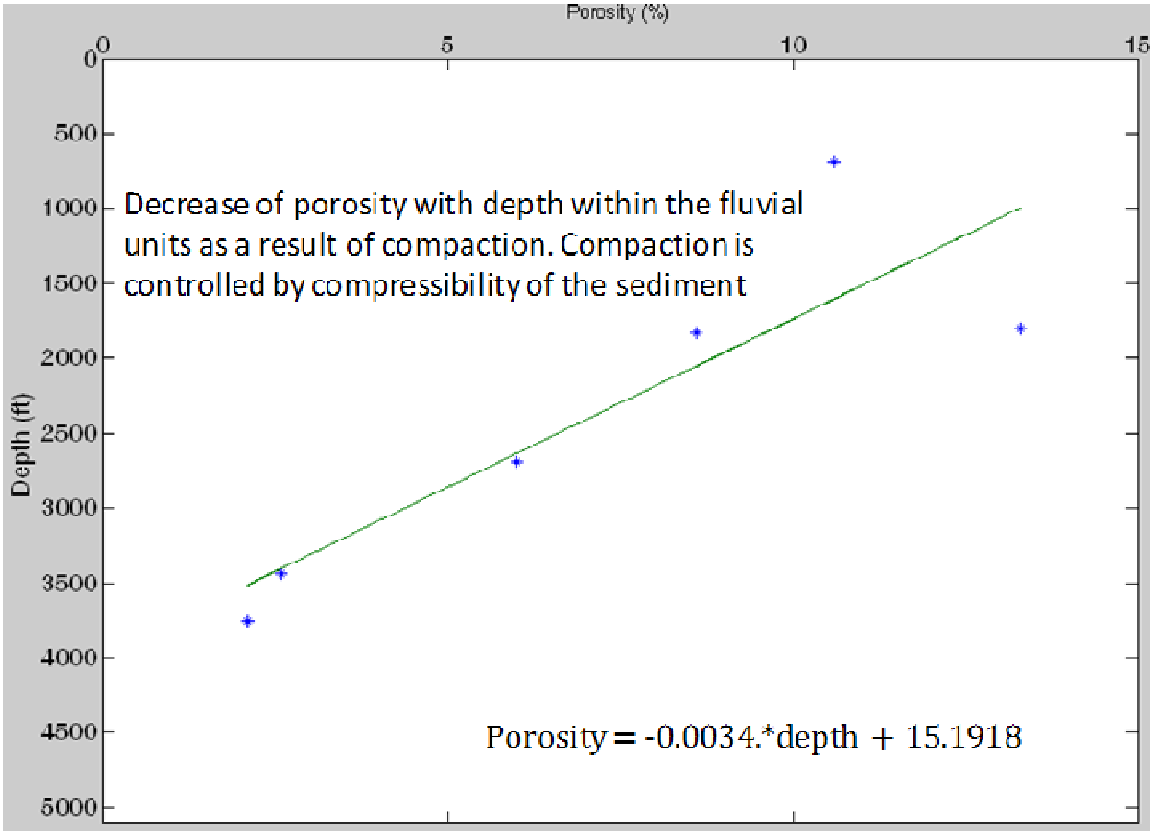

Figure 3.4: Linear decrease of porosity with depth (with correlation of -0.8712). This was observed for data points in other parts of the study locations with the exception of the Norris Lightsey that lacks significant correlation with depth.

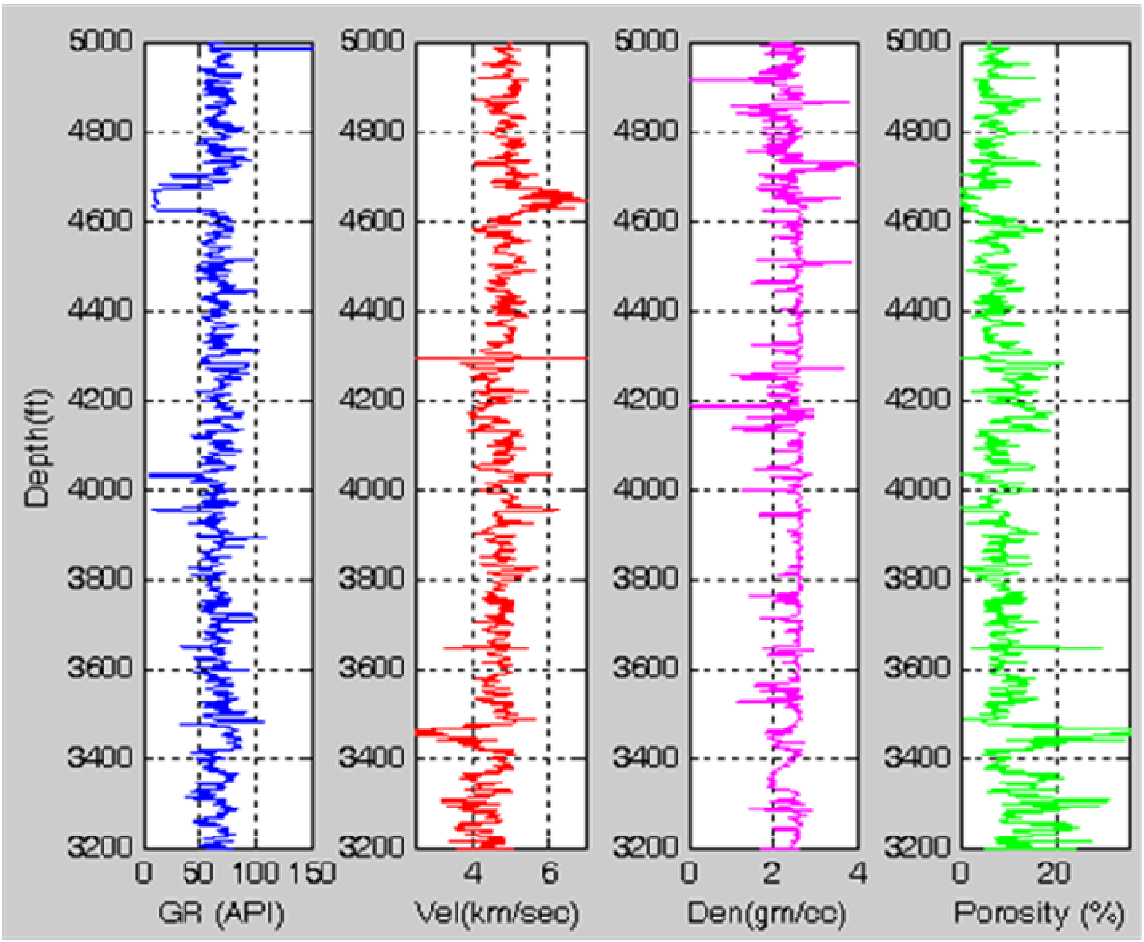

Figure 3.5: Plots of Gamma ray (GR), velocity, density and porosity from the Norris Lightsey well. The significantly low GR signatures and high velocity around 4650 ft is caused by diabase intrusion.

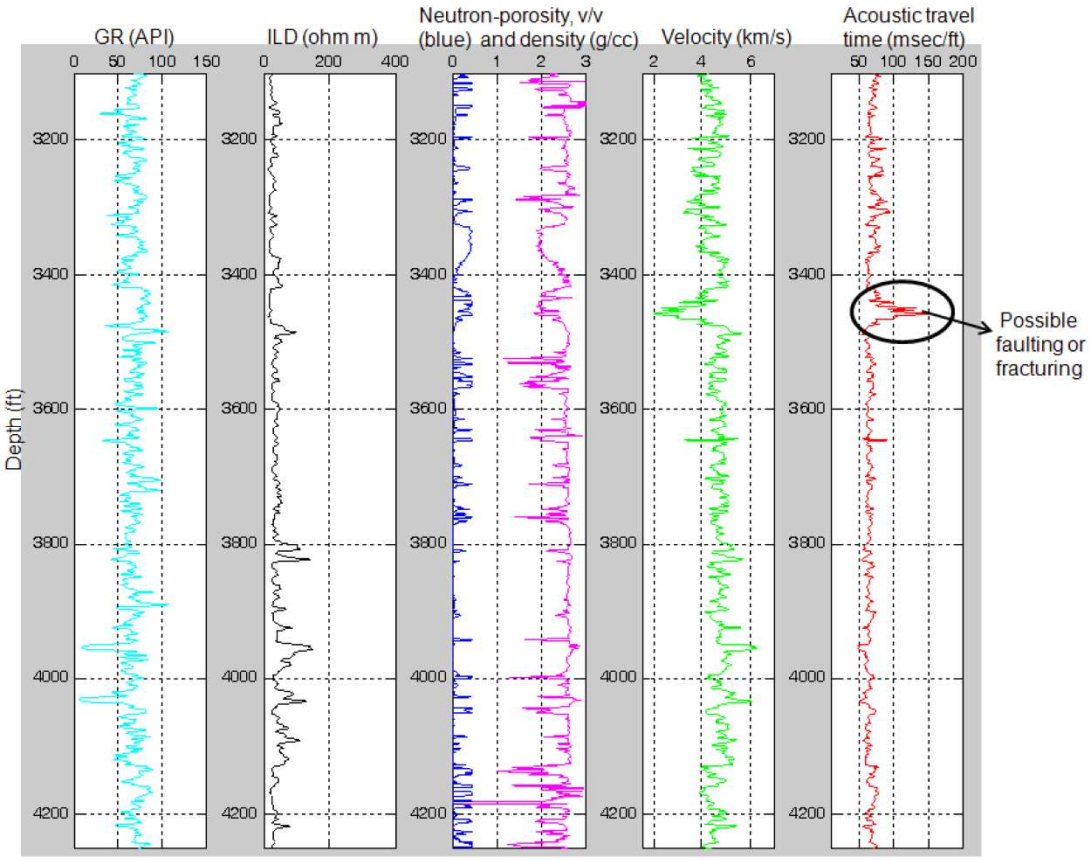

Figure3.6: Analysis of the acoustic travel time (sonic) log with other well logs provides petrophysical evidence for a possible structurally/fault-induced abnormal pore pressure condition at depth in the Norris Lightsey well.

3.8. CONCLUSIONS

Two regimes of porosity-permeability distribution are recognized within the Triassic-Jurassic SGR basin based on the interpretation of porosity/permeability depth profiles. The first regime, which is characterized by low porosities and permeabilities as well as manifests a linear dependency with depth, provides evidence for a compacted, deformed basin. The second regime, which appears to be restricted to the Norris Lightsey area of the basin, shows a non-linear dependency with depth. This non-

conformity to the normal compaction trend, in which porosities decrease linearly or exponentially with depth may likely result from altered or secondary porosities caused by faulting or fracturing at depth. The existence of these different regimes of porosity and permeability within the basin suggests the SGR basin may not be a single extensional basin but a subset of basins with presumably distinct geo-hydrologic systems. The observed low permeabilities throughout the basin suggest minimal risk with induced seismicity. The low permeabilities especially for the CC-3 well and Dunbarton are below the range of seismogenic permeability that can trigger induced seismicity with fluid injection (Talwani et al., 2007).

Furthermore, the depth dependencies of porosity/permeability distribution throughout the SGR basin is a function of tectonically induced post depositional processes such as compaction, uplift and erosion as well as possible faulting that have shaped the evolution of the SGR basin following the major phase of rifting.

CHAPTER FOUR

PERMEABILITY PREDICTIONS IN THE RED BEDS AND AN ANALYSIS OF THE EFFECTS OF CO_2 ON SEISMIC VELOCITY IN THE TRIASSIC RED BEDS

4.1. OVERVIEW

A key observation in the experimentally derived porosity and permeability data for the SGR red beds formations (Figure 2.1 and Table 2.3) is the significantly low permeability values (generally less than 1 mD), and the variations in these low values are significantly larger when compared to the variations in porosity between the study locations . This holds true regardless of the nature of the red beds facies (that is whether or not these are coarse-grained or fine-grained facies). The key issue is whether or not permeability can be uniquely predicted from porosity for these tight red beds. These red beds are characterized by sparsely distributed porosity and permeability based on the availability of data. Permeability predictions are necessary in the absence of information from well data to help provide insights into permeability changes at critical reservoir depths not covered or sampled by core analysis. The high cost ($10M - $100M) associated with drilling, logging and coring a new well for petrophysical characterization equally justify the need for permeability predictions to provide the basis for key, sensitive decisions about subsequent reservoir characterization requiring inputs from porosity and permeability.

Previous studies for permeability predictions have relied on the connection between permeability and other rock properties to establish a plausible correlation. Fabricius et al., (2007) show that while permeability cannot be derived alone from P-wave velocity or using the Vp/Vs (ratio of P-wave to S-wave velocities), combining Vp/Vs with porosity allow for permeability prediction in carbonates. Permeability predictions from sonic data and porosity have been presented by Klimentos and McCann (1990); Akbar et al. (1993), and Prasad (2003). And while Klimentos and McCann (1990) made a case for a possible correlation between permeability and P-wave attenuation, Prasad (2003) disputed/contradicted this claim. Overall, existing permeability predictive models are often site-specific and data dependent, and so it is important to assess whether or not existing models would work for the SGR's poorly sorted, fine-grained and coarse grained red beds, and what modifications would be needed to boost reliability or accuracy of predictions.

The existence of distinct porosity-permeability regimes and the strong correlation between porosity and permeability within the SGR's lacustrine deposits are explored to derive a relationship between porosity and permeability. Existing models such as the modified Kozeny-Carman relation (Mavko and Nur, 1997) and the method of Flow Zone Indicator (FZI) (Prasad, 2003) were also employed to assess reliability of permeability predictions for the SGR red beds. Permeability predictions from porosity alone and from the method of FZI were subsequently applied to well data from the Norris Lightsey to provide insights into reservoir changes at depths not covered by core-derived laboratory data. An attempt to predict permeability from resistivity was

undertaken and the results show a close match between predicted and measured permeability.

4.2. INTRODUCTION

Permeability expresses the ease or difficulty with which a reservoir allows for passage of a fluid. It is a physical rock property that is controlled primarily by the pore throat which is a function of the pore space (Schon, 2011, Mavko et al., 2003, Dvorkin et al., 2009). Darcy (1856) expressed permeability for a cylindrical core/rock sample (with length L and cross sectional area A) as the ratio of the product of the flow per unit time (in cm/s) and viscosity μ (in cp) to the products of the cross sectional area (in cm^2), the pressure drop across the sample and the reciprocal of the length of the rock. The physical expression for permeability follows from Darcy (1856).

$$k = Q\mu/A(\Delta P/L) \qquad (4.1)$$

where: K = permeability in darcy (unit) , Q= flow per unit time in cm/s, μ is the dynamic viscosity of the fluid (cp), A is the cross sectional area of the rock in cm^2, L is length in cm and ΔP is the pressure drop across the sample.

Unlike permeability, which is a function of the volumetric and geometrical properties as well as connectivity of the pores within a rock (Prasad, 2003, Alam et al., 2011), porosity depends primarily on the volume property of the rock. It is the ratio of the pore volume to the total volume of the rock. In general, permeability as a volume property of a rock should relate with porosity and by implication can be influenced by grain size, shape and sorting. A rock with large and uniformly rounded grains typically

exhibits high porosity and permeability. However, poor sorting and presence of fine grain materials like clay will reduce permeability even if the porosity is high. Cementation, compaction and/or lithification as well as fracturing (especially in non-clastic formations) are other factors that can alter the primary or original permeability of a rock.

Core derived permeability values for the SGR red beds (Table 3.1) are very low and generally less than 1Md for most study locations making these red beds to be classified as tight reservoirs. Compositionally, these confined red bed units are heavily mixed with siltstone and mudstone (Figure 4.1) that generally favors low permeability. The lack of in-situ permeability data from the available deep drilled wells within the basin hampers the ability to understand changes at strategic subsurface depths.

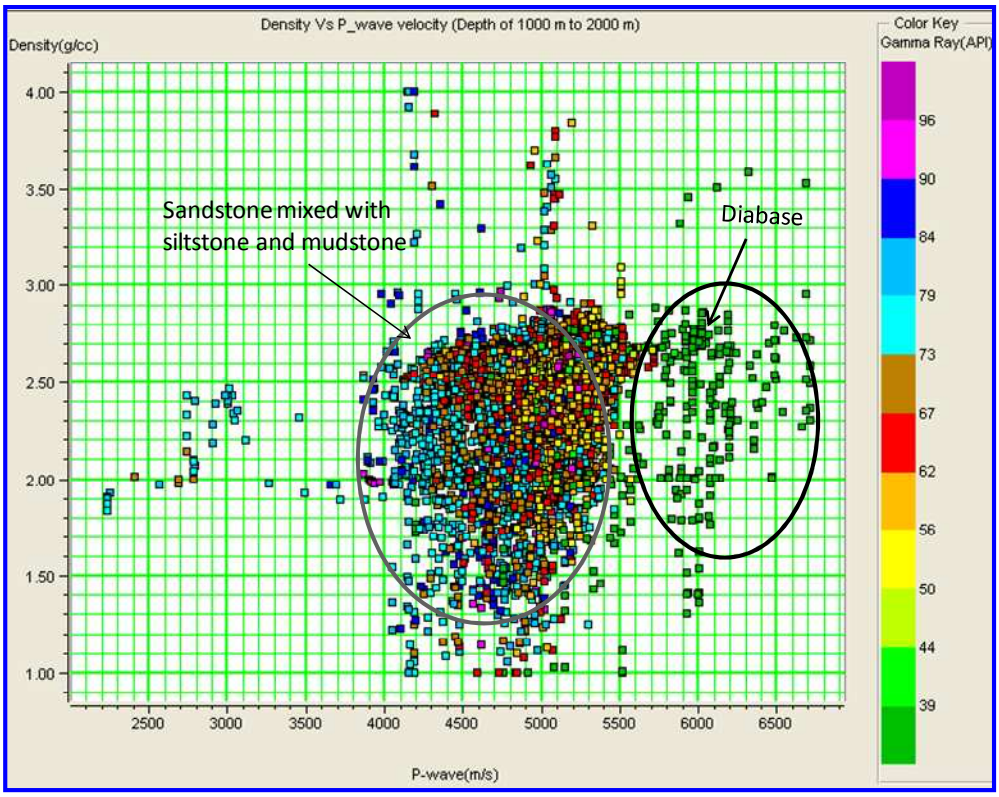

Figure 4.1: Lithologic composition of the red beds showing siltstone and mudstone

For reservoir characterization studies for oil and gas exploration and CO_2 storage that often require estimation of reservoir storage capacity as well as amount of recoverable hydrocarbon or amount of fluid injectivity, understanding and quantifying permeability changes at well logging scale become critically important. Permeability estimates at the reservoir level can or may subsequently be extended or upscaled to the seismic scale to accommodate areas not sampled by the well. This can be done through implementation of appropriate rock physics transforms from core scale to reservoir scale and then to seismic scale using statstical rock physics to help account for uncertainties.

Furthermore, existing approaches to permeability predictions are usually data dependent and site specific, and as such may have to be modified to be applicable to a given site. Moreover, these existing techniques like the Kozeny Carman relation (Kozeny, 1927 and Carman, 1937) do have limitations that may limit the reliability or accuracy of predictions. The tight nature of the SGR's red beds, their general lack of sorting and poor rounding of grains may present a significant challenge to the applicability of these models. In this study, we demonstrate rock physics relation relations based on the use of porosity data, and a combination of porosity and resistivity for permeability predictions in the SGR's red beds. Details of the strategies and assumptions adopted for these predictions are presented.

This chapter also contains fluid substitution modeling to provide an understanding of the impact of CO_2 saturation on seismic velocity. This will be necessary to aid the design of appropriate and cost effective monitoring strategy should CO_2 injection be undertaken. Whether or not time-lapse seismic technology, which is the common practice for reservoir fluid monitoring, can be deployed would depend on the degree of seismic sensitivity to time-dependent, dynamic reservoir changes arising from the interactions of CO_2 with the brine-filled reservoir. Fluid substitution based on the use of Gassmann's equation (Gassmann, 1951) was carried out to help predict changes in seismic velocity with uniform CO_2 saturation.

4.3. EXISTING APPROACHES TO PERMEABILITY PREDICTIONS

1. Permeability from Porosity:

Historically, the first attempt at successful prediction of permeability from porosity and specific surface area was conducted by Kozeny (Kozeny, 1927; Prasad, 2003, and Alam et al., 2011). The Kozeny derivation discussed below was extracted from Schon (2011). The derivation was based on a porous rock sample consisting of cross-sectional area A and length L. The length is made up of a number, n, of straight capillary tubes in parallel, and with the spaces between the tubes sealed by a cementing material. Assuming the capillary tubes are all of the same radius r (cm) and length L (cm), the flow rate q (cm^3/s) through this bundle of tubes according to Poiseuille's equation is:

$$q = \left(\frac{n\Pi r^4}{8\mu}\right)\frac{\Delta P}{L} \qquad (4.2)$$

where the pressure loss ΔP over length L is expressed in dynes/cm^2. The flow of fluids through these n capillaries can also be approximated by Darcy's law as:

$$q = \left(\frac{\kappa A_C}{\mu}\right)\frac{\Delta P}{L} \qquad (4.3)$$

where AC is total cross sectional area, including cemented zones, of this bundle of capillary tubes. Using equations (4.2) and (4.3) and solving for k gives:

$$k = \frac{n\Pi r^4}{8A_C} \qquad (4.4)$$

The porosity is given by:

$$\phi = \frac{V_p}{V_b} = \frac{n\Pi r^2 L}{A_C L} = \frac{n\Pi r^2}{A_C} \qquad (4.5)$$

Substituting $A_C = n\mathbf{\Pi}r2/\phi$ from equation 4.5 into equation 4.4 will give a simple relationship between permeability and porosity for pores of the same size and radii equal to r:

$$k = \frac{\phi r^2}{8} \qquad (4.6)$$

Where k is in cm^2 (1 cm^2 = 1.013 x 10^8 darcy) or in μm^2 (1mD = 9.871 x 10-4μm^2) and ϕ is a fraction. Let s_{Vp} be the internal surface area per unit of pore volume, where the surface area As for n capillary tubes is $n(2\mathbf{\Pi}rL)$ and the pore volume Vp is $n(\mathbf{\Pi}r^2L)$.

Therefore:

$$S_{V_P} = \frac{A_S}{V_P} = \frac{n(2\Pi rL)}{n(\Pi r^2)L} = \frac{2}{r} \qquad (4.7)$$

If SVgr is the specific surface area of a porous material or the total area exposed within the pore space per unit of grain volume, then for a bundle of capillary tubes, the total area exposed, At, is equal to the internal surface area As; and the grain volume, Vgr, will be AcL(1-ϕ). Therefore:

$$S_{V_{gr}} = \frac{n(2\Pi rl)}{A_c L(1-\phi)} = \frac{2\Pi rn}{A_c(1-\phi)} = \frac{n\Pi r^2}{A_c}\left(\frac{2}{r}\right)\frac{1}{1-\phi} \qquad (4.8)$$

A combination of equations 4.6, 4.7 and 4.8 gives:

$$S_{Vgr} = S_{VP}\left(\frac{\phi}{1-\phi}\right) \qquad (4.9)$$

Equation 4.6 can be expressed as:

$$k = \left(\frac{\phi}{2}\right)\frac{1}{(2/r)^2} = \left(\frac{1}{2s_{Vp}^2}\right)\phi \qquad (4.10)$$

Substituting for svp from Equation 4.10 yields:

$$k = \left(\frac{1}{2s_{vgr}^2}\right)\frac{\phi^3}{(1-\phi)^2} \qquad (4.11)$$

According to Schon (2011), the above equations are based on the assumption that the porous rock can be represented by a bundle of straight capillary tubes. However, the average path length that a fluid particle must travel is actually greater than the length L of the core sample. The departure of a porous medium from being made up by a bundle of straight capillaries can be measured by the tortuosity coefficient, τ, which is expressed as:

$$\tau = \left(\frac{L_a}{L}\right)^2 \qquad (4.12)$$

where La is actual flow path and L is the core length. Thus, for a bundle of tortuous capillary tubes, Poiseuille's law becomes:

$$q = \left(\frac{n\Pi r^4}{2\mu}\right)\ \frac{\Delta P}{L\sqrt{\tau}} \qquad (4.13)$$

Combining this equation with Darcy's equation (equation 4.3) and using the same approach as above, one can show that Equations 4.6, 4.10 and 4.11, respectively become:

$$k = \left(\frac{r^2}{8\tau}\right)\phi \qquad (4.14)$$

$$k = \left(\frac{1}{2\tau s_{vp^2}}\right)\phi \tag{4.15}$$

$$k = \left(\frac{1}{2\tau s_{vgr^2}}\right)\frac{\phi^3}{(1-\phi)^2} \tag{4.16}$$

where k is permeability in μm^2, ϕ is porosity, τ is tortuosity, and S_{vgr} is the specific surface area per unit grain volume. The product 2τ is equivalent to the Kozeny constant, Kz. Carman reported that the values of Kz can be approximated by 5 for most porous materials. In as much as Kz = Ksτ = 5, equation 15 can be written as follows:

$$k = \left(\frac{1}{5 s_{vgr^2}}\right)\frac{\phi^3}{(1-\phi)^2} \tag{4.17}$$

As stated in Schon (2011), Equation 4.16 is the most popular form of Kozeny equation, but in practice K_z is variable and much greater than 5 for a porous rock. According to Prasad 2003, equation 4.16 assumes that the pores are cylindrical with circular cross-sections, and that some authors such as Amaefule et al. (1993) came up with a modified expression for equation 4.16 to include different pore shapes as shown in equation 4.18 below.

$$k = \left(\frac{1}{F_s K_z s_{vgr}^2}\right)\frac{\phi^3}{(1-\phi)^2} \tag{4.18}$$

The Mavko-Nur modification of the Kozeny-Carman expression (Mavko et al., 2003) is expressed as follows:

$$k = \left(\frac{d_{Mean}^2}{72\tau^2}\right)\frac{\left(\phi-\phi_p\right)^3}{\left[1-\left(\phi-\phi_p\right)\right]^2} \tag{4.19}$$

where d_{Mean} is the mean grain size; τ is tortuosity, ϕ is the total porosity and ϕ_p is the percolation porosity. Percolation porosity is the porosity when the pore is disconnected and does not contribute to flow. It is between 1 to 3% (Mavko et al., 2003).

A further modification of the Kozeny-Carman relation which enables grouping of porosity and permeability units as flow zone indicators was introduced by Amaefule et al. (1993) and employed in Prasad (2003), and Alam et al., (2011). The Flow Zone Indicator (FZI) is related to the reservoir quality index, can be computed from measured porosity and permeability and may account for the inherent limitations in the Kozeny equation in 4.14. To do this for a simple capillary model, the pore radius can be described in terms of the specific internal surface to yield (Schon, 2011):

$$S_{pore} = \frac{2\pi r}{\pi r^2} = \frac{2}{S_{pore}} \; or \; r = \frac{2}{S_{pore}} \qquad (4.20)$$

Substituting equation 4.20 into equation 41.4 above yields permeability k to be

$$k = \frac{1}{8}\,\phi\frac{r^2}{\tau^2} = \frac{1}{2}.\phi.\frac{1}{S_{pore}^2}.\frac{1}{\tau^2} \qquad (4.21)$$

Further adjustment to equation 4.21 to account for the shape and geometry of the pore channels results in

$$k = \frac{1}{Fs.\tau^2}.\phi.\frac{1}{S_{pore}^2} \qquad (4.22)$$

where the quantity $FS.\tau^2$ represents the shape and geometry of the pore and is referred to as the Kozeny constant ($Kz = Fs.\tau^2$). Permeability is also dependent on the pore body radius in addition to the pore throat radius. Equation 4.22 can be modified by adding the ratio of pore throat to pore radius (Γ) to give

$$\sqrt{\frac{k}{\phi}} = \frac{\Gamma}{2\sqrt{FS}} . \frac{r}{\tau} = \frac{\Gamma}{\sqrt{FS}} . \frac{1}{\tau} \frac{1}{S_{pore}} \qquad (4.23)$$

In defining the Reservoir Quality Index (RQI), Leverett (1940) equated the expression sqrt(k/ϕ) as a rock property. Thus equation 4.23 can be re-written as

$$\sqrt{\frac{k}{\phi}} = \frac{\Gamma}{2\sqrt{FS}} . \frac{r}{\tau} = \frac{\Gamma}{\sqrt{FS}} . \frac{1}{\tau} \frac{1}{S_{pore}} \qquad (4.24)$$

The right hand side of equation 4.24 indicates that the term sqrt (k/ϕ) is controlled by specific internal surface or pore size, tortuosity, pore shape, and pore-throat to pore-body ratio. Consequently, it encompasses relevant textural properties that control permeability. Altunbay et al. (1997), and Prasad (2003) defined the RQI as follows (and with permeability expressed in mD)

$$RQI = 0.0314 \sqrt{\frac{k}{\phi}} \qquad (4.25)$$

A simplification of equation 4.18 by Amaefule et al. (1993) enables the RQI to be expressed in terms of the FZI as follows:

$$\log(RQI) = log\ (\epsilon) + \log(FZI) \qquad (4.26)$$

where ϵ is the ratio of the pore volume to grain volume and is defined as

$$\epsilon = \frac{\phi}{1-\phi} \tag{4.27}$$

The FZI is given by

$$FZI = \frac{1}{\sqrt{F_s}\tau S_{Vgr}} \tag{4.28}$$

FZI can be also be expressed as

$$FZI = \frac{0.0314}{\epsilon}\sqrt{\frac{k}{\phi}} \tag{4.29}$$

Equation 4.29 relates the RQI to the ratio of the pore volume and grain volume. According to Prasad (2003), reservoir units with FZI values within a narrow range belong to one hydraulic unit that is these have similar pore throats and will therefore form a flow unit.

2. Permeability from Velocity

By grouping and sorting rocks into hydraulic units which are based on pore space properties, Prasad (2003) shows that permeability can be reliably predicted from velocity. In this work (Prasad, 2003), the pore space properties were developed from flow zone indicators derived from measured values of porosity and permeability. Prasad (2003) further demonstrated that attenuation, though equally affected by pore geometry, is not a good predictor for permeability. Another example of permeability prediction from velocity based on a case study from North Sea Chalk was discussed in Alam et al. (2011).

3. Permeability-Pressure/Stress Relationship

In general, permeability decreases with increasing confining stress and/or increasing effective/differential pressure due to closure of pores and cracks within the rock. Schon (2011) reported a non-linear decrease of permeability with pressure with changes in permeability more significant at lower confining stresses and less significant at higher effective pressures (Fatt, 1953). In addition, the pressure dependence of permeability is stronger in weak, unconsolidated sedimentary rocks or fractured rocks than more lithified, and well consolidated rocks (Schon, 2011). The lithified nature of the SGR red beds may not allow for significant sensitivity of permeability to changes of effective pressure under the influence of confining stress. This can change under dynamic conditions. Permeability changes measured under low confining stresses for the Berkeley sandstone (Figure 4.2) show a linear decrease with confining stress.

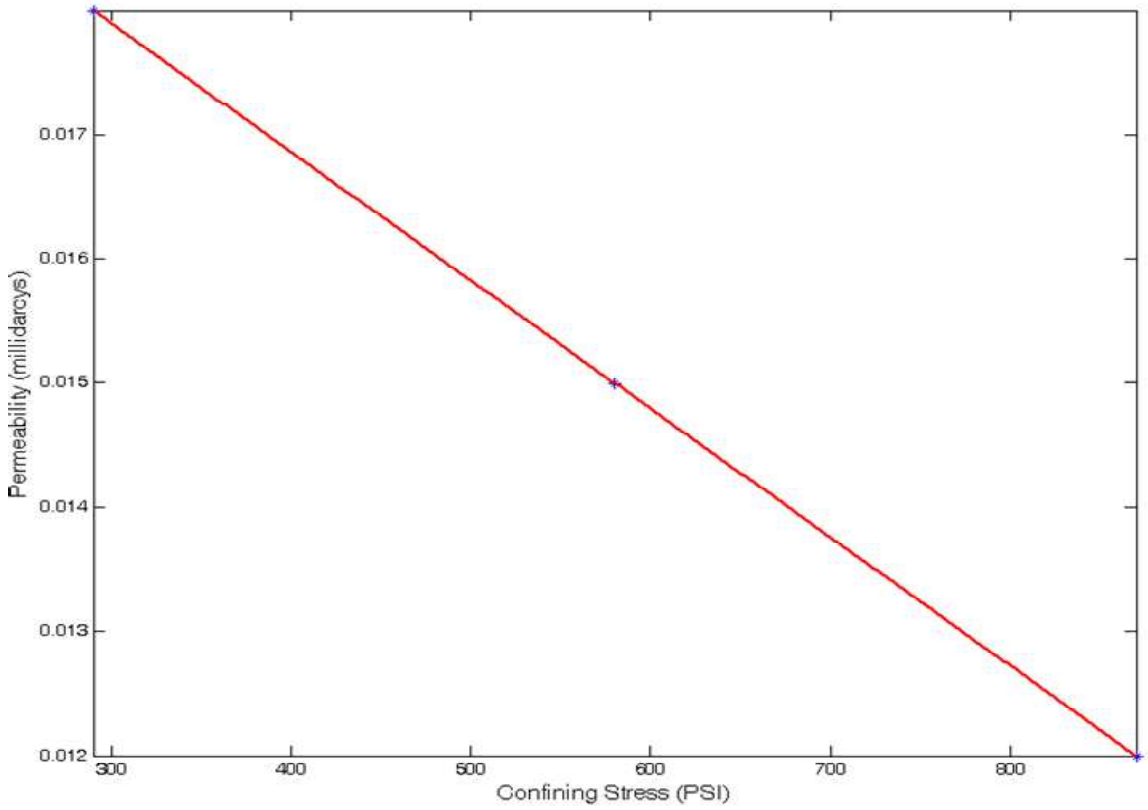

Figure 4.2: Permeability as a function of confining stress in the Berkeley sandstone/red beds in South Carolina.

4. Permeability from Electrical Resistivity

Attempts have been made in the past by several authors (Archie, 1942; Worthington, 1997;, Katz and Thompson, 1986; and Gomez et al., 2010) to calculate permeability from resistivity. The resistivity-permeability relations from these authors typically employ the formation factor, amount of clay content, and other predetermined information about pore geometry such as grain size, specific surface area, tortuosity and the cementation factor or exponent. A recent study by Gomez et al. (2010) suggests that establishing a strong correlation between resistivity and permeability is quite difficult

due to large data scatter between formation factor and resistivity, especially at low porosity (Archie, 1942; and Gomez et al., 2010).

4.4. METHODS AND RESULTS OF PERMEABILITY PREDICTIONS IN THE RED BEDS

The existence of distinct porosity-permeability regimes within the SGR basin provides a clue to establish a unique correlation between porosity and permeability since existing empirical relations to predict permeability from porosity are usually site-specific. The sparsely distributed nature of data, as well as the large variations between porosity and permeability for the fluvial and fluvial-alluvial deposits (Figure 4.3) does not allow a good, linear correlation to be established.

On the other hand, the porosity-permeability distribution for the lacustrine deposits from the Norris Lightsey (Figure 4.4) shows a strong correlation between these porosity and permeability. By assigning a grain size of 250 μm, tortusoity 2.5 and percolation porosity 0.03, the modified Kozeny-Carman relation (equation 4.19; Mavko et al., 1998) appears to significantly predict permeability (with a correlation of 0.9) from the core derived porosity for the Norris Lightsey red beds (Figure 4.4). Grain sizes 200 μm and 300 μm under predict and over predict permeability derived from the Kozeny-Carman relation when compared with the measured values (Figure 4.4). The modified Kozeny-Carman estimates based on grain size 250 μm closely match the predicted permeability by linear fit (Figure 4.4). The fit between porosity and permeability for the Norris Lightsey significantly predicts the calculated permeability values from the measured values (Figure 4.5). The implication of this result suggests that permeability

may be uniquely predicted from porosity in tight clastic rocks exhibiting same depositional environment and without significant variations in the spatial distribution of porosity and permeability. Assuming the effects of the pore geometry and connectivity are negligible since these are poorly sorted samples, a reliable prediction can be implied.

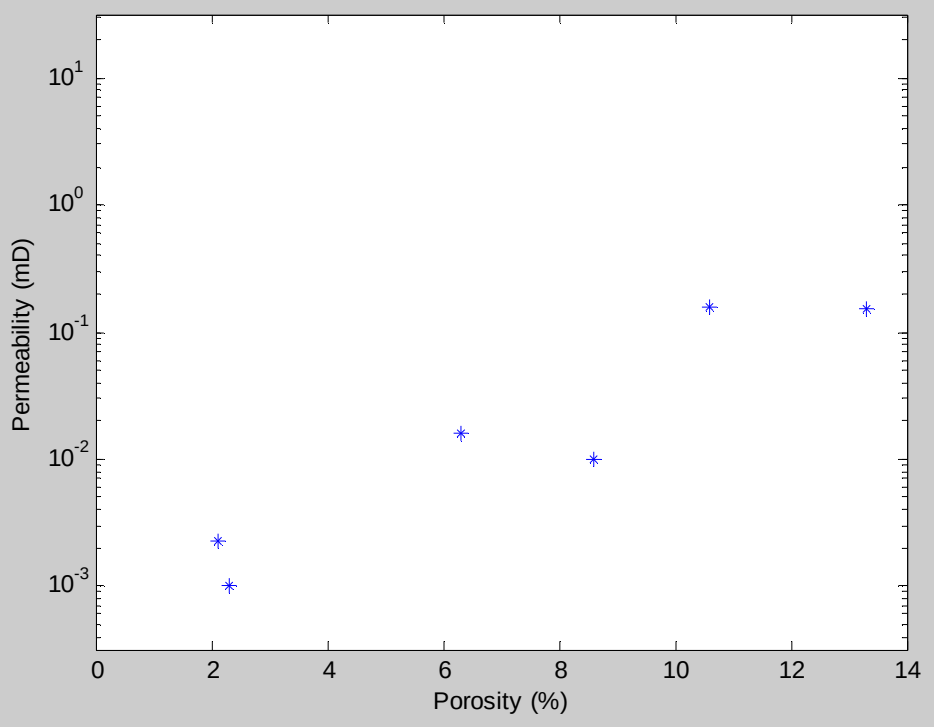

Figure 4.3: Permeability-porosity relationship for the fluvial and/or fluvial-alluvial deposits within the SGR basin.

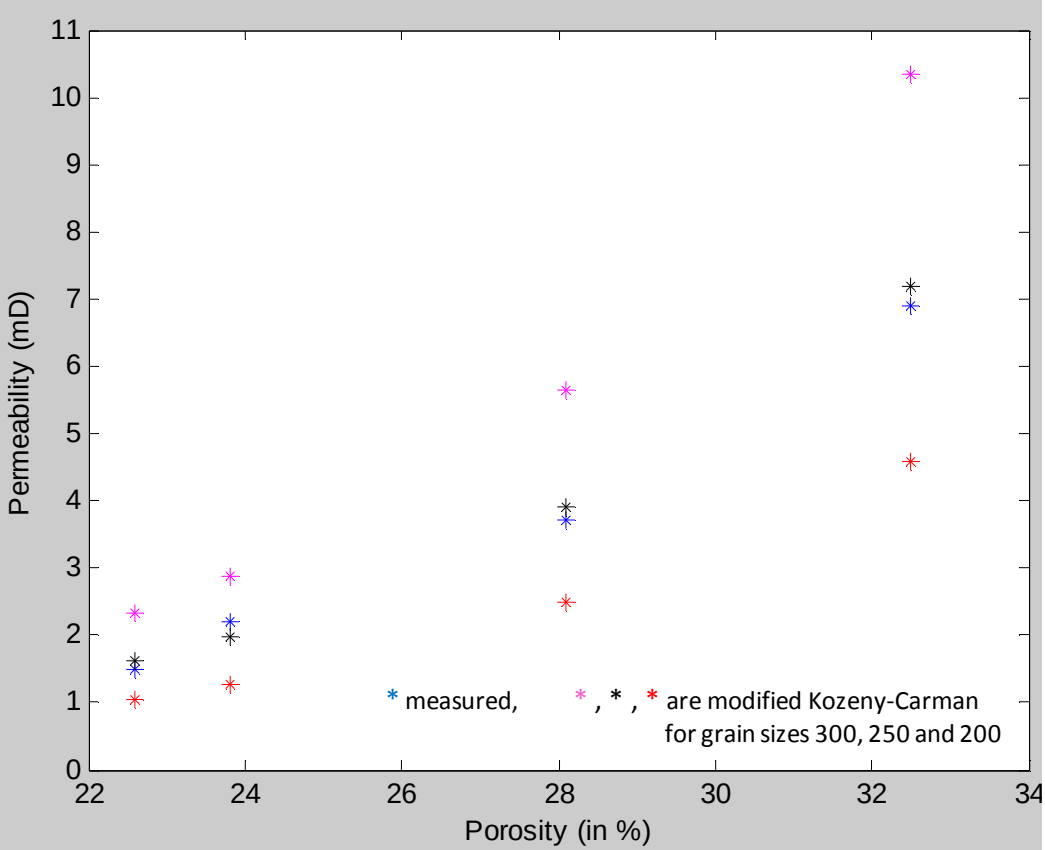

Figure 4.4: Porosity-Permeability distribution for the Norris Lightsey Red beds showing measured permeability as well as the ones calculated using the modified Kozeny-Carman relation.

Extending the linear fit derived for the permeability prediction to the log scale allows for changes in permeability with depth to be seen (Figure 4.6). The observed changes are consistent with changes seen in the resistivity, velocity and porosity logs (Figure 4.6). The Flow Zone Indicator (FZI) approach based on equation 4.29 allows for a division of the porosity and permeability data for the SGR red beds into flow zone units shown in figure 4.7. Majority of the data (especially the Norris Lightsey data) falls within

the FZI of 0.35. By applying FZI 0.35 enables a reasonable prediction of permeability changes with depth at reservoir scale (Figure 4.8).

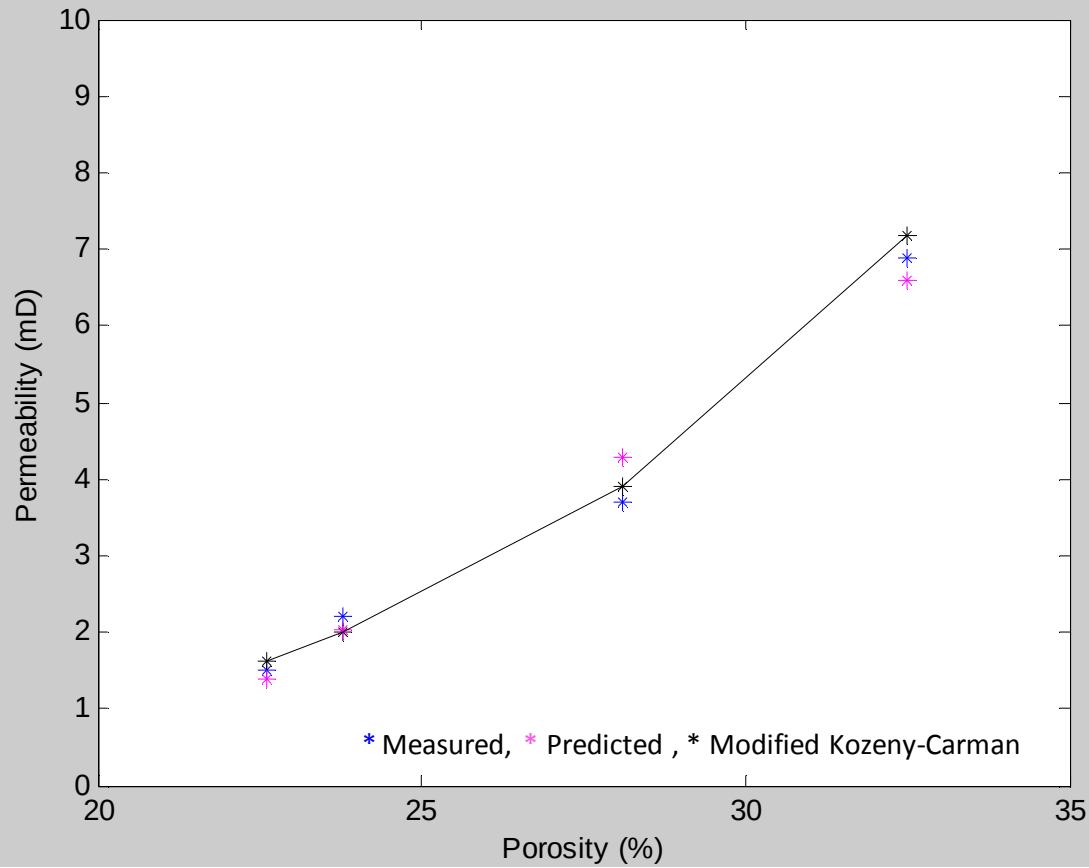

Figure 4.5: Permeability versus Porosity for the lacustrine red beds within the SGR basin. Correlation equation gives permeability = 0.5255 * porosity – 10.4818.

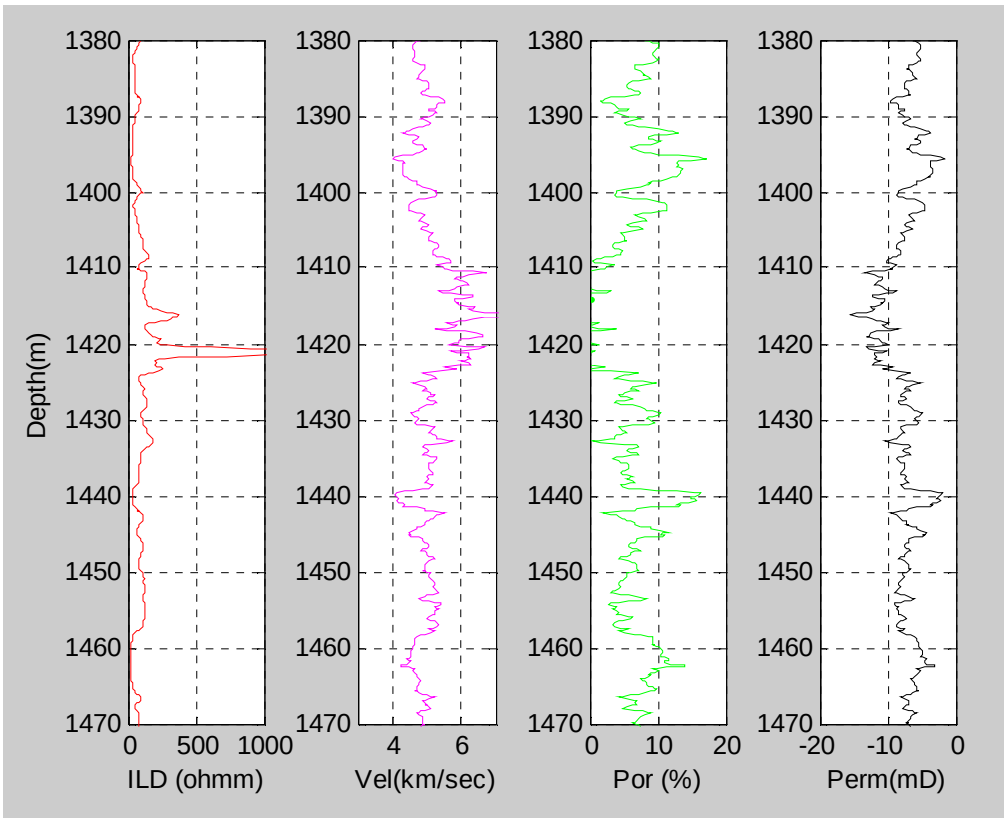

Figure 4.6: Predicted permeability at the reservoir scale using Kozeny-Carman. The observed highs in the ILD, Vel and the lows seen in the Por log at around 1420 m are due to presence of diabase. Porosity changes within the red beds units around 1400, 1440 and 1465 m are significant. Notice that the derived permeability follows same trend as the porosity log.

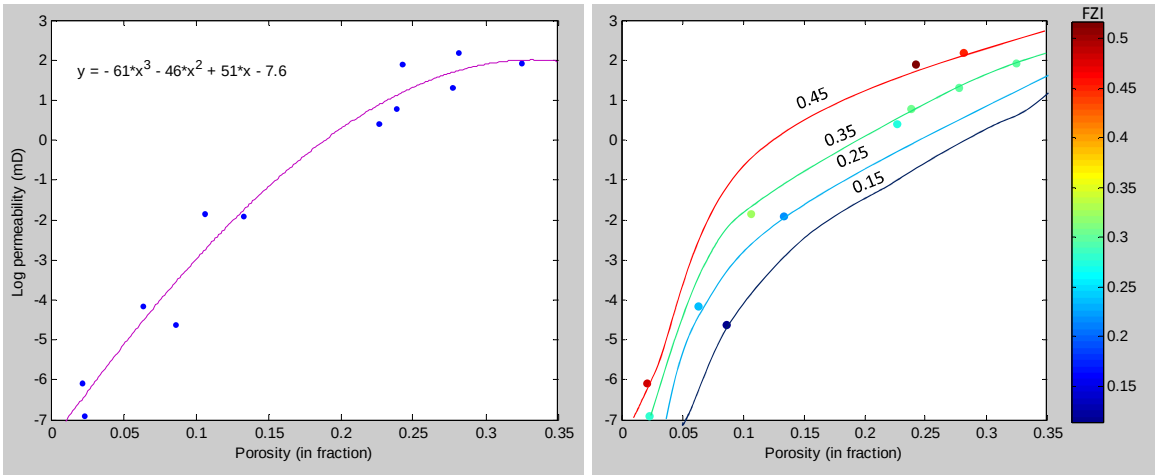

Figure 4.7: Permeability based on the concept of Flow Zone Units (FZI). The FZI computed from equation 4.19 are shown on the right. The flow zone intervals are shown by different colors in the color bar.

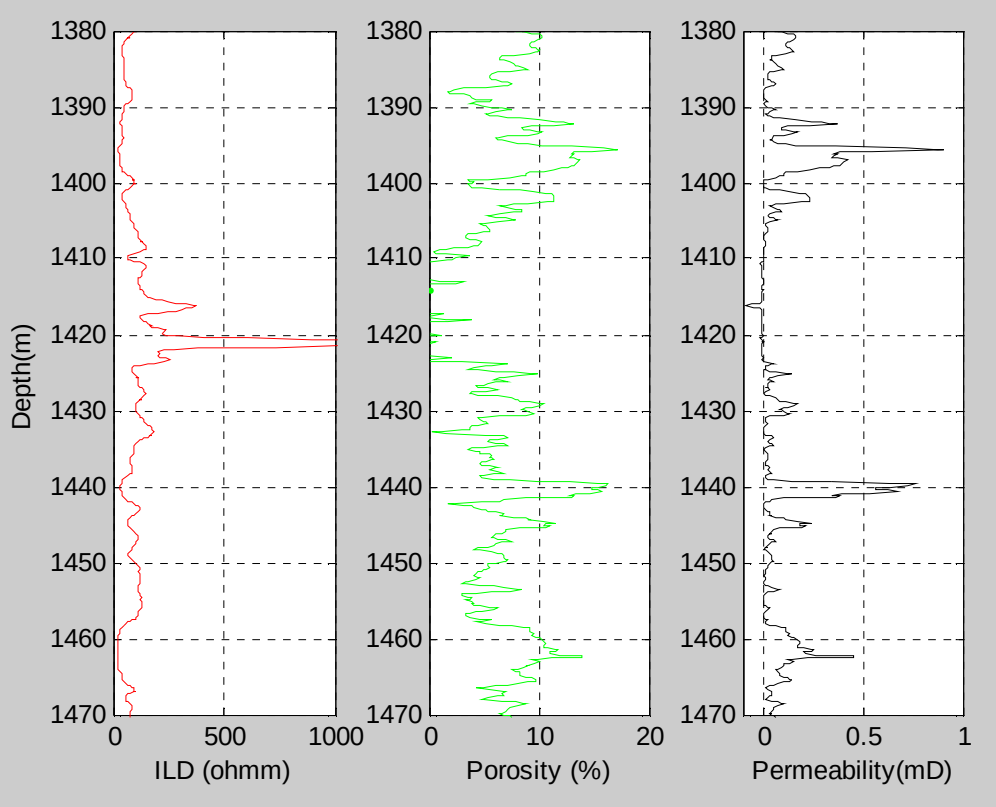

Figure 4.8: Predicted permeability changes at the reservoir scale using flow zone interval 0.35 (as shown/computed in Figure 4.7 above).

The third approach is to predict permeability from resistivity using the available data from the Norris Lightsey. In general, the resistivity of a rock is influenced by factors that such as resistivity of the pore fluid, porosity and degree of water or brine saturation, temperature, tortuosity or distribution of pore channels as well as the composition of the rock. The factors do control permeability, and hence it may be possible to establish a link between resistivity and permeability. Mathematically, the ratio of the resistivity of the rock when filled with 100% water (R_O) to the resistivity of the pore water (R_w) is a constant defined by the Formation Resistivity Factor F. The Formation factor F is related to porosity based on Archie (1942) as follows:

$$R_O = FR_W \qquad (4.30)$$

$$F = {}^{a}/_{\phi^m} \qquad (4.31)$$

where a and m represent the cementation exponent and the tortuosity, respectively. For sandstone (which is the case in this study), a = 1.13 and m = 1.73 according to the Timur equation (Timur, 1968). R_O is related to the true resistivity or measured resistivity at water saturation S_w and at saturation exponent n of 2 (Gomez et al., 2010) by the relation below

$$R_O = R_t {S_w}^n \qquad (4.32)$$

Using equation 4.31 based on the Timur expressions for sandstone, and the porosity data from the Norris Lightsey , the formation factor F was calculated. The values of F subsequently used to determine the resistivity of the brine-saturated rock R_O. Assuming 100% water saturation, R_o will be the same as R_t from equation 4.23 above. Rw estimated to be about 0.09 ohm m from the Schlumberger Log interpretation charts-Gen 9 (Schlumberger, 2000) based on a predetermined brine concentration of about 35, 000 PPM of Nacl at borehole temperature 149 ^{0}F for the Norris Lightsey well. A plot of the resistivity of the brine-saturated rock R_O versus porosity is shown in Figure 4.9. The relationship allows porosity to be determined from resistivity as well. By substituting porosity as a function of resistivity into the empirical relationship between porosity and permeability in Figure 4.5, permeability can be determined from the core-derived resistivity values as shown in Figure 4.10. The permeability-resistivity plot shows similar trend to the porosity-resistivity trend (Figure 4.9). The permeability prediction from

resistivity appears quite close with the measured values but not for all data points (Figure 4.11).

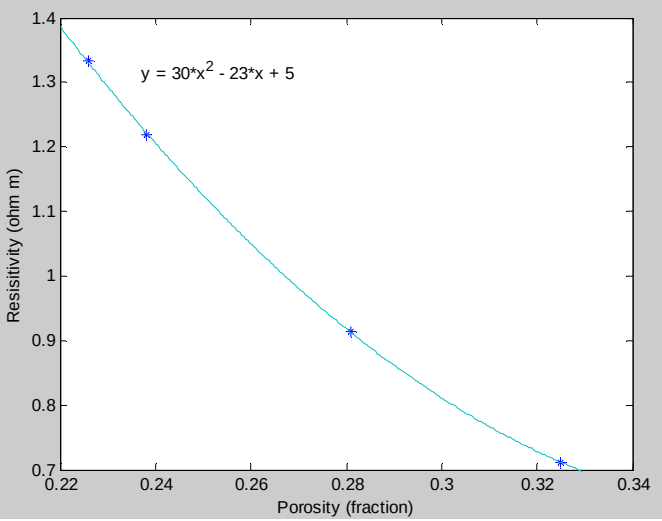

Figure 4.9: Resistivity-Porosity Relationship for the Norris Lightsey data.

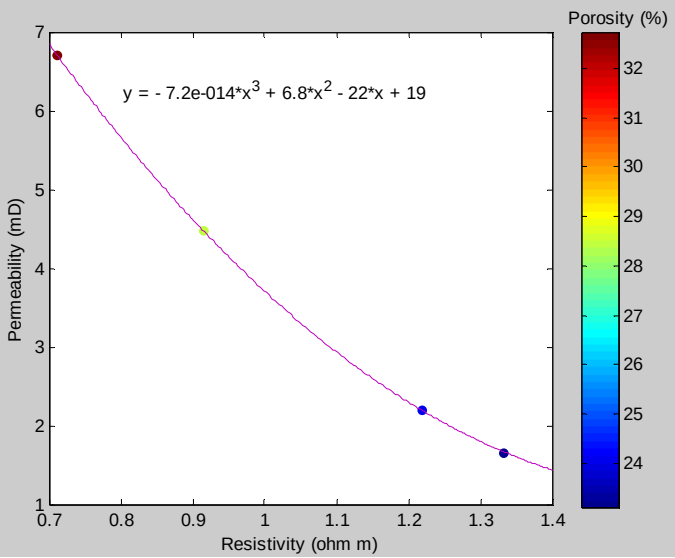

Figure 4.10: Predicted permeability versus resistivity color coded by porosity.

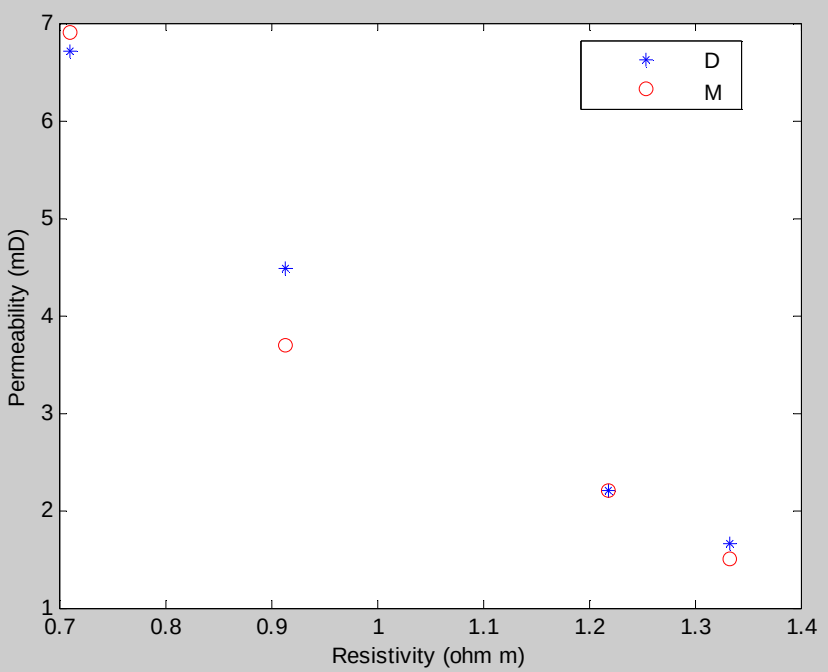

Figure 4.11: Resistivity-derived permeability (D) versus measured resistivity (M)

4.5. DISCUSSION OF RESULTS OF PERMEABILITY PREDICTIONS

Within the limits of available core-derived laboratory data, four different approaches for permeability predictions for the red beds within the SGR basin have been attempted. Firstly, by taking advantage of the distinct porosity permeability regimes within the basin, a strong correlation between porosity and permeability can be established for the Norris Lightsey lacustrine red beds (Figure 4.5). The strong correlation obtained between the measured permeability and the porosity-derived permeability (Figure 4.5) indicates this relationship can be explored to uniquely predict permeability from porosity in tight sandstones with similar textural composition as the case of the Norris Lightsey lacustrine deposits. Secondly, the predicted permeability from the modified Kozeny-Carman relation also shows a good match with the measured permeability (Figure 4.5). The draw back with the porosity-derived permeability and the

Kozeny-Carman derived estimates is that both approaches do not seem to work for all the data sets from the identified depositional environments within the basin. The sparsely distributed nature and large variations in the regional distribution of measured porosity and permeability within the basin do not favor predictions from porosity alone as well as by using the modified Kozeny-Carman relation (Mavko and Nur, 1997). Using the FZI approach (Figure 4.7) help overcome these shortcomings and permeability changes at depth at the reservoir scale can be predicted (Figure 4.8). The predicted permeability changes at the reservoir scale are generally which is consistent with in-situ laboratory measurements and generally follow the same trend with actual porosity changes with depth based on information from the porosity log. The 4th approach based on prediction from resistivity provides a reasonable match between the predicted and the measured permeability for the Norris Lightsey lacustrine red beds (Figures 4.10 to 4.11).

The implications of the observed strong positive correlation between permeability and porosity (Figure 4.5) are that a possible strong dependency of permeability on physical quantities (Figure 4.12) such as velocity and density that have inverse relationships with porosity may be implied for the SGR red beds. Porosity correlates significantly well with density especially for fluid-saturated rocks, and the degree of correlation can be influenced by the densities of the rock matrix and pore fluid (Mavko et al., 2003, and Schon, 2011). Velocity increases as porosity decreases due to increasing depth of burial and effects of compaction. Consequently, permeability should decrease with increasing density and velocity due to closing of cracks and other

connectivity responsible for fluid flow. The dependency of porosity on compaction also implicitly implies that modeling the effects of compaction and/or cementation may help understand or predict depth-dependent permeability changes within a formation.

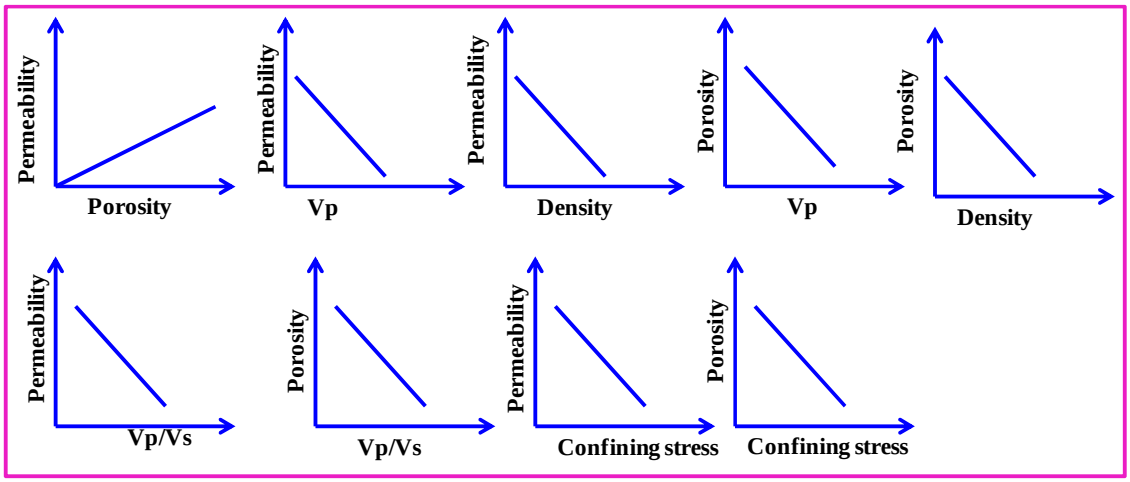

Figure 4.12: Schematic of theoretical considerations for permeability and porosity predictions for the SGR red beds based on available petrophysical data from this study.

In the absence of permeability data from deep drilled well and the exorbitant cost associated with drilling and logging a new well, it is possible to predict permeability for the SGR red beds at the core scale and results can be transformed to the reservoir scale to enable changes in permeability with depth at zones not covered by cores to be predicted. The output can also aid in subsequent geologically constrained reservoir simulation studies and subsurface characterization for insights into reservoir changes. Moreover, seismically derived elastic properties can be transformed into reservoir properties through an inversion process that takes into consideration the issue of non-uniqueness arising from the band-limited nature of seismic data, areas and depths not sampled by core and well data as well as inherent uncertainties in well to seismic ties.

The inversion process can be carried out through Bayesian formulation, by optimization or error minimization and/or by stochastic simulation to yield multiple realizations of the desirable reservoir properties such as changes in porosity and permeability (Spikes et al., 2007, Grana and Della Rossa, 2010).

4.6. ANALYSIS OF THE EFFECTS OF CO_2 ON SEISMIC VELOCITY IN THE RED BEDS

The ability to understand and quantify seismic dependency on reservoir changes with CO_2 saturation will be important to design the right monitoring techniques for CO_2 storage. The changes that may be detected seismically can be different for different basins. Variations in the physical composition, textural and mineralogical characteristics of rocks can impact physical properties that determine whether or not reservoir changes with fluid injection or production can be detected. The need to have insights into the physics of the rock-CO_2 interactions under the SGR reservoir conditions motivate this physical modeling of the potential effects of CO_2 on seismic properties.

Moreover, time-lapse seismic monitoring of fluid recovery and/or injection is not new (Lumley, 1995; Harris et al., 1995, Wang et al., 1998, and Akintunde, 2010) but whether or not this can be feasibly and economically implemented for a given geologic reservoir setting depends on production/injection induced changes in the acoustic velocity and density of the fluid-saturated rock. The tight nature of the SGR red beds may present a significant challenge to subsurface monitoring using time-lapse seismic imaging technology. Given the history of seismicity within the South Carolina area, the issue of whether or not CO_2 injection might trigger seismicity will also need to be

critically examined especially if the storage were to involve large scale deployments. Zoback and Gorelick (2012) discussed the potential risk that large scale storage of CO_2 may pose if the right geologic conditions, like the presence of weak, poorly cemented sandstones as found in the Utsira Formation in Norway, are not in place. To ensure safe sequestration and provide quick warnings and necessary remedial action in case of leakage, subsurface monitoring will be critically important. Understanding the nature of the effects of CO_2 on the Triassic-Jurassic rocks will allow for a proper planning and design of the right subsurface CO_2 monitoring techniques for pre- and post-injection scenarios (White, 2008; Vanorio et al., 2011, and Williams and Chadwick, 2012). This could range from using an active seismic source to passive seismic monitoring including possible monitoring for induced seismicity (Verdon et al., 2010). The potential to monitor typically rely on saturation changes that dominantly affect the P-wave velocity. This in turn is dependent on the bulk modulus of the rock that is related to both the bulk modulus of the rock matrix and that of the reservoir fluids (Akintunde, 2010). An investigation of the potential effects of CO_2 on seismic velocity for a brine-filled red bed formations encountered at the Norris Lightsey (Figure 4.13) was carried out using Gassmann's equation, velocity information derived from well data and other appropriate properties of rock and fluid (Batzle and Wang, 1992; Nur, 1989; and, Mavko et al., 2003).

The expressions for Gassmann's equations (Gassmann, 1951) are as follows:

$$K_{sat} = K_s \frac{\phi K_{dry} - (1+\phi) K_f K_{dry} / K_s + K_f}{(1-\phi) K_f + \phi K_s - K_f K_{dry} / K_s} \qquad 4.33$$

$$K_{dry} = K_s \frac{1-(1-\phi)K_f K_{sat}/K_s - \phi K_{sat}/K_f}{1+\phi-\phi K_f + \phi K_s/K_f - K_{sat}/K_s} \quad 4.34$$

$$G_{sat} = G_{dry} \quad 4.35$$

Where: K_{sat}, K_{dry} and K_s are the bulk moduli of the fluid-saturated and dry rock and the solid frame of the rock respectively; K_f is the effective bulk modulus of the pore fluid and ϕ is porosity; G_{sat} is the shear modulus of rock with fluid and G_{dry} is the shear modulus of the dry rock. For a mixture of fluids, the effective bulk modulus K_f is provided by Wood's equation (Mavko et al., 2003).

$$1/K_f = \sum_i S_i / K_i \quad 4.36$$

Where, S_i is the i^{th} fluid saturation and such that $\sum S_i = 1$ and K_i is the i^{th} fluid modulus.

Other physical properties of interest needed to complete fluid substitution to predict changes in the velocity of a saturated rock from the dry state are the expressions for P-and S-waves velocities (Vp and Vs) and density.

$$V_P = \sqrt{\frac{K+(4/3)G}{\rho}} \quad 4.37$$

$$V_S = \sqrt{\frac{G}{\rho}} \quad 4.38$$

where; V_P and V_s are the compressional- and shear-wave velocities in a homogeneous and isotropic elastic material, and ρ is density. The density of the saturated rock is expressed as follows (Mavko et al., 2003):

$$\rho_{sat} = (1-\phi)\rho_{dry} + \phi\sum_i S_i \rho_i \qquad 4.39$$

where S_i is the i^{th} fluid saturation such that $\sum S_i = 1$ and ρi is the i^{th} fluid density.

By applying Gassmann's equation and the properties of CO_2 under supercritical conditions (Wang and Nur, 1989; Akintunde et al., 2013b) the P-wave velocity for the fluid saturated rock changes by about 6% (Figure 4.13). This velocity saturation curve shows a dramatic change around 10% CO_2 saturation. Beyond this saturation threshold, the changes in velocity are generally negligible and appear to be flat as CO_2 saturation increases above 10 to 15% (Figure 4.13). The degree of seismic sensitivity to fluid saturations will depend on porosity and density, and bulk modulus of the rock as well as the amounts and compressibility of CO_2. Intuitively, the injection will increase the pore pressure thereby reducing the effective pressure and with a consequent decrease in velocity. The degree of seismic sensitivity to time-dependent reservoir changes will depend on the concentration of CO_2 and the effects of changes in effective pressure. Core derived stress-dependent measurements of the effects of CO_2 on seismic velocities can be used to aid the interpretation of time-lapse seismic data to monitor injection and post injection changes with CO_2 saturations.

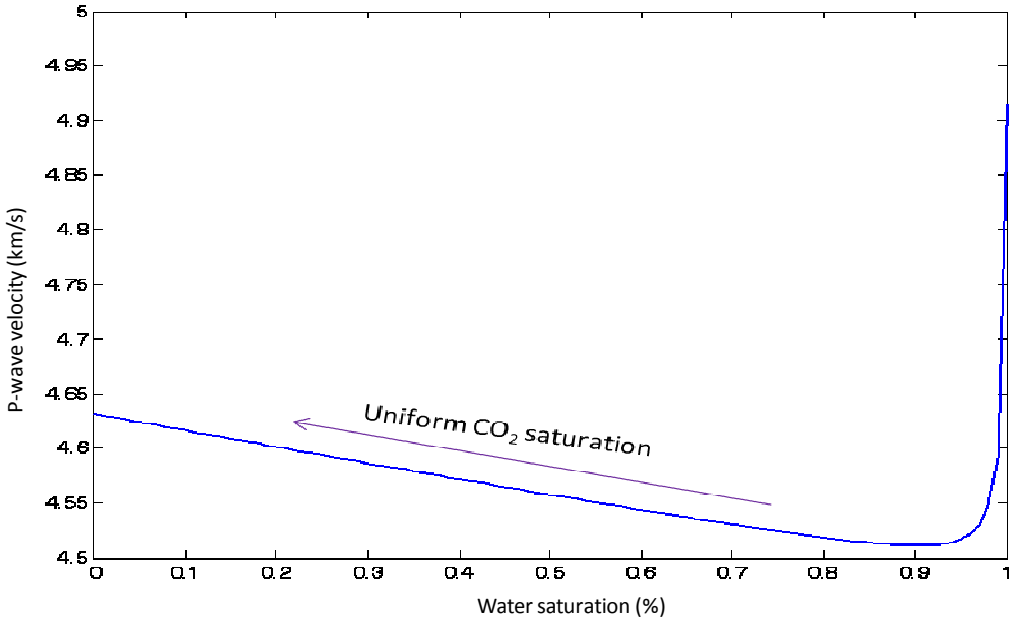

Figure 4.13: Velocity-saturation behavior velocity with CO_2 saturation for a Triassic red bed reservoir encountered at the Norris Lightsey (based on Gassmann, 1951).

In the absence of core derived laboratory measurements of P-wave velocity (Vp) and their stress dependency for the SGR's Norris LIghtsey reservoir, conditioned data set (Figure 4.14) from Vernik (1997) was used to model the effects of CO_2 saturations on the P-wave velocity of the brine-filled reservoir under stress dependency. The associated velocity for the type III stress behavior discussed in Vernik (1997) closely reflects the geo-reservoir conditions for the Norris Lightsey red beds or sandstone reservoir setting. Using the 10% CO_2 saturation (or 90% water/brine saturation) threshold in Figure 4.13, Vp decreases by about 4% to 10% when compare with the 100% water saturation (Figure 4.15).

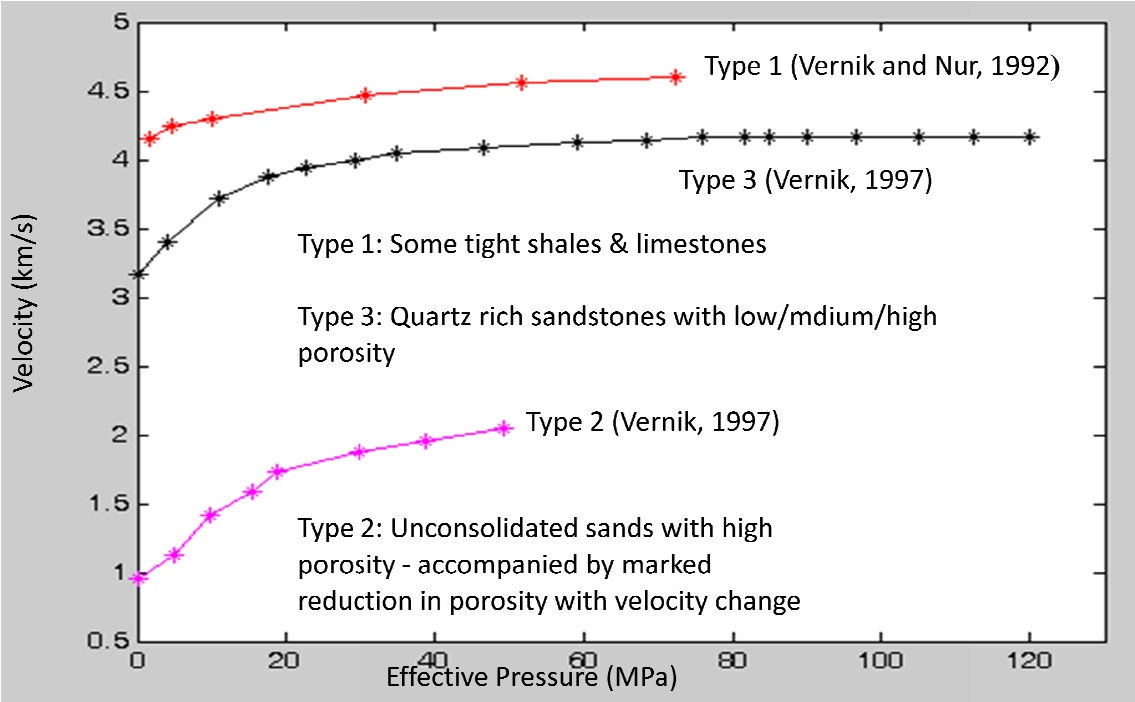

Figure 4.14: Velocity-stress dependency in sedimentary rocks (modified from Vernik, 1997)

In the dry rock, the effects of increasing confining pressure, and by implication increasing effective pressure, will lead to an increase in velocity due to closing of cracks and this is more noticeable at lower confining and/or effective pressure. On the other hand, increasing the pore pressure with fluid injection will result in a decrease in effective pressure with a consequent perturbation in velocity due to opening of cracks and pores. The velocity can either increase or decrease depending on the type of fluid. For 100% water saturation, the velocity increases relative to the dry rock velocity due to the large bulk modulus of water (Figure 4.15). With introduction of CO_2 into the brine-filled rock, the velocity decreases due to the high compressibility (or low bulk modulus) of CO_2 and the net increase in the density of the saturated rock.

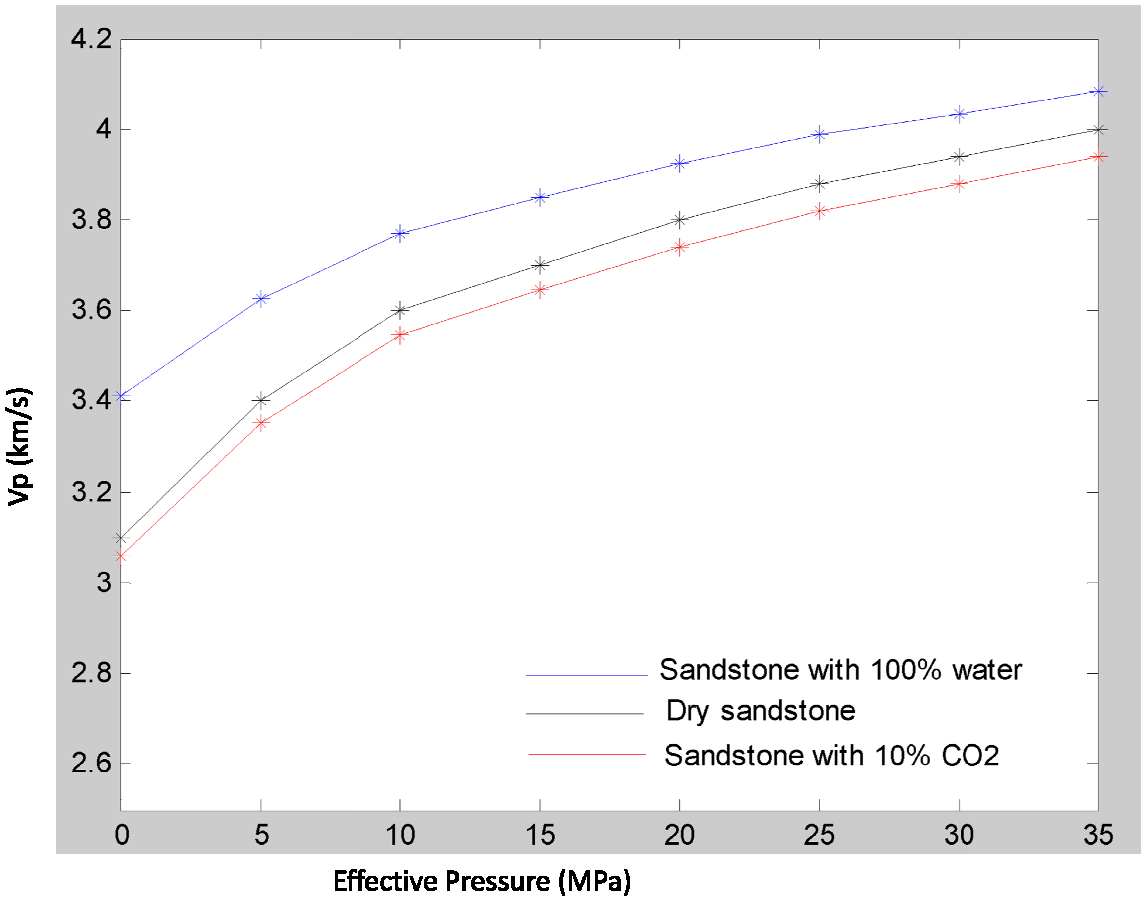

Figure 4.15: Effects of CO_2 on P-wave seismic velocity (V_p) under the influence of effective pressure changes. Data for dry sandstone modified from Vernik (1997) to reflect reservoir conditions at the Norris Lightsey. Effects of 100% water (blue curve), and 10% CO_2 with 90% water (red curve) saturations on the behavior of the seismic velocity are shown.

The degree of seismic sensitivity to fluid saturation and pressure will also depend on the rock's porosity. Modeling results (Figure 4.16) shows that seismic sensitivity to CO_2 effects will be expected to be lower in a low porosity reservoir. The implication for low porosity in a consolidated sandstone similar to the deeply buried red beds encountered at the Norris Lightsey and the Clubhouse Crossroads #3 (Figure 1.1) is that seismic properties are likely going to be heavily stress dependent with CO_2 saturations.

Stress dependency of seismic properties like velocity is generally higher in high porosity consolidated rocks compare to low porosity, lithified rocks. At the same time, high porosity and unconsolidated sandstone reservoirs are generally highly sensitive to changes in Vp with fluid saturations, and as such are well suited to the use of conventional time-lapse seismic monitoring (surface to surface, surface to borehole and/or borehole to borehole acquisition geometries). Pressure management and/or passive seismic monitoring would be suitable for subsurface monitoring in low porosity rocks where stress dependency of seismic properties may be quite obvious.

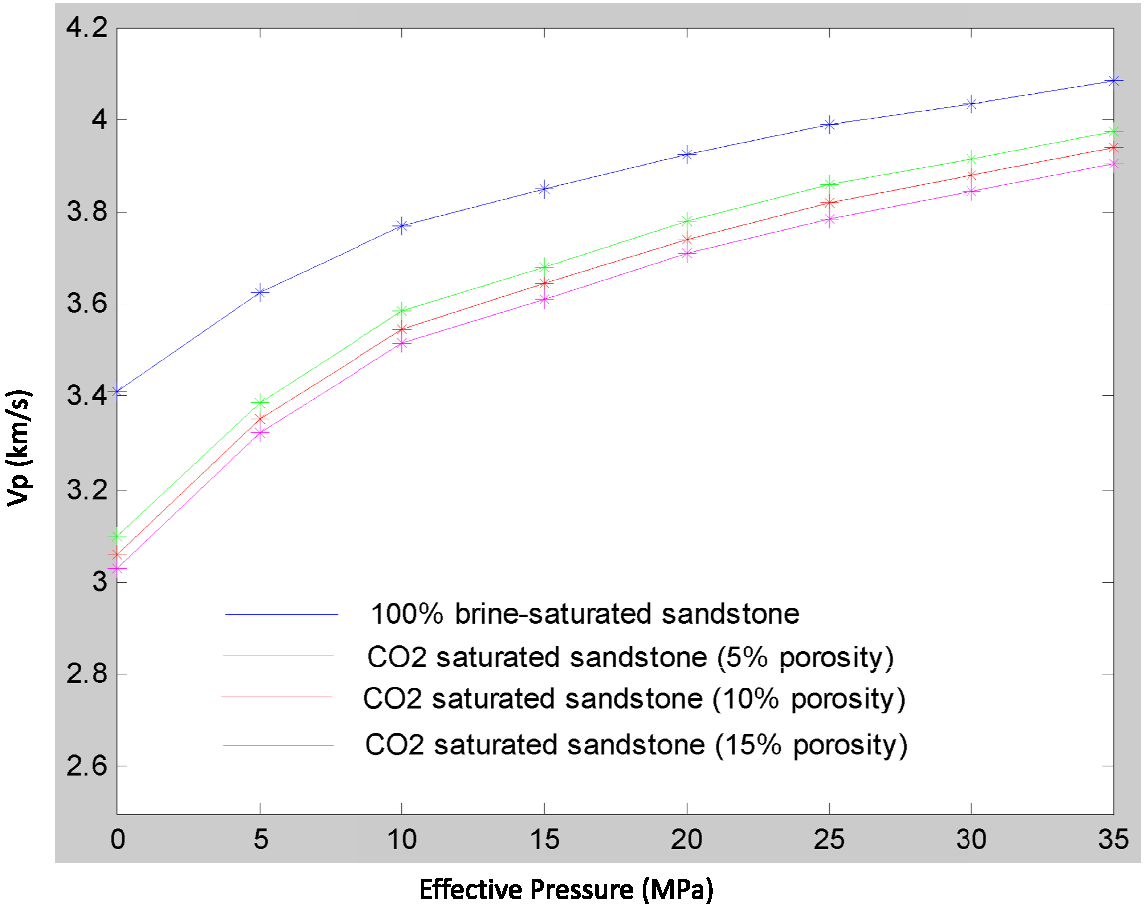

Figure 4.16: Effects of CO_2 saturations on seismic velocity under different porosities.

Over time, and following hydrodynamic trapping, CO_2 will fully dissolve and react with minerals in the rock through solubility and mineral trapping. Under this scenario, the expected geochemical changes will need to be monitored to assess the long term fate of the injected CO_2.

4.7. CONCLUSIONS

By predicting permeability for the SGR red beds, it could be possible to understand and quantify permeability changes with depth at the reservoir level in the absence of direct measurements from well logs. Porosity-derived permeability for the SGR red beds from the Norris lightsey lacustrine location has been aided in part by the observed strong correlation between porosity and permeability as well as the ability to establish flow zone units from measured porosity and permeability. The flow zone unit technique, as used in Prasad (2003) and Alam et al. (2011), can help to overcome short comings inherent in the Kozeny-Carman relation for permeability prediction. The lack of correlation between porosity and permeability within the fluvial and fluvial-alluvial tight red beds, (due mostly to the large scatters and sparsely distributed data sets) makes it difficult to predict permeability from porosity alone and from the use of the Kozeny-Carman relation.

The FZI method provides improved prediction for permeability regionally within the basin using all available data compared to the modified Kozeny-Carman approach. We found out that the predicted permeability is consistent with the measured permeability and follows same trend with the changes from the porosity log. The ability to predict permeability from resistivity and porosity is demonstrated in the Norris

Lightsey data. The resistivity-derived permeability based on the assumption of a fully brine-saturated rock and incorporating reservoir temperature and porosity as well as the Archie's tortuosity and cementation factor, shows a reasonable match with measured permeability. The factors that control the true resistivity of a formation or the resistivity of the fluid saturated rock also influence both porosity and permeability. By relating the true resistivity to porosity and establishing a linear relationship between porosity and permeability, we show that it is possible to predict permeability from resistivity.

Analysis of Gassmann's derived velocity for the CO_2 saturated porous-reservoir show that the P-wave velocity changes as CO_2 replaces brine. Ability to monitor the short and long terms of supercritical CO_2 injection under reservoir conditions will depend on the degree of seismic sensitivity to the effects of fluid saturation and changes in pore pressure caused by injection of CO_2. Modeling results incorporating variations in effective pressure show that P-wave velocity changes by up to 10% with CO_2 saturations. Seismic sensitivity to CO_2 saturations will also depend on the reservoir's porosity, and with a high porosity rock showing more sensitivity than a low porosity rock. In the absence of cores from the Norris Lightsey to conduct experimental evaluation of the effects of CO_2 on seismic velocity, fluid substitution modeling is important to understand the physics of the rock-CO_2 interactions. The result can be used to provide the basis for an assessment of the potential to monitor, help in the designing of optimum and cost-effective monitoring strategy as well as serve to aid interpretation of any time-lapse seismic images for the purpose of subsurface monitoring.

CHAPTER FIVE

SUMMARY OF RESEARCH GOALS AND ACCOMPLISHMENTS

This research was driven by the United States Department of Energy (DOE) funded geological characterization of the SGR basin for safe and permanent CO_2 storage as part of the growing global response and urgency to curtail rising concentrations of atmospheric CO_2, and by implication reduce global warming. The research is motivated by the scientific importance of uncovering: (1) geophysical observations for improved understanding of the tectonic evolution of the SGR basin, and (2) key seismic and rock properties critical to study prospects for CO_2 storage in the SGR basin.

The objectives and scope of research were to: (1) provide enhanced imaging of the SGR basin through time, depth, post-processing and geologically constrained interpretations of SeisData6, and (2) examine the CO_2 storage potential and tectonic significance of rock properties through petrophysical investigations involving: laboratory experiments, quantitative and qualitative analyses of well logs, analyses of thin sections, x-ray diffraction data, x-ray computed tomographic data, and physical modeling of the effects of CO_2 on seismic P-wave velocity.

The SGR basin was formed in an extensional tectonics setting about 215-175 Ma during the break up of Pangea and opening of the Atlantic. It is buried below the Cretaceous-Cenozoic Coastal Plain sediments in parts of South Carolina, Georgia, Florida

and Alabama. It is mostly filled with red beds (sandstone) that are capped by basalt flows and/or diabase sills as observed from deep wells in the South Carolina part of the basin. The study approach has involved seismic reprocessing and the use of rock physics techniques.

Reprocessing was carried out on the approximately 200 km SeisData6 seismic reflection profile in southeast Georgia in order to identify and interpret subsurface reflectors for evidence of the buried Triassic basin and its underlying characteristics. The key research issues were to: (1) determine the true characteristics (such as stratigraphy, structure, extent and thickness) of the buried basin which have remained unknown; (2) investigate the presence or absence of a basaltic layer on top of the Triassic sediments; (3) evaluate the regional significance of basalt within the SGR basin and its potential to serves as a seal for CO_2 storage; and (4) investigate whether or not the low angle Augusta fault identified in other studies in the vicinity of the Piedmont-Coastal Plain boundary extends underneath the Coastal Plain in the study area.

In order to assess address these issues, seismic reprocessing involving was carried out on the S_6 Coastal Plain profile. The reprocessing steps involved: (1) initial data analysis to understand noise and signal characteristics and (2) designing and applying appropriate workflows necessary to improve the signal to noise ratio. The workflows consist of processes such as vibroseis correlation, geometry assignment, trace editing, elevation statics, true amplitude recovery, deconvolution, residual statics correction, velocity analysis and Normal Moveout (NMO) correction, common-midpoint

stacking, poststack enhancement, poststack time migration, and depth conversion. The goal is to produce a good quality image suitable for identification and interpretation of subsurface reflectors for evidence of the buried Triassic basin and its underlying characteristics. Proper assignment of the two-dimensional (2-D) land geometry is a critical aspect of the prestack processing steps and is a part of the reason for reprocessing. The accuracy and reliability of other critical tasks such as velocity analysis and stacking depends on the accuracy of the 2-D source-receiver geometry. Reprocessing was followed by interpretation, analyses of results and interpretations, as well as the regional implications of these results for subsurface CO_2 storage within the basin.

Our new interpretations have helped to substantiate the presence of a buried Triassic basin beneath the southeast Georgia Coastal Plain. It is 2.2 km deep and 170 km wide, and appears to coincide with the subsurface convergence of the previously named Riddleville and Dunbarton basins in Georgia and South Carolina, respectively. No basalt was found in this basin contrary to previous studies, and the reinterpreted absence of basalt is consistent with Heffner et al. 2012 showing that basalt is not prevalent throughout the main SGR basin.

Structurally, the basin defines an asymmetric half-graben possibly bounded by normal faults. The observed seismic discontinuities in the southeast part of the line suggest that the delineated basin appears to be bounded in the southeast by Triassic normal faults which may have been reactivated during Cretaceous time. Our data show

no clear evidence for the Augusta fault that was identified in other studies in the vicinity of the Piedmont-coastal plain boundary in Georgia and South Carolina.

We estimate, based on the new interpretations from S_6 and analysis of the additional Triassic-Jurassic wells presented in Heffner et al. (2012), that the onshore areal extent of basalt within the SGR basin is about 2,700 to 2,800 km^2. New results further show that the origin of the "J" reflector is not restricted to basalt/diabase sequence only. It is a regional geologic marker over different strata. The absence of basalt from study area does not preclude subsurface CO_2 storage within the basin, diabase sills exist that could serve as a seal for CO_2 storage so long as the regional extent and sealing integrity of these diabase sills are properly evaluated. Absence of basalt implies that erosion, uplift and possibly faults reactivation may have limited the regional extent basaltic flows extruded during post-rifting and by extension the magmatism that characterized the Eastern North American Margin (ENAM).

The petrophysical analysis of the basin has focused on the scientific importance and tectonic implications of the critically important physical properties of the red beds for CO_2 storage. In addition, understanding basin evolution through compaction and diagenetic processes require information at the petrophysical scale (not provided at the seismic scale). Knowledge of and predictions for fluid flow and pressure regimes within the basin will be difficult without high-resolution information from in-situ petrophysical/rock physics data such as porosity and permeability.

The goal of the rock physics aspect of this study is to examine the CO_2 storage potential and tectonic significance of key physical rock properties of the Triassic-Jurassic formations (sandstones or red beds as well as the basalt flows and diabase sills) that characterize the SGR-basin fill. Central to this goal are the following objectives: (1) understand and quantify the spatial distribution of porosity and permeability, (2) understand the internal composition and microstructure of the basalt flows and diabase sills, (3) evaluate impacts of porosity and permeability on subsurface suitability for CO_2 storage, (4) investigate the influence of depositional processes on rock properties, (5) investigate impacts of tectonic setting including compaction on rock properties, (6) predict permeability for the Triassic red beds, and (7) understand the physics of the rock-CO_2 interactions through fluid substitution modeling in order to provide a basis to assess suitability for subsurface monitoring as well as to help provide insights into the appropriate monitoring strategy for the SGR reservoir conditions.

A variety of methods were implemented to address the rock physics research objectives. These were laboratory experiments on cores from selected sites within the basin with availability of Triassic and Jurassic samples, analyses of thin sections, X-ray diffraction and X-ray computed tomographic data, quantitative interpretation of well logs and physical modeling to understand the effects of compaction and CO_2 on rock properties. The key, substantial and new findings are that: (1) the SGR basin manifests distinct porosity-permeability regimes that are influenced by the depositional environments, (2) present-day porosity and permeability within the basin has been altered by physical processes and that the key controls on porosity and permeability are

poor sorting, fine-grained nature of the sediments, small pore throats and tectonically induced processes, (3) while 3.73 to 13.23 Gt CO_2 may be stored within the basin, the low permeability presents a challenge for injectivity, (4) the observed variations in the core-derived porosity and permeability suggest presence of moderately to highly compartmentalized reservoir systems, and that (5) the changes in porosity with depth imply a highly compacted, deformed basin as well as a basin with a history of significant uplift and erosion. The existence of distinct porosity-permeability regimes implies distinct geo-hydrologic systems within the SGR basin. The potential to store 3.73 to 13.23 Gt CO_2 is particularly significant to the global need to store 4 Gt CO_2 annually if geologic sequestration were to be truly effective to help stabilize the rising concentrations of atmospheric CO_2. The generally low permeability favors safe storage and suggests minimal risk with induced seismicity. The permeability values especially for Dunbarton and Clubhouse Crossroads parts of the basin are below the seismogenic permeability that may trigger induced seismicity with fluid injection (Talwani et al., 2007).

In the absence of permeability data from a deep drilled well, results show that it is possible to predict permeability for the SGR basin tight red beds, and that such predictions can help to understand permeability changes alongside porosity changes at critical subsurface depths that may or are not covered by core-derived data. The output from the permeability predictions can also provide input into reservoir simulation studies for subsequent dynamic reservoir property evaluation either at the reservoir or seismic scale. Strong, linear correlation obtained between porosity and permeability for

the fluvial samples from the Norris lightsey show that permeability can be predicted from porosity alone. The predicted permeability from porosity matches with Kozeny-Carman derived estimates as well as with the measured permeability. Results further show that the method of flow zone indicator will work best for permeability predictions regionally within the basin.

Permeability based on the flow zone indicator approach provides a good, reasonable estimate of permeability changes at the reservoir level for the Norris Lightsey case and shows trends consistent with observed changes from the sonic-derived porosity log. Permeability obtained from resistivity and porosity shows a reasonable fit with the measured permeability, implying that the true resistivity of a formation can be a useful tool for permeability prediction within the Triassic red bed formations of the SGR basin.

Gassmman computed fluid substitution modeling incorporating variations in effective pressure shows a decrease in P-wave velocity of up to about 10% with CO_2 saturations. This change is within the limit of seismic detection for time-lapse seismic and suggest this may be deployed to monitor the impacts of CO_2 changes both short and long terms. The presence of low porosity reservoirs within the SGR red beds formations suggest pressure management/monitoring will be important if CO_2 were to be injected in a low porosity red beds. Monitoring will be important to assess storage efficiency, as well as help to evaluate the potentials for any leakage and induced seismicity (Zoback and Gorelick, 2012) that could compromise or threaten storage integrity. The

sealing/leaking capacities of any inferred faults would also need to be properly evaluated.

BIBLIOGRAPHY

Ackerman, H.D., 1983, Seismic refraction study in the area of the Charleston, South Carolina, earthquake, in Gohn, G.S., ed., Studies Related to the Charleston, South Carolina, Earthquake of 1886 - Tectonics and seismicity: U.S. Geological Survey Professional Paper 1313, p. F1-F20.

Akbar, N., J. Dvorkin, and A. Nur, 1993, Relating P-wave attenuation to permeability: Geophysics, 58, 20-29

Akintunde, O.M., 2010, Time-lapse seismic imaging of coal bed methane reservoir from the Powder River Basin, Wyoming, USA. Lambert Academic Publishing

Akintunde, O.M., Knapp, C.C., Knapp, J.H., Prasad, M. and Olsen, P.E., 2011, Porosity and Permeability of Triassic-Jurassic Formations of the South Georgia Rift Basin: Potential Implications for CO_2 Storage: Abstract presented at 2011 Fall Meeting, American Geophysical Union, San Francisco, California, 5-9 December.

Akintunde, O.M., C. Knapp, D.M. Heffner, J.H. Knapp, and J. Shafer, 2011, Reinterpretation of the "J" Basalt Reflector from Seismic Data Reprocessing across the Coastal Plain of Southeastern Georgia: Potential Implications for Long-term CO_2 Sequestration , AAPG, Annual Convention & Exhibition, Houston, Texas, AAPG Search and Discovery Article #80174

Akintunde, O.M., C.C. Knapp, J.H. Knapp, and D.M. Heffner, 2013a, New constraints on buried Triassic basins and regional implications for subsurface CO_2 storage from the SeisData6 seismic profile across the Southeast Georgia coastal plain. Environmental Geosciences, V.20., No.1, PP. 17-29.

Akintunde, O.M., C. Knapp, and J. Knapp, 2013b, Petrophysical characterization of the South Georgia Rift basin for supercritical CO_2 storage: a preliminary assessment. Environmental Earth Sciences, doi 10.1007/s12665-013-2355-6.

Alam, M.M., I.L. Fabricius, and M. Prasad, 2011, Permeability prediction in chalks, American Association of Petroleum Geologists (AAPG) Bulletin, V. 95, No.11, PP. 1991-2014.

Albritton, D.L., and, L.G. Meira Filho, 2001, Climate Change 2001: The Scientific Basis: Contribution of Working Group I to the Third Assessment Report of the Intergovernmental Panel on Climate Change technical Summary, IPCC, Geneva, Switzerland

Al-Chalabi, M., 1973, Series approximation in velocity and traveltimes computations: Geophysical prospecting, 21, 783-795

Altunbay, M., D. Georgi, and H.M., Takezaki, 1997, Permeability prediction for carbonates: still a challenge? Presented at the Middle East Oil Show and Conference, 15-18 March, Bahrain, paper SPE 37753.

Amaefule, J.O., M. Altunbay, D. Tiab, D.G. Kersey, and D.K. Keelan, 1993, Enhanced reservoir description: Using core and log data to identify hydraulic (flow) units and predict permeability in uncored intervals/wells: SPE Paper 26436, 1-16.

Archie, G.E., 1942, The electrical resistivity log as an aid in determining some reservoir characteristics : Transactions of the American Institute of Mining, Metallurgical, and Petroleum Engineers, 146, 54-62

Athy, L.F., 1930, Density, porosity and compaction of sedimentary rocks. Bull. Am. Ass. Pet. Geol. 14, 1-24

Bachu, S., Gunter, W.D., Perkins, E.H., 1994, Energy Conversion Management 35, 269-279.

Bachu, S, 1996, Aquifer disposal of carbon dioxide: hydrodynamic and mineral trapping – proof of concept, Hitchon, B., Ed.; Geosciences Publishing, Sherwood Park, Alberta, Canada

Batzle, M., and Wang, Z., 1992, Seismic properties of pore fluids: Geophysics, 57, 1396–1408.

Behrendt, J.C., R.M. Hamilton, H.D. Ackermann, V.J. Henry, and K.C. Bayer, 1983, Marine multichannel seismic reflection evidence for Cenozoic faulting and deep crustal structure near Charleston, South Carolina, in G.S. Gohn, ed., Studies related to the Charleston, South Carolina earthquake of 1886 - Tectonics and seismicity: United States Geological Survey Professional Paper 1313, p. J1-J29.

Behrendt, J.C., 1986, Structural interpretation of multichannel seismic reflection profiles crossing the southeastern United States and the adjacent continental margin – decollements, faults, Triassic(?) basins and Moho reflections in M. Barangi and L. Brown, eds., Reflection seismology: the continental crust: American Geophysical Union Geodynamics Series, v. 14, p. 201 – 214

Biot, M.A., 1956a, Theory of propagation of elastic waves in fluid saturated porous solids. I. Low frequency range: J. Acous. Soc. Amr., 28, 168-178

Biot, M.A., 1956b, Theory of propagation of elastic waves in fluid saturated porous solids. II. High frequency range: J. Acous. Soc. Amr., 28, 179-191.

Bloch, S., 1991, Empirical prediction of porosity and permeability in sandstones: American Association of Petroleum Geologists Bulletin, v.75, no. 7, p.1145-1160.

Bonini, W.E., and G.P. Woollard, 1960, Subsurface geology of North Carolina-South Carolina Coastal Plain from seismic data: AAPG Bulletin, v. 44, p. 298-315.

Bramlett, K.W., D.T., Secor., Jr., and D.C. Prowell, 1982, The Belair fault: A Cenozoic reactivation structure in the eastern Piedmont: Geological Society of American Bulletin, v. 93, p. 1109-1117.

Burruss, R.C., S.T. Brennan, P.A. Freeman, M.D. Merrill, L.F. Ruppert, M.F. Becker, W.N. Herkelrath, Y.K. Kharaka, C.E. Neuzil, S.M. Swanson, T.A. Cook, T.R. Klett, P.H. Nelson, and C.J. Schenk, 2009, Development of a Probabilistic Assessment Methodology for Evaluation of Carbon Dioxide Storage. U.S.G.S. Open File Report – 1035.

Carman, P.C., 1937, Fluid flow through granular beds: Trans. AICHE, 15, 150-166

Castle, R.J., 1974, Theory of normal moveout. Geophysics 59, 983-999

Chowns, T.M., and Williams, C.T., 1983, Pre-Cretaceous rocks beneath the Georgia Coastal plain – regional implications, in Gohn, G.S., ed., Studies Related to the Charleston, South Carolina, Earthquake of 1886 – Tectonics and seismicity: US Geological Survey Professional paper 1313, p. L1-L42.

Claerbout, J.F., and S.M. Doherty, 1972, Downward continuation of moveout-corrected seismograms. Geophysics 37, 741-768

Cook, F.A., L.D. Brown, S. Kaufman, J.E. Oliver, and T.A. Petersen, 1981, COCORP seismic profiling of the Appalachian orogen beneath the Coastal Plain of Georgia: Geological Society of America Bulletin, v. 92, p. 738-748.

Core Laboratories Analysis Report, 1984, for Texaco Inc. Essex Exploration and Production Company, Norris C. Lightsey No. 1 Well Wildcat, Colleton County, South Carolina.

Daniels, D.L., and I. Zeitz, 1978, Geological interpretation of aeromagnetic maps of the Coastal Plain region of South Carolina and parts of North Carolina and Georgia: U.S. Geological Survey Open-File Report 78-261, 47 p.

Daniels, D.L., Zietz, I, and Popenoe, P., 1983, Distribution of subsurface lower Mesozoic rocks in the southeastern United States as interpreted from regional aeromagnetic and gravity maps, in Gohn, G.S., ed., Studies Related to the Charleston, South Carolina, Earthquake of 1886 – Tectonics and seismicity: U.S. Geological Survey Professional paper 1313, p. K1-K24.

Darcy, H., 1856, Les Fontaines Publiques de la Ville de Dijon, Dalmont, Paris.

Dietz, R.S., and J.C. Holden, 1970, Breakup of pangea: Scientific American, v. 223, P.30.

DOE-NETL, 2008, Methodology for Development of Geologic Storage Estimates for Carbon Dioxide, Capacity and Fairways Subgroup, of the Geologic Working Group, DOE Regional Carbon Sequestration Partnerships, p.27-30

Dillon, W.P., K.D. Klitgord, and C.K. Paul, 1983, Mesozoic development and structure of the continental margin off South Carolina, in G.S. Gohn, ed., Studies related to the Charleston, South Carolina earthquake of 1886 - Tectonics and seismicity: United States Geological Survey Professional Paper 1313, p. N1-N16

Dillon, W.P., K.D. Klitgord, and C.K. Paul, 1983, Mesozoic development and structure of the continental margin off South Carolina, in G.S. Gohn, ed., Studies related to the Charleston, South Carolina earthquake of 1886 - Tectonics and seismicity: United States Geological Survey Professional Paper 1313, p. N1-N16.

Domoracki, W.J., 1995, A geophysical investigation of geologic structure and regional tectonic setting at the Savannah River Site, South Carolina: PhD dissertation, Virginia Polytechnic Institute and State University, Blacksburg, Virginia, 236p

Dvorkin, J., N. Derzhi, Q. Fang, A. Nur, B. Nur, A. Grader, C. Baldwin, H., Tono, and E, Diaz, 2009, From micro to reservoir scale: permeability from digital experiments. The Leading Edge, Vol. 28, No. 12, pp. 1446-1452

Energy Information and Administrative (EIA), 2007, United States Department of Energy International Energy Outlook, May 2007, in http://www.eia.doe.gov/oiaf/ieo/pdf/0484.

Fabricius, I.L., G. Baechle, G.P. Eberli, and R. Weger, 2007, Estimating permeability of carbonate rocks from porosity and Vp/Vs. Geophysics, Vol. 72, No.5 P. E185-E191.

Fatt, I., 1953, The effect of overburden pressure on relative permeability. Pet. Trans. AIME 198, 325-326.

Gassmann, F. 1951, Elastic waves through a packing of sphere. Geoph.16, 673-685.

Gohn, G.S. 1983, Geology of the basement rocks near Charleston, South Carolina – Data from detrical rock fragments in lower Mesozoic(?) rocks in Clubhouse Crossroads test hole #3, in Gohn, G.S., ed., Studies Related to the Charleston, South Carolina, Earthquake of 1886 – tectonics and seismicity: US Geological Survey Professional Paper 1313, p. E1-E22.

Gohn, G.S., B.B. Houser, and R.R. Schneider, 1983b, Geology of the lower Mesozoic(?) sedimentary rocks in Clubhouse Crossroads test hole #3 near Charleston, South Carolina, in G.S. Gohn, ed., Studies related to the Charleston, South Carolina earthquake of 1886 - Tectonics and seismicity: United States Geological Survey Professional Paper 1313, p. D1-D17.

Goldberg, D.S., D.V. Kent, and P.E. Olsen, 2010, Potential on-shore and off-shore reservoirs for CO2 sequestration in Central Atlantic Magmatic Province Basalts: Proceedings of the National Academy of Sciences, v. 107, p. 1327-1332.

Gomez, C.T., J. Dvorkin, and T. Vanorio, 2010, Laboratory measurements of porosity, permeability, resistivity, and velocity on Fontainebleau sandstones. Geophysics, Vol. 75, No.6, P. E191-E204.

Gottfried, D., C.S. Annell, and G.R. Byerly, 1983, Geochemistry and tectonic significance of subsurface basalts near Charleston, South Carolina: Clubhouse Crossroads test holes #2 and #3, in G.S. Gohn, ed., Studies related to the Charleston, South Carolina earthquake of 1886 - Tectonics and seismicity: United States Geological Survey Professional Paper 1313, p. A1-A19.

Grana, D., and E. Della Rossa, 2010, Probabilistic petrophysical properties estimation integrating statistical rock physics with seismic inversion. Geophysics 75, no. 3, O21-O37.

Hames, W.E., P.R. Renne, and C. Ruppel, 2000, New evidence for geologically instantaneous emplacement of earliest Jurassic Central Atlantic Magmatic Province Basalts on the North American margin: Geology, v. 28, no. 9, p. 859-862.

Hamilton, R.M., J.C. Behrendt, and H.D. Ackermann, 1983, Land multichannel seismic reflection evidence for tectonic features near Charleston, South Carolina, in G.S. Gohn, ed., Studies related to the Charleston, South Carolina earthquake of 1886 - Tectonics and seismicity: United States Geological Survey Professional Paper 1313, p. 11-118.

Han, D., A. Nur, and Morgan, D., 1986, Effects of porosity and clay content on wave velocities in sandstones. Geophysics, Vol. 51, No.11, P. 2093-2107.

Harris, J.M., R.G. Nolen-Hoeksema, R.T., Langan, M. Van-Schaack, S.K., Lazaratos, and J.W. Rector, 1995, High resolution cross well imaging of a West Texas Carbonate Reservoir: Part1- Project summary and interpretation: Geophysics 60, 667-681.

Hatcher Jr., R.D., Howell, D., and Talwani, P., 1977, Eastern Piedmont fault system: Speculation on its extent: Geology, v.5, p. 636-640

Heffner, D.M., Knapp, J.H., Akintunde, O.M., and Knapp, C., 2012, Preserved extent of Jurassic flood basalt in the South Georgia Rift: A new interpretation of the J horizon. Geology, V.40, no. 2, p. 167-170

Holbrook, W.S., and Kelemen, P.B., 1993, Large igneous province on the United States Atlantic margin and implications for magmatism continental breakup: Nature, v. 364, p. 433-436.

Hovorka, S.D., R.C. Smyth, J. Paine, S. Tinker, and I. Duncan, 2006, Downscaling capacity estimates from a regional to a site scale – case study in the South Eastern US Gulf Coast Carbon Center at the Bureau of Economic Geology, University of Texas at Austin.

Iverson, P.W., and Smithson, S.B., 1983, Reprocesses COCORP southern Appalachian reflection data: Root zone to Coastal Plain: Geology, v. 11, p. 422-425.

Katz, A.J., and A.H. Johnson, 1986, Quantifying prediction of permeability in porous rock: Physical Review B, 34, no. 11, 8179-8181.

Keelan, D.K., 1986, Automated Core Measurement System for enhanced core data at overburden conditions, Society of Petroleum Engineer (SPE) Rocky Mountain Regional Meeting, Montana.

Ketcham, R.A., and Carlson, W.D., 2001, Acquisition, optimization and interpretation of X-ray computed tomographic imagery: Applications to the geosciences. Computers and Geosciences, 27, 381-400.

King, M.S., 1966, Wave velocities in rocks as a function of changes in overburden pressure and pore fluid saturants. Geophysics, Vol. XXXI, No. 1, PP. 50-73.

Klimentos, T., and C. McCann, 1990, Relationships among compressional wave attenuation, porosity, clay content, and permeability in sandstones: Geophysics, 55, 998-1014.

Klinkenberg, L.J., 1941, The permeability of porous media to liquids and gases, Drilling and Production Practice, American Petroleum Inst., pp. 200-213.

Knapp, C.C., O.M. Akintunde, and J.H. Knapp, 2012, New constraints on buried Triassic basins of the Eastern North American Margin and implications for regional tectonics from reanalysis of SeisData6 seismic profile. 2012 fall meeting, AGU, San Francisco, Calif., 3-7 Dec.

Koide, H, Tazaki, Y, Noguchi, Y, Nakayama, S, Iijima, M, Ito, K and Shindo, Y, 1993, Subterranean containment and long-term storage of carbon dioxide in unused aquifers and in depleted natural gas reservoirs. Energy Conversion and Management, vol. 33 (5-8), pp. 619-626.

Kozeny, J., 1927, Ueber Kapillare Leitung des Wasers in Boden: Sitzungsberichte der Akademie der Wissenschaften in Wien, 136, 271-305.

Lanphere, M.A., 1983, 40Sr/39Ar ages of basalt from Clubhouse Crossroads test hole #2, near Charleston, South Carolina, earthquake of 1886, in G.S. Gohn, ed., Studies related to the Charleston, South Carolina earthquake of 1886 - Tectonics and seismicity: United States Geological Survey Professional Paper 1313, p. B1-B8.

Leverett, M.C., 1940, Capilarry behavior in porous solids. Trans. AIME 142, 152-169

Lindholm, R.C., J.M. Hazlett, and S.W. Fagin, 1979, Petrology of Triassic-Jurassic conglomerates in the Culpeper basin, Virginia. Journal of sedimentary Petrology, v. 49, no.4, p. 1245-1261

Liu, G., and R. Roaldset, 1994, A new decompaction model and its application to the northern North Sea. First Break 12, 81-89.

Lumley, D.E., 1995, 4-D seismic monitoring of an active steamflood: 65th Annual International Meeting., Society of Exploration Geophysics, expanded abstracts, 203-206.

Lumley, D. D. Sherlock, T. Daley, L. Huang, D. Lawton, R. Masters, M. Verliac,, and D. White, 2010, Highlights of the 2009 SEG Summer Research Workshop on CO2 Sequestration. The Leading Edge, Vol. 29, No.02, P. 138-145.

Maher, H.D., 1987, Kinematic history of mylonitic rocks from the Augusta fault zone, South Carolina and Georgia: American Journal of Science, v. 287, p. 436-445.

Maher, H.D., R.D. Dallmeyer, D.T. Secor Jr., and P.E. Sacks, 1994, 40Ar/39Ar constraints on the chronology of Augusta fault zone movement and late Alleghanian extension,

southern Appalachian Piedmont, South Carolina and Georgia: American Journal of Science, v.294, p. 428-448.

Marine, W., 1974, Geohydrology of buried Triassic Basin at Savannah River Plant, South Carolina: American Association of Petroleum Geologists Bulletin, v.58, no.9, p. 1825-1837.

Marine, W., and G.E. Siple, 1974, Buried Triassic Basin in the Central Savannah River Area: Geological Society of America Bulletin, v. 85, P. 311-320.

Marion, D., H. Nur., and D. Han, 1992, Compressional velocity and porosity in sand-clay mixtures. Geophysics, Vol. 57., No.4, P.554-563.

Mavko, G., and A. Nur, 1997, The effect of percolation threshold in the Kozeny-Carman relation: Geophysics, 62, 1480-1482, doi: 10.1190/1.1444251.

Mavko, G., T. Mukerji, and J. Dvorkin, 2003, The rock physics handbook: Cambridge University Press.

McBride, J.H., Nelso, K.D., and Brown, L.D., 1987, Early Mesozoic basin structure and tectonics of the southeastern United States as revealed from COCORP reflection data and the relation to Atlantic rifting: Canadian Society of Petroleum Geologists Memoir 12, p. 173-184

McBride, J.H. Nelson, K.D. & Brown, L.D., 1989, Evidence and implications of an extensive early Mesozoic rift basin and basalt/diabase sequence beneath the southeast Coastal Plain. Geological Society of America Bulletin, v. 101, p. 512-520.

McGrail, B.P. H.T. Schaef, A.M. Ho, Y. Chien, J.J. Dooley, and C.L. Davidson, 2006, Potential for carbon dioxide sequestration in flood basalts, Journal of Geophysical Research, Vol. 111, B12201, p. 1-13.

Miall, A.D., 1996, The geology of fluvial deposits. Springer-Verlag Berlin Heidelberg New York

Nelson, P.H., 2005, Permeability, porosity, and pore-throat size – a three dimensional perspective. Petrophysics December, 452-455

Nur, A., and G. Simmons, 1969, The origin of small cracks in igneous rocks. Int. J. Rock Mech. Min. Sci., Vol. 7, pp. 307-314.

Nur, A., 1989, Four-dimensional seismology and (true) direct detection of hydrocarbons: The petrophysical basis: The Leading Edge, 8, no. 09, 30-36.

Olsen, P.E., A.J. Froelich, D.L. Daniels, J.P. Smooth, and J.W. Gore, 1991, Rift basins of early Mesozoic age in J.W. Horton and V.A. Zullo, eds., The Geology of the Carolinas, v. 50, p. 142-170.

Petersen, T.A., Brown, L.D, Cook, F.A., Kaufman, S, and Oliver, J.E., 1984, Structure of the Riddleville basin from COCORP seismic data and implications for reactivation tectonics: Journal of Geology, v. 92, p. 261-271.

Phillips, J.D., 1983, Paleomagnetic investigations of the Clubhouse Crossroads basalt in G.S. Gohn, ed., Studies related to the Charleston, South Carolina, earthquake of 1886, in G.S. Gohn, ed., Studies related to the Charleston, South Carolina earthquake of 1886 - Tectonics and seismicity: United States Geological Survey Professional Paper 1313, p. C1-C18.

Planke, S., Alvestad, E., and Eldholm, O. 1999, Seismic characteristics of basaltic extrusive and intrusive rocks, The Leading Edge 18, 342-348

Popenoe, P., and I. Zietz, 1977, The nature of the geophysical basement beneath the Coastal Plain of South Carolina and northeastern Georgia, in D.W. Rankin, ed., Studies related to the Charleston, South Carolina, earthquake of 1886 - A preliminary report: United States Geological Survey Professional Paper 1028, p. 119-137.

Prasad, M, 1997, Effects of pore pressure and differential pressure on compressional wave velocity and quality factor in Berea and Michigan sandstones, Geophysics, Vol. 62, No.4, P. 1163-1176.

Prasad, M, 2002, Acoustic measurements in unconsolidated sands at low effective pressure and overpressure detection: Geophysics, vol. 67, no. 2, P. 405-412.

Prasad, M, 2003, Velocity-permeability relations within hydraulic units, Geophysics, Vol. 68, No.1, P.108-117

Ratcliffe, N.M., W.C., Burton., R.M. D'Angelo, and J.K., Costain, 1986, Low-angle extensional faulting, reactivated mylonites and seismic reflection geometry of the Newark Basin margin in eastern Pennsylvania: Geology, v. 14, p. 766-770.

Reid, M.S., R.W. Aucott, R.W. Lee, and, R.A. Renken, 1986, Hydrologic and geologic analysis of a well in Dorchester County, South Carolina: United States Geological Survey Water-Resources Investigation Report 86-4161, p. 23.

Revil, A., D. Grauls, O. Brevart, 2002, Mechanical compaction of sand/clay mixtures. J. Geophys. Res. 107 (B11), 2293, ECV11-1-ECV11-15

Schaef, H.T., B.P. McGrail, and A.T. Owen, 2009, Basalt-CO_2-H2O Interactions and Variability in Carbonate Mineralization Rates, Science Direct, Energy Procedia 1, 4899-4906

Schilt, F.S., L.D. Brown, J.E. Oliver, and S. Kaufman, 1983, Subsurface structure near Charleston, South Carolina: Results of COCORP reflection profiling in the Atlantic Coast Plain, in G.S. Gohn, ed., Studies related to the Charleston, South Carolina earthquake of 1886 - Tectonics and seismicity: United States Geological Survey Professional Paper 1313, p. H1-H19.

Schlumberger, 2000, Log interpretation charts, Schlumberger Oilfield Communications, Sugar Land, Texas

Schlumberger Oil Field Glossary, 2012, Boyle's law single cell under formation evaluation in http://www.glossary.oilfield.slb.com/Display.cfm?Term=Boyle%27s%20Law%20Single%20Cell

Schon, J.H., 2011, Physical Properties of Rocks – Handbook of Exploration and Production- Volume 8, Elsevier, p.17-70.

Sheriff, R.E., and L.P. Geldart, 1983, Exploration seismology vol.2, data processing, Cambridge University Press.

Siple, G.E., 1967, Geology and ground water of the Savannah River Plant and vicinity, South Carolina: United States Geological Survey Water-Supply Paper, v. 1841, p. 113.

Smyth, R.C. 2007, Potential sinks for geologic storage of carbon dioxide generated in the Carolinas. US Bureau of Econ Geol, summary report 1-14.

Snipes, D.S., W.C. Fallaw, V. Price, and, R.J. Cumbest, 1993, The Pen Branch fault: Documentation of late cretaceous-tertiary faulting: Southeastern Geology, v. 33, No.4. p. 195-218.

Spikes, K., T. Mukerji, J. Dvorkin, and G. Mavko, 2007, Probabilistic seismic inversion based on rock-physics models. Geophysics 72, No. 5, R87-R97

Swanson, M. T., 1986, Preexisting fault control for Mesozoic basin formation in eastern North America: Geology, v. 14, p. 419-422.

Talwani, P, 1977, A preliminary shallow crustal model between Columbia and Charleston, South Carolina, determined from quarry blast monitoring and other geophysical data, in Rankin, D.W., ed., Studies Related to the Charleston, South

Carolina, Earthquake of 1886 – A preliminary report: U.S. Geological Survey Professional Paper 1028, p. 177-187.

Talwani, P., L. Chen, and K. Hahalaut, 2007, Seismogenic permeability, Ks: Journal of Geophysical Research, Vol. 112, B07309, doi: 10.1029/2006JB004665.

Tans, P., 2012, Trends in atmospheric carbon dioxide at Mauna Loa. U.S. Department of Commerce NOAA (National Oceanic and Atmospheric Administration). http://www.esrl.noaa.gov/gmd/ccgg/trends/. Accessed 27 December 2012

Timur, A., 1968, An investigation of permeability, porosity, and residual water saturation relationships for sandstone reservoirs. Log Analyst July-August, 8-17.

Traverse, 1987, Pollen and spores date origin of rift basins from Texas to Nova Scotia as early late Triassic: Science, v. 236, p. 1469-1472

Vanorio, T., A. Nur, and Y. Ebert, 2011, Rock physics analysis and time-lapse rock imaging of geochemical effects due to the injection of CO_2 into reservoir rocks. Geophysics, Vol. 76, No.5, P. 023-033.

Verdon, J.P., J.M. Kendall, and C.S. Maxwell, 2010, A comparison of passive seismic monitoring of fracture stimulation from water and CO_2 injection: Geophysics, Vol. 75, no.3. P. MA1-MA7.

Vernik, L., and A. Nur, 1992, Ultrasonic velocity and anisotropy of hydrocarbon source rocks: Geophysics, 5, 727-735.

Vernik, L., 1997, Predicting porosity from acoustic velocities in siliciclastics: A new look. Geophysics, Vol. 62, No. 1, P. 118-128

Wang, Z., and, A. Nur, 1989, Effects of CO_2 flooding on wave velocities in rocks with hydrocarbon. SPE Reservoir Engineering, Nov. P.429-436

Wang, Z., E.C. Michael, and R.T. Langan, 1998, Seismic monitoring of a CO_2 flood in a carbonate reservoir. Geophysics Vol.63, No.5. PP. 1604-1617.

White, D.J. 2008, Geophysical monitoring in the IEA GHG Weyburn-Midale CO_2 monitoring and storage project: 78th Annual International Meeting, SEG, Expanded Abstracts, 2846-2849.

Williams, G., and A. Chadwick, 2012, Quantitative seismic analysis of a thin layer of CO_2 in the Sleipner injection plume: Geophysics, Vol. 77, No.6, R245-R256

Worthington, P., 1997, Petrophysical estimation of permeability as a function of scale: Developments in Petrophysics, in M. A. Lovell, and P.K. Harvey, eds., Geological Society Special Publications, 122, 159-168.

Wyllie, M.R.J., A.R. Gregory, and L.W. Gardner, 1956, Elastic wave velocities in heterogeneous and porous media, Geophysics 21, 41-70

Yantis, B.R., J.K. Costain, and, H.D. Ackermann, 1983, A reflection seismic study near Charleston, South Carolina, in G.S. Gohn, ed., Studies related to the Charleston, South Carolina earthquake of 1886 - Tectonics and seismicity: United States Geological Survey Professional Paper 1313, p. G1-G20.

Yilmaz, O., 2001, Seismic data analysis: processing, inversion, and interpretation of seismic data Volume 1: Tulsa, Society of Exploration Geophysicists, 998 p.

Ziegler, P.A., 1983, Hydrocarbon potential of the Newark rift system: Eastern North America: Northeastern Geology, v.5, no. ¾, p. 200-208

Zoback, M.D., and S.M. Gorelick, 2012, Earthquake triggering and large-scale geologic storage of carbon dioxide. Proceedings of the National Academy of Sciences (PNAS) 109 (26) 10164-10168.